A NOISE REDUCTION BASED COMPUTED TOMOGRAPHY IMAGE ENHANCEMENT

THESIS

SUBMITTED TO

BABASAHEB BHIMRAO AMBEDKAR UNIVERSITY

LUCKNOW

BABASAHEB
BHIMRAO
AMBEDKAR
UNIVERSITY

LUCKNOW

प्रज्ञा शील करुणा

ESTABLISHED 1996

FOR THE DEGREE OF

Doctor of Philosophy

IN

COMPUTER SCIENCE

Submitted by

Manoj Diwakar

(Enrolment no: 956/13)

Supervisor

Dr. Manoj Kumar

Assistant Professor

DEPARTMENT OF COMPUTER SCIENCE

SCHOOL OF INFORMATION SCIENCE & TECHNOLOGY

BABASAHEB BHIMRAO AMBEDKAR UNIVERSITY

(A Central University; NAAC-'A' GRADE)

VIDYA VIHAR, RAEBARELI ROAD, LUCKNOW-226 025

2017

Candidate's Declaration

I hereby declare that I have completed research work for the full time prescribed and that the thesis embodies the results of my investigation conducted during the period I worked as Ph.D. research scholar. I further declare that to the best of my knowledge the thesis does not contain part of any work submitted for the award of any degree either in this Institute /University or any other Institute/ University.

(Manoj Diwakar)
Research Scholar

BABASAHEB BHIMRAO AMBEDKAR UNIVERSITY
LUCKNOW
प्रज्ञा शील करुणा
ESTABLISHED 1996

Babasaheb Bhimrao Ambedkar University
(A Central University)
Vidya Vihar, Rae Bareli Road, Lucknow - 226 025.
बाबासाहेब भीमराव अम्बेडकर विश्वविद्यालय
विद्या विहार, रायबरेली रोड, लखनऊ - 226 025

Certificate

This is to certify that the thesis titled "**A Noise Reduction based Computed Tomography Image Enhancement**" submitted by **Mr. Manoj Diwakar** is an original research work and has not been previously submitted in part or full for the award of any other degree or diploma to this or any other University.

The thesis submitted to Babasaheb Bhimrao Ambedkar University, Lucknow satisfies all the requirements as stipulated in the *Doctor of Philosophy (Ph.D.) regulations-1999 as amended in 2008/2010/2013* and it is fit for submission and evaluation for the award of the degree of Doctor of Philosophy of the University.

(Dr. Manoj Kumar)

Date: Supervisor

(Prof. Sanjay K. Dwivedi)

Head of the Department

Phone : +91 (0) 522 2440826, 2440827, 2441515, 2441615, 2441888, 2442190 (EPABX) Fax : +91 (0) 0522 2440821
Grams : BABVERSITY E-mail : root@dbraulko.ren.nic.in

BABASAHEB BHIMRAO AMBEDKAR UNIVERSITY
LUCKNOW
प्रज्ञा शील करुणा
ESTABLISHED 1996

Babasaheb Bhimrao Ambedkar University
(A Central University)
Vidya Vihar, Rae Bareli Road, Lucknow - 226 025.
बाबासाहेब भीमराव अम्बेडकर विश्वविद्यालय
विद्या विहार, रायबरेली रोड, लखनऊ - 226 025

Viva-Voce Certificate

This is to certify that thesis entitled "**A Noise Reduction based Computed Tomography Image Enhancement**" submitted by **Mr. Manoj Diwakar** under the supervision of **Dr. Manoj Kumar**, to the Department of Computer Science, Babasaheb Bhimrao Ambedkar University (A Central University) Lucknow, India, in the fulfillment of the requirement for the degree of Doctor of Philosophy in Computer Science has been approved after an oral examination of the same in collaboration with an external examiner.

Signature of External Examiner

Date:

Place: Lucknow

HEAD
Department of Computer Science,
Babasaheb Bhimrao Ambedkar University
(A Central University) Lucknow, India

Phone : +91 (0) 522 2440826, 2440827, 2441515, 2441615, 2441888, 2442190 (EPABX) **Fax :** +91 (0) 0522 2440821
Grams : BABVERSITY **E-mail :** root@dbraulko.ren.nic.in

Abstract

Today, Computed Tomography (CT) is one of the highly efficient indispensable tools in medical science for clinical purpose. Due to software and hardware limitations, and statistical uncertainty of all physical measurements in Computed Tomography, the unwanted noise appears in CT images. The presence of noise is one of the main factors to degrade the visual quality of the CT images. Because of the image degradation, the experts are not able to identify the correct information from the medical images. Therefore, this thesis investigates the methods for noise reduction in CT images while preserving their main structures. The goal of work is to improve the signal to-noise ratio without loss of spatial resolution or structures of the CT images. Hence, image denoising is an essential processing step preceding visual and automated analyses.

This thesis is concerned with the methods for CT image enhancement using image denoising concepts which can be capable to preserve edges and maintain high visual quality. Before start the CT image denoising, a brief description of CT imaging is presented which is followed by the problems of CT image denoising, motivation for the studies and a brief review of some salient work in the related fields. Further, some necessary concepts, definitions and algorithms for CT image denoising are also discussed. The thesis is attained by various approaches using spatial and transform based denoising techniques.

The first contribution of the thesis has been presented for CT image denoising using total variation (TV) method in spatial domain where a modification on total variation algorithm has been performed. In this work, a new exponentially directional weighted function (EDWF) has also been introduced based on the difference between L_1 and L_2 norms. Furthermore, a numerical algorithm has been designed to solve the minimization problem of EDWF using iterative Split Bregman method.

In next contribution, Wavelet based noise reduction technique has been developed

to improve the image quality where adaptive Wiener filtering and Wavelet Packet Threshold (WPT) algorithm are used. The Noisy CT image is decomposed using Discrete Wavelet Transform (DWT), where approximation part is filtered using WPT algorithm and detail part is filtered by the adaptive Wiener filtering. By using the decomposition level, the wavelet packet tree coefficients are calculated using optimal linear interpolation shrinkage function. Denoised image is acquired using wavelet packet reconstruction and inverse DWT. Further, to improve the results, this method has been modified by using the concepts of Wiener filtering and method noise in wavelet domain. In this modified work, a discrete wavelet transform (DWT) is performed over the noisy CT images. The high frequency wavelet coefficients are modified using local Wiener filtering. The first intermediate result is obtained using inverse discrete wavelet transform (IDWT). For better edge preservation, first intermediate result is subtracted from the input noisy image and processed using wavelet packet thresholding. The outcome of wavelet packet thresholding is the second intermediate result. Both intermediate results are added to obtain the final denoised CT image.

Another contribution to denoise the CT images with edge preservation in tetrolet domain (Haar-type wavelet transform) has been developed where a locally adaptive shrinkage rule is performed by using circular shift on high frequency tetrolet coefficients in such a way that noise can be reduced more effectively. Further this scheme is modified using method noise concept. In this modified work, NLM filter and circular shift based wavelet packet thresholding methods are used for CT image denoising.

The next contribution has been designed, developed and evaluated in wavelet domain using intra scale dependency based approach where many intermediate steps are performed using method noise and wavelet based thresholding concepts. This work is divided into two phases. In first phase, input CT image is separately denoised using different patch size where denoising is performed based on thresholding and its method noise thresholding. The outcome of first phase provides more than one denoised images. In second phase, block wise variation based aggregation is performed

in wavelet domain to get the final outcome. Further, this scheme is modified using inter scale dependency where bilateral filter and bivariate shrinkage rule is used in dual-tree complex wavelet transform.

The last contribution of the thesis has been designed, developed and evaluated using Wavelet, Curvelet and Non-subsampled Contourlet transforms. In this work, Wavelet and Curvelet transforms based CT image denoising is performed using method concept. Further, this work is modified using Curvelet and Non-subsampled Contourlet transforms where Curvelet and Non-subsampled Contourlet transforms based CT image denoising is performed using thresholding and aggregation concept to get the sharp and smooth CT images.

The salient contributions of the work described in this thesis are given, with the future scope of work in this field.

To verify the performance of all CT image denoising schemes, the qualitative and quantitative evaluations are performed. The experimental results of proposed schemes are visually analyzed. Apart from visual analysis, the proposed schemes are also verified with some standard performance metrics such as Image Quality Index (IQI) and Peak Signal-to-noise Ratio (PSNR) and so on. The proposed schemes are also compared with some standard similar existing methods or state-of-the-art methods, and it is observed that performance of proposed schemes are superior to existing similar methods in terms of visual quality and performance metrics.

Acknowledgements

Starting with my thanking note, I first of all thank GOD for providing me the opportunity to pursue higher studies under the guidance of Dr. Manoj Kumar, Assistant Professor, Department of Computer Science, Babasaheb Bhimrao Ambedkar University, Lucknow. I feel privileged to express my sincere regards and gratitude to my supervisor for his valuable guidance, and constant encouragement throughout the course of my research work. The critical comments, rendered by him during the discussions are deeply appreciated.

I pay my hearted and deep tributes to all the researchers in the world around, working for the development of Science and Technology for the betterment and enlightenment of the society and feeling to be the part of that community gives me a great pride and pleasure.

The award of degree Doctor of Philosophy is one of the hardest deserving achievements. People struggle for it and achievement not easily found. During the entire research works some valuable people conceived their enormous positions in my heart. In this regard, I am grateful to the University and express my deep sense of gratitude to its Honble Vice-Chancellor for delivering this great opportunity to me.

I convey my sincere thanks to Prof. Vipin Saxena, Dean, SIST, Prof. Sanjay K. Dwivedi, Head, Department of Computer Science, Department Research Committee and all other faculty members of department namely Dr. Deepa Raj, Dr. Narendra Kumar and Dr. Shalini Chandra for their motivation and support during the research. I would also like to show my gratitude to the Department of Computer science, for the provision of the best equipment and pleasant office environment required for good quality research. I would like to thank all administrative and supporting staffs of the University for providing the comfortable environment and help.

I would also like to thank Dr. Rakesh Kumar, Medical officer, State Allopathy

Dispensary, Lucknow (U.P.), India for his valuable suggestions and CT related questions.

I particularly would like to deeply appreciate the great help of research scholars Smita Agrawal, Ankita Vaish and Sonam, who always kept the healthy research environment and extended their full cooperation during my research. They have given me support, and a joyful and wonderful university life. I am also grateful to my friends Ganesh Chandra, Kamlesh Verma and many more for their timely help and the moral support they provided me during my research work.

I wholeheartedly thank my parents, my wife and all other family members for their enduring patience and for providing the moral support during the course of this work.

I thank University Grants Commission, India for the financial support to carry out this research work.

Lucknow (Manoj Diwakar)

February, 2017

List of Figures

List of Tables

Table of Contents

CHAPTER 1

Introduction

Chapter 1

Introduction

This chapter introduces the thesis work, some background of Computed Tomography such as CT image reconstruction and noise in CT images, problems of CT image denoising, describes motivation leading to the presentation of this thesis, brief literature review and outline of the thesis.

1.1 General Introduction

Computed Tomography (CT), invented by Godfrey N. Hounsfield [59] in 1972, was the first method that allowed to generate non-overlapping axial slices of the internal structure of a humans body without opening it [16, 113]. The Nobel prize awarded to Hounsfield [59] and Cormack [29] for their work on the initial CT device which signifies the importance of CT [60].

Today, CT is associated with high efficiency in radiologic diagnostics and has become an important tool in medical examinations. Computed tomography (CT), originally known as computed axial tomography (CAT or CT scan), is a medical imaging method employing tomography where digital geometry processing is used to generate a three-dimensional image of the internals of an object from a large series of two-dimensional X-ray images taken around a single axis of rotation [124]. Computed

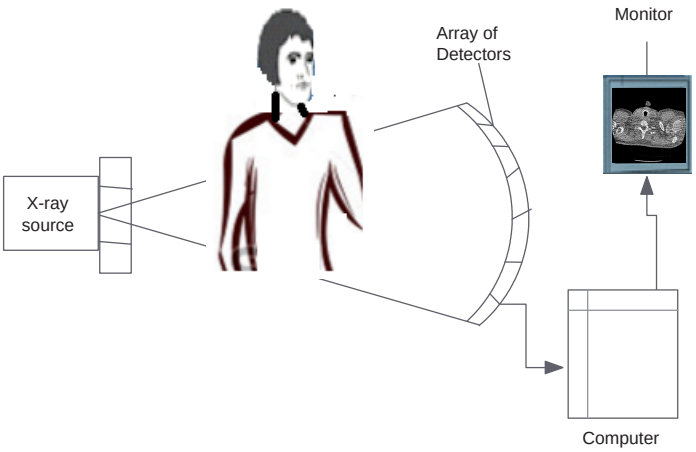

Figure 1.1: CT Scan System

Tomography (CT) is a powerful nondestructive evaluation (NDE) technique for producing 2-D and 3-D cross-sectional images of an object from flat X-ray images. The characteristics of the internal structure of an object such as dimensions, shape, internal defects and density are readily available from CT images. The process through radon and inverse radon transform on the information received through the passage of an X-ray beam, an image can be reconstructed, is known as CT imaging. The CT scan system is illustrated in figure 1.1.

In Computed Tomography, X-rays are projected with various angles over the human body where soft and hard tissues of human body are observed by the detector. More X-rays are observed on the higher density tissue such as bones and detectors receive weak signal and change into electrical signals. These electrical signals are converted into the digital data by analog/digital converter. The data in the digital matrix can be changed into small boxes ranging from black to white gray through digital/analog converter. Finally, raw data (collected from various angles) are further

mathematically computed using Radon transform and CT images are reconstructed. To reconstruct the CT images, radon transform is very popular using backprojection concept. Backprojection is the most common concept used to reconstruct the CT images. The back projecting to the raw data with respective directions is generally known as backprojection [75].

1.1.1 Radon Transform

The 2D Radon transformation is the projection of the image intensity along a radial line oriented at a specific angle. The Radon transformation shows the relationship between the 2-D object and its projections [140].

Suppose a 2-D function integrating along the line as shown in figure 1.2, whose normal vector is in θ direction, results in the $g(s, \theta)$ function which is the projection of the 2D function $f(x, y)$ on the axis s of θ direction. When s is zero, the g function has the value $g(0, \theta)$ which is obtained by the integration along the line passing the origin of (x, y) coordinate. The points on the line whose normal vector is in θ direction and passes the origin of coordinate satisfy the equation:

$$x \cos\theta + y \sin\theta = 0 \tag{1.1.1}$$

Integration along the line whose normal vector is in θ direction and that passes the origin of (x, y) coordinate means the integration of $f(x, y)$ only at the points satisfying the previous equation. With the help of the Dirac delta function δ, which

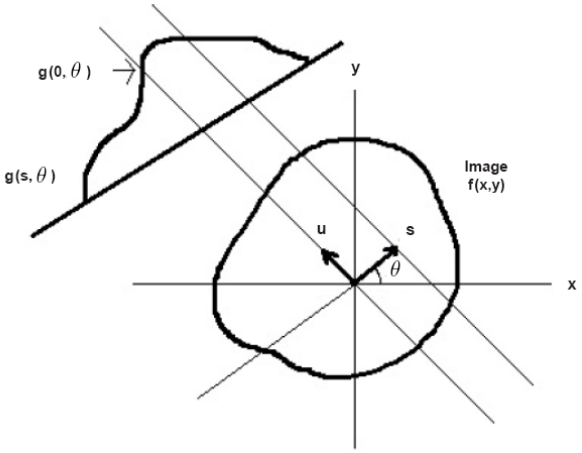

Figure 1.2: Radon Transform

is zero for every argument except to 0 and its integral is one, $g(0, \theta)$ is expressed as:

$$\int \int f(x, y) \cdot \delta(x \cos\theta + y \sin\theta) dx dy \tag{1.1.2}$$

Similarly, the line with normal vector in θ direction and distance s from the origin is satisfying the following equation:

$$x \cos\theta + y \sin\theta - s = 0 \tag{1.1.3}$$

Therefore, the general equation of the Radon transformation is acquired as:

$$g(s, \theta) = \int \int f(x, y) \cdot \delta(x \cos\theta + y \sin\theta - s) dx dy \tag{1.1.4}$$

The inverse of Radon transform is given by the following equation:

$$f(x, y) = \int_{-\pi/2}^{\pi/2} g(s, \theta) d\theta \tag{1.1.5}$$

However, backprojection is conceptually simple, it does not correctly solve the inverse problem. To reconstruct the CT image, a simulation based example is

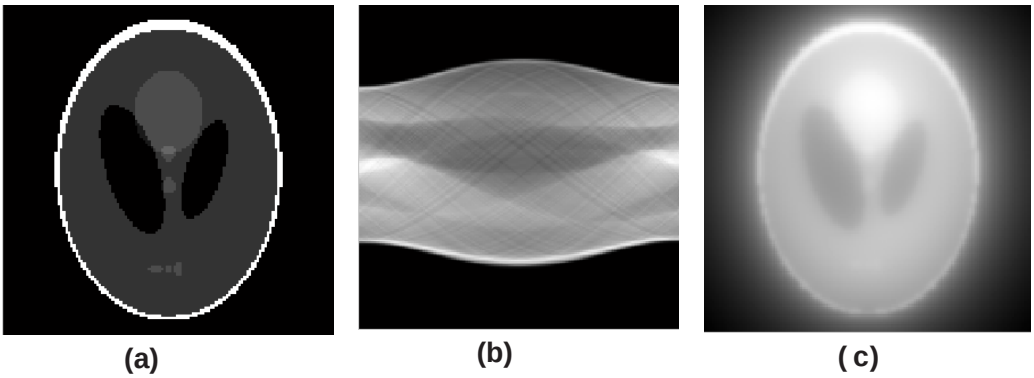

Figure 1.3: Image reconstruction using Radon Transform

shown in figure 1.3. In this example, a phantom image as shown in figure 1.3(a) is taken as an input object and Radon transform is applied to the phantom image by choosing $\theta = 180$. A raw data is collected from each angel. This raw data can be represent in the form of the image which is known as Sinogram as shown in figure 1.3(b). Finally, inverse Radon transform is performed over the Sinogram to obtain the reconstructed CT image as shown in figure 1.3(c). However, reconstructed CT image as shown in figure 1.3(c) is very blurry. To overcome from the blurry effects, filter backprojection is widely used in CT image reconstructions. To correct this, the projections are first filtered in the Fourier domain by a filter such as ramp filter and then the filtered projections are projected using radon transform. An example of image reconstruction using filtered backprojection is shown in figure 1.4.

There are many factors which affect the quality of reconstructed CT images. Some of major factors affecting image quality are:

- Blurring: CT image may be blurred due to various reasons such as appropriate

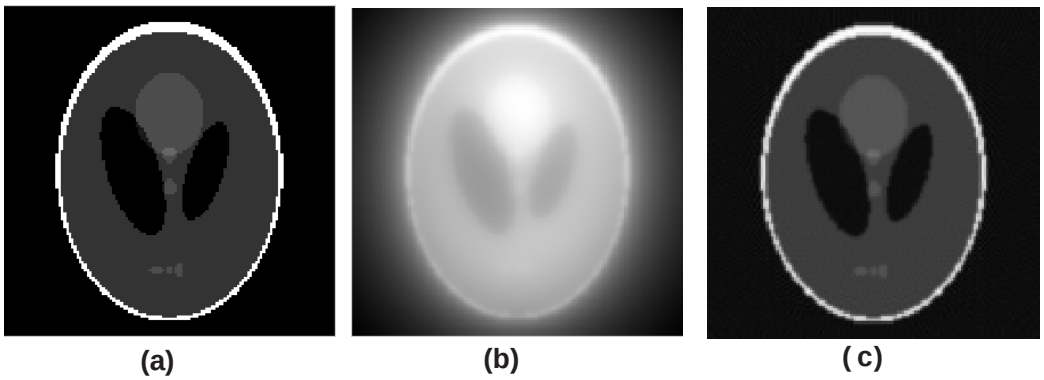

Figure 1.4: Image reconstruction using filtered backprojection: (a) Phantom image, (b) Unfiltered image, and (c) Filtered image

protocol factor values, patient movement, etc.

- Field Of View (FOV): A selected region to reconstruct the CT image is known as field of view. If a reconstructed CT image is too small or too big, it is hard to find the abnormalities and the quality of CT image may be degraded.

- Artifacts: Distortion or an error in an image and unrelated from object is known as an artifact. The quality of CT images is also degraded because of various types of artifacts such as metal, equipments, etc.

- Visual Noise: Noise is an undesired information that degrades the visual effect of an image. Due to acquisition and transmission in CT imaging, the noise is appeared that leads to poor image quality. Noise is also generated because of many mathematical computations at the time of reconstruction of CT images. The noise contains very less value which is embedded with a clean pixels to make the pixel noisy.

In this thesis, we are focusing on the noise suppression to enhance the quality of noisy CT images. CT image quality can be improved by developing algorithms to reduce the noise from CT images. These algorithms can be further used in order to reduce the radiation dose. Generally, the process of noise suppression is known as image denoising.

1.1.2 Noise in CT reconstructed images

Generally, noise in reconstructed CT images are introduced mainly by two reasons. First, a continuously varying error due to electrical noise or roundoff errors, can be modeled as a simple additive noise, and second reason is the possible error due to random variations in detected X-ray intensity. To differentiate tissues (soft and hard), CT numbers are defined by using Hounsfield unit (HU) [59] for CT image reconstruction. Hounsfield unit (HU) scale is displayed in figure 1.5, where some CT numbers are defined. The CT number for a given tissue is determined by the X-ray linear attenuation coefficient (LAC). Linearity is the ability of the CT imaging to assign the correct Hounsfield unit (HU) to a given tissue. A good linearity is essential for quantitative analysis of CT images. Suppose we have two voxels of identical tissues and these voxels are transmitted into CT numbers for CT image reconstruction. Both CT numbers should be same but there is a small variation. This is a statistical variation which is considered as image noise. Because CT noise appears as fluctuations in CT numbers, a measurement of image noise can be estimated from these fluctuations, and such a measurement can be determined from a regions of interest (ROIs) on a CT

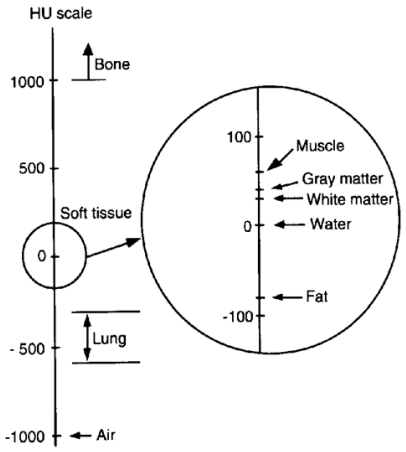

Figure 1.5: Hounsfield unit (HU) scale [59]

scan image. The measurement can be performed using statistical ROI function which is calculated by the average and standard deviation (SD) of the CT numbers for the enclosed pixels. The resultant statistical distribution is most likely to be bell-shaped curve. The amount of noise can be determined by calculating the magnitude of random fluctuations in the CT numbers which is also know as standard deviation (SD). Larger value of SD means higher noise in CT images. This statistical distribution shows that the mean value of the noise is equal to the noise variance and it can be analyzed that the signal-to-noise ratio is proportional to the square root of the X-ray dose. Therefore, the relative amount of quantum noise at the detector elements can be decreased by increasing dose. With the known noise distribution at the detector, CT images are reconstructed using reconstruction method such as filtered backprojection method. The problem to identify noise in CT image is that all the intermediate steps, like interpolations or filtering with the convolution kernel, introduce correlations to the noisy data. Due to these dependencies, the noise distribution in the final CT

image is usually unknown.

The distribution of noise in CT image can be determined by many approaches. By repeating scans of the same object can give an ideal noise distribution but impractical to perform on the patients. In another approach, noise is added to the raw data and multiple noise simulations and reconstructions are performed to analyze the distribution of noise in CT images. However, this approach is time consuming because of repeat simulations. A more elegant approach is to analyze the noise distribution analytically using a noise model at the time of the reconstruction process. In this approach, the distribution of noise in CT image can be derived by estimating the noise variance through reconstructions algorithms. However, the distribution of noise in CT image can be accurately characterized using a Poisson distribution. But for multi-detector CT (MDCT) scanner, the noise distribution is more accurately characterized by the Gaussian distribution. Various literatures [117, 118, 15, 13, 14] also confirm that the noise in CT images is generally an additive white Gaussian noise.

After noise analysis in CT images, CT image quality can be improved by developing algorithms to reduce the noise from CT images. These algorithms can be further used in order to reduce the radiation dose. Generally, the process of noise suppression is known as image denoising. Some major problems of image denoising are given below.

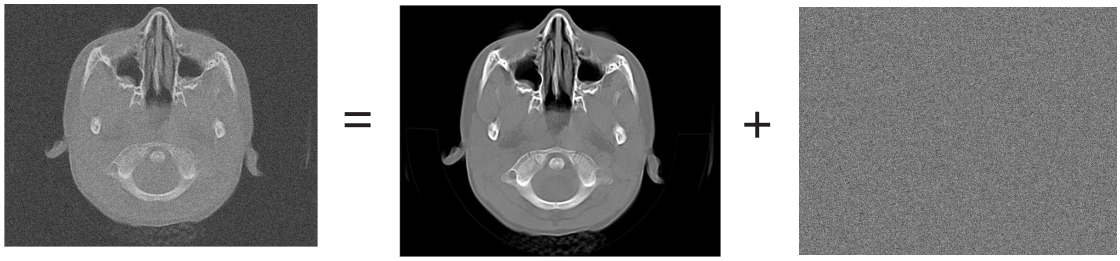

Figure 1.6: A noisy image is the sum of the clean image and the noise component.

1.2 Problems of CT image denoising

Image denoising is the problem of finding a clean image from a noisy image [54]. In most cases, it is assumed that the noisy image is the summation of original image and a noise component, as shown in figure 1.6. Hence denoising is a procedure which reduces the existing noise in an image and minimizes the loss of features in a clean image. CT Image denoising can be better performed with the prior knowledge about CT images and the noise. Without prior knowledge, the accuracy of CT image denoising can not be effectively improved.

The problem of CT image denoising can be mathematically presented as follows:

$$X = Y + \eta \tag{1.2.6}$$

where, X is the noisy image, Y is the clean image to be estimated from X and η is a noise component.

The goal of image denoising is to suppress the noise from the CT images with preserving clinical details so that CT image can be useful for diagnosis purpose. Digital image processing plays a key role to suppress the noise from the CT images

[54, 62]. Conventional smoothening and sharpening filters are the most popular filters for noise reduction in digital images. Smoothening filters are not sufficient for effective noise reduction, especially for higher noise. Also it may harm the detail parts such as edges due to smoothness factor. Sharpening filters have a tendency to reduce the noise and sharp the edges but, not impressive to preserve small details. This is the major problem of image denoising in medical image analysis because missing structures can give an inaccurate analysis of CT images which may harmful for the life of a human. However, various methods have been investigated but still noise reduction is a challenging task. The main challenges for noise reduction in CT image are:

- Flat regions should be flat.
- Image boundaries should be preserved (no blurring).
- Texture details should not be lost.
- Global contrast should be preserved.
- New artifacts should not be generated.

1.3 Motivation for the Study

Due to statistical uncertainty of all physical measurements in Computed Tomography, the noise is introduced in the measurement of intensities propagates through the reconstruction algorithm to the resulting CT slices. The noise in CT reconstructed

images is also dependent on the amount of radiation dose [30, 67, 69, 126]. Generally physicians are demanding a good quality of CT images to diagnose the problem. The good quality of CT images can be obtained by increasing the radiation dose. Unfortunately, these higher radiation doses may increase the risk to generate the cancer cells in the human body [32, 68, 93]. The risk of higher radiation dose for children is 2-3 times greater than the risk to adults [48, 95, 150, 108]. Hence, the demand for reducing the radiation dose arises but this might degrade the quality of an image in terms of noise. Decreasing the radiation dose may increase the noise which may affect the details needed for clinical diagnosis. There is need to make a tradeoff between noise and radiation dose. Reducing the radiation dose without losing the image quality is a challenging task. If it becomes possible that the noise can be reduced or removed from low dose CT image while preserving all clinically relevant details, then higher radiation dose is further not required to generate the good quality CT images. But how the noise can be reduced without degrading and preserving diagnostically relevant content of the noisy CT images? This motivates us and increase the interest in the development of new techniques or methods to enhance noisy CT images with a possibility to increase signal-to-noise ratio and have a scope for further reduction of X-ray radiation dose. The main objectives covered in this thesis are to develop efficient denoising algorithms for CT images corrupted with Gaussian noise with effectively retain the significant features in images.

1.4 Brief Literature Review

With the invention of CT, the research of noise reduction in CT has been come into existence. The first articles [122] and [28] of CT image denoising were published shortly after the invention of CT, where the concept of low-pass filtering was used. Authors concluded that the noise is effectively reduced and also enhanced the detectability of big objects from the noisy CT image. However, these methods have major problems such as over-smoothing of edges and decreasing the detectability of small structures.

Over the years, various techniques [8, 109, 151, 152] have been investigated for controlling the noise in CT scan imaging. Projection based techniques in CT works on raw data or sinogram which comes through Radon transform where noise filtering was applied on raw data using linear or non-linear filters followed by filtered back-projection (FBP) [46, 78, 83]. Many iterative reconstruction approaches for noise suppression in CT have also been investigated [41, 80] by optimizing statistical objective functions. Iterative reconstruction techniques have the advantage that the noise statistics in the projections can directly be taken into account during the reconstruction process. The disadvantage, however, is the high computational cost of iterative methods. The other popular techniques are based on post-processing approaches. The main goal of these techniques are the structure-preserving reduction of pixel noise in reconstructed CT-images and improved signal-to-noise ratio (SNR)

without increasing the radiation dose. A very important requirement for any noise reduction in CT images is that all clinically relevant image contents must be preserved. Especially, edges and small structures should not be affected.

Various methods have been investigated for image denoising as discussed in [102, 64]. Generally, images can be denoised into two domains: (i) spatial and (ii) transform domains.

1.4.1 Spatial domain filtering

Initially, in spatial domain, linear filters were used to denoised the images but it was not successful for preserving details over the images. Mean filtering was used to reduce the Gaussian noise but for high noise it produces blurry images. To overcome that, wiener filtering [100] was further used. With non-linear filters in spatial domain, the noise is removed without any attempt to explicitly identify it. Spatial filters employ a low pass filtering on group of pixels with the assumption that the noise occupies the higher region of frequency spectrum. Generally, linear filters are used to remove noise but blurring problem may occur [2].

Naidich et al. [104] analyzed the effect of low dose on CT images and found that low dose can also help to provide CT images for diagnosis purpose. However, the quality of CT images is not as good as conducted by high dose CT images. Mayo et al. [92] also tested on low dose CT images and observed that the photon detectors adapting less data will create the visual noise in the reconstructed CT images. They concluded that low dose CT images also meet with diagnostic requirements and further image

processing algorithms would help to improve the quality of CT images.

Recently, least square fidelity minimization [153, 154, 155, 156] concept is also popular to remove the Gaussian noise from images. To minimize the least square fidelity term, many regularization functions have been investigated such as Tikohonov, anisotropic diffusion and Total variation methods. Tikohonov method [70, 135] is the simplest one in which data fidelity term is minimized with L_2 norm regularization, but it over smooths the detail parts of images [38, 107]. To overcome that, anisotropic diffusion based methods have been proposed to enhance the details of the images by stopping the diffusion at the edges, but it blurs the noisy edges [23, 43]. In parallel with anisotropic diffusion [114, 147], Total variation (TV) based regularization was proposed to overcome the smoothness in denoised images. From various studies, it can be found that TV methods perform better for noise suppression in medical images, but it has a problem of unwanted stair-artifacts [25, 120, 142, 143]. The advantages of TV and anisotropic diffusion were combined to improve the drawbacks of TV method and the combination is called as anisotropic total variation method [121].

Rudin-Osher-Fatemi (R.O.F.) model [121] was proposed to provide the smooth and denoise images by TV method using L_2 norm fidelity optimization. The authors [121] also discussed the computational difficulty because of non-linearity and non-differentiability. Therefore, R.O.F. model was further modified to avoid these difficulties and improved the performance of image denoising [24]. A non-differential TV method was introduced using Bregman iteration and got the success to minimize

the problems. Later, Bregman iteration was improved by using linearization function [53]. Further, it was extended to minimize the L_1 regularization by introducing Split Bregman method [36, 84, 111, 148]. Recently, various methods [18, 19, 20, 22, 27] have been proposed using Split Bregman method by modifying norms as well as regularization terms. Some authors also proposed the mixed models such as $L_2 - L_1$ [86, 161], higher degree based image denoising [61] and gradient-based algorithms for constrained total variation [7]. However, the results of mixed model based image denoising are improved over the classical TV method and some of the state-of-the-art methods, but still blocking effects can be observed near the noisy edges. To solve the blocking effects in TV model, a method [134] was proposed based on exponentially TV method. Further, image denoising was performed by Split Bregman using exponential TV function. This method gives better noise reduction.

In [6, 66], authors addressed the directional derivatives of an images and image denoising was performed on the basis of choosing directional TV function. The directional derivatives give better edge and texture preservation. Recently, total variation methods were improved such as coefficients driven based total variation [3], nonnegativity constrained based TV [79] and so on, to attenuate the noise from the noisy CT images.

To gain better edge preservation, Zhang et al. [159] introduced a denoising scheme based on dictionary learning on low dose CT images in projection domain. To improve the quality of reconstructed CT images, the authors performed on sinogram where

penalized weighted least-square (PWLS) approach is used. Here, dictionary learning based denoising was performed using statistical characteristic of noise by considering weighted least-squares and CT image was reconstructed using filtered back projection (FBP) algorithm from the denoised sinogram. This work performs well for the projected data. Experimental evaluation also indicates that low dose CT images have been denoised effectively. Mechlem et al. [94] also proposed a CT image denoising scheme based on dictionary learning method. Here, denoising was performed on dual energy computed tomography images. The authors examined dictionary learning algorithm for dual energy CT aimed at exploiting the high spatial correlation between images obtained from different energy spectra. Both low and high energy images were divided into small patches, and for denoising, they combined the respective patches with the help of weighted mean using linear transformation. These combined patches were further processed using conventional dictionary denoising method. The experimental evaluation indicates that their proposed algorithm gives better outcomes in compare to conventional dictionary denoising in terms of qualitative and quantitative image quality measures.

Generally, the images are denoised based on the analysis of neighbour pixels. With this motivation, Okada [110] proposed a method for CT image denoising using weight neighboring pixels depending on the intensity differences. The implementation time of this method is little bit higher however it provides less smoothed CT images with higher spatial resolution. For better edge preservation, Al-Ameen et al. [4] proposed

a phase-preserving algorithm to denoise CT images. The phase preserving is an excellent noise reduction method, but it suppresses the specific details from the processed images supposing them as noise. Therefore, phase-preserving algorithm is modified using Wiener filter that uses 2D Gaussian point spread function. The advantages of this algorithm are better preservation of the minor medical details and an improvement in noise suppression. The performance of proposed methodology has been tested by using universal image quality index and peak signal-to-noise ratio metrics. Results show major improvement not only in noise attenuation but also in preserving the small details. In an another approach, Lanzolla et al. [81] analyzed the effects of different noise reduction filters on computed tomography (CT) images. The authors introduced a denoising method based on the combination of Gaussian and Prewitt operators for CT image denoising. Simulation results indicate that their algorithm enhanced the image quality and also permitted to use low radiation dose protocol in CT examinations. Zheng et al. [160] introduced a new method for low dose CT image denoising using Pointwise Fractal Dimension where a modified pointwise fractal dimension (PWFD) function, named as pointwise box-counting dimension (PWBCD) was performed for calculating weight value of each pixel using NLM. The function was further used to calculate the variance between the two comparable windows to estimate the required weights. This method gives sharp and smooth denoised images but may lose small structures. Trinh et al. [137] proposed an optimal weight denoising method where patch wise filtering was performed based on defined database of

standard image blocks. This method depends on the standard image data-set which is not applicable for all images, especially when there is only the noisy CT images.

In recent years, Bilateral [136] and Non-local means (NLM) [17] filters are very popular for image denoisng. Bilateral filter is a non-linear, edge-preserving and noise-reducing smoothing filter used for image denoising. Intensity value at each pixel in an image was replaced by a weighted average of intensity values from nearby pixels. Unlike local smoothing filters, non-local means does not update a pixel value with an average of the neighbour pixels, instead that, NLM filter updates a pixel using a weighted average of the pixels judged to be most similar where neighborhood comparisons is done within a specified search window. Both bilateral and Non-local means filters give good results in terms of noise reduction and preserving clinical information. Giraldo et al. [52] presented a comparative study of two noise reduction methods for computed tomography images: Bilateral filter and nonlocal means. The authors compared both techniques against those from a commercially available weighted filtered back-projection (WFBP) method. The authors tested their results over real CT images as well as simulated phantom images. It was observed from result analysis that both methods are providing better denoising by weighted filtered back-projection (WFBP) method. Manduca et al. [91] presented a novel locally adaptive projection space denoising algorithm for low-dose CT image where locally adaptive bilateral sinogram filtering with a CT noise model was used. Due to bilateral filtering, the edge information in the sinogram is preserved and it helps to provide smooth

denosied CT images. Li et al. [85] presented an adaptive nonlocal means filtering based on local noise level for CT denoising where a modified nonlocal means (NLM) algorithm is proposed to denoise the CT image. Due to modification in NLM filtering, the cost computational is additionally increased while the resultant image is giving better outcomes in compare to standard NLM methods. Wu et al. [149] proposed a parallelized nonlocal means denoising method where the pixels were filtered depending on the self-similarity feature of the pixel with different noise reduction levels through large-scale areas. However, this method provides sharp and smooth denoised CT images. If the image size is large, the process time of this method is also much higher. Demerit of this method is that it removes the small details from the noisy CT image and also takes high operation time. To overcome that, Hashemi et al. [58] presented a study on CT image denoising using total variation (TV) method where they analyzed that some of the small structures was removed while denoising using TV method. To overcome that, they proposed a modified nonlocal TV method, called probabilistic NLTV (PNLTV) for CT image denoising. Here, Non-locality allows the proposed method to preserve the image texture by enabling proposed stopping criterion. From the result analysis, it was analyzed that PNLTV has a capability to keep fine details unchanged and provide sharp and smooth denoised images. Ai et al. [1] proposed a new scheme based on an adaptive tensor-based principal component analysis (AT-PCA) algorithm for low-dose CT image denoising. Using neighborhood pixels, patches were selected and similar patches were searched by providing training

the patches for further processing. Further, Tensor-based PCA was used to obtain transformation matrices where coefficients were sequentially shrunk by the linear minimum mean square error. The shrunked patches were obtained and aggregation was performed on all shrunked patches to get the denoised images. The experimental evaluation was performed on CT images and it was observed that this method can suppress the noise, enhance the edges, and improve the image quality more effectively than NLM filtering.

1.4.2 Transform domain filtering

The most investigated transform in denoising is Wavelet Transform [90] where the input data is decomposed into its scale-space representation. In wavelet based thresholding, a threshold value is estimated and small wavelet coefficients in high frequency subbands are removed by using the estimated threshold value and large wavelet coefficients are kept preserve. Wavelet based denoising algorithms basically involve three steps. First, an image is transformed into a wavelet domain. Next, denoising is effected on the wavelet coefficients, and finally the denoised image is obtained by applying the inverse wavelet transform on the denoised wavelet coefficients.

Linear filters in transform domain such as Wiener filter in the wavelet domain yield optimal results when the signal corruption can be modeled as a Gaussian process and the accuracy criterion is the mean square error (MSE) [131]. However, designing a filter based on this assumption frequently results in a filtered image that is more visually displeasing than the original noisy signal, even though the filtering operation

successfully reduces the MSE.

The most popular method in transform domain is non-linear based thresholding. Wavelet coefficient thresholding scheme of denoising is based on the idea that the energy of the signal to be defined concentrates on some of the wavelet coefficients, while the energy of noise spreads throughout all wavelet coefficients. Similarity between the basic wavelet and the signal to be defined plays a very important role, making it possible for the signals to concentrate on fewer coefficients. The effectiveness of thresholding depends on the estimation of an appropriate threshold.

In another approach, Moulin et al. [103] introduced a method for image denoising using Gaussian mixture model (GMM) and the Generalized Gaussian Distribution (GGD) over the wavelet coefficients. Although GGD is more accurate, GMM is simpler to use. For better enhancement of images, Chang et al. [26] introduced the use of adaptive wavelet thresholding for image denoising, by modeling the wavelet coefficients as a generalized Gaussian random variable, whose parameters are estimated locally (i.e., within a given neighborhood). Sanches et al. [123] conducted a Bayesian denoising algorithm to suppress the additive white Gaussian and multiplicative noise described by Poisson and Rayleigh distributions from CT images. The algorithm was based on the Maximum a Posteriori (MAP) criterion, and edge preserved priors which suppressed the distortion of relevant anatomical details. The main contribution of their algorithm is provided a Bayesian denoising algorithm followed by the Sylvester Lyapunov equation to suppress additive and multiplicative noise from CT images.

The experimental evaluation indicates that proposed algorithm works well for noise suppression and edge preservation. Recently, Fathi et al. [44] proposed an efficient algorithm for image denoising which performs adaptive thresholding methods in the Wavelet packet transform domain using optimal linear interpolation. Experiments were evaluated on medical as well as natural test images which were corrupted by various noise levels. The analysis of the results indicate that the method performs well in most of the cases and more visually pleasant than other wavelet based denoising methods. The computational cost of the proposed method is also modest. Yasuda et al. [157] proposed a new and smooth shrinkage function using noise distribution approach for CT image denoising. They analyzed that spatial frequency of noise exists in the same frequency band with the signal, it is impossible to completely remove the noise. However, wavelet shrinkage rules enables position scale processing, and it is possible to reduce noise components effectively without degrading high frequency signal components. Denoising performance of this scheme was compared with a conventional thresholding and filtering method. They also discussed that the preservability of diagnostic information and reduction of X-ray dose. They concluded that preservability of signals and denoising performance were obtained better with the proposed shrinkage function, if this method is applied to low-dose noisy images. Also conclude that reduction in the patient radiation dose can be achieved without degrading diagnostic information.

Wang et al. [145] introduced a method to improve the robustness of denoising

algorithm where noise was estimate based on the concept of the pixel pattern classifier. Moreover, robust adaptive directional lifting (RADL) algorithm was performed at each pixel level to enhance the denoising performance. The denoising performance of RADL algorithm improved in terms of edges and texture preservation. Firoiu et al. [47] presented a method based on the Bayesian approach of wavelet based thresholding for image denoising. To perform denoising, hyper analytic wavelet transform (HWT) is performed with some intermediate wavelets thresholding using bishrink filter. The results have been analyzed using different wavelet basis such as Haar, DB2, etc. However, the results are slightly different by using other wavelet basis but wavelets Daubechies-10 performed better denoising in most of the cases. Mohideen et al. [101] presented a method using multi wavelet with hard thresholding over the mammographic images. Initially, the contrast and faint details are improved with some preprocessing concepts. Image suppression has been performed where multi wavelet transforms are performed for better edge preservation. To find the noise variance, Laplacian random model is generalized at each subbands and thresholding has been performed using hard thresholding function. The performance of denoising method depends on estimated threshold value. However the results are improved but for higher noise the results are not up to the mark. Max Migonette [96] introduced a method using wavelet based thresholding for image denoising. However, the noise was suppressed effectively but blurring problem still occurs. To avoid blurring, a post processing deconvolution step has been performed.

Based on inter-scale and intra-scale dependencies in wavelet coefficients, Romberg et al. [119] analyzed that Hidden Markov Models (HMM) effectively work for inter-scale based image denoising. While Random Markov Field (RMF) models are more efficient to capture intra-scale correlations in image denoising. The complexity of local structures is not well described by Random Markov Gaussian densities whereas Hidden Markov Models can be used to capture higher order statistics. The correlations between coefficients at same scale are modeled by Hidden Markov Chain Model whereas the correlation between coefficients across the chain is modeled by Hidden Markov Trees (HMT). Once the correlation is captured by HMM, maximization expectation is used to estimate the required parameters and from those, denoised signal is estimated from noisy observation using well known MAP estimator. A disadvantage of HMT is the computational burden of the training stage. To avoid that, Malfait et al. [89] proposed a model where each neighborhood of wavelet coefficients was described as a Gaussian scale mixture (GSM) and an independent hidden random scalar multiplier. In another approach, Knas et al. [74] proposed a denoising algorithm using Gaussian filter and adaptive Prewitt Mask for computed tomography images. The process of denoising was performed on the basis of Markov Random Field (MRF) model. The results obtained from proposed scheme gives better results than standard approach of using only the MRF. It takes less time to execute the proposed algorithm.

H. Rabbani [117] proposed image denoising algorithm where each coefficients in

each subband were suppressed using steerable pyramid with a Laplacian probability density function (PDF) with local variance. Within this framework, they performed a method for image denoising based on designing a maximum a posteriori (MAP) estimator, which relied on the zero-mean Laplacian random variables with high local correlation. Results were analyzed with several published methods such as Bayes least squared Gaussian scale mixture (BLS-GSM) technique that was a state-of-the-art denoising technique and it was observed that proposed algorithm works well for image denoising. Further, Rabbani et al. [118] extended his work and proposed a novel noise reduction algorithms that was used to improve the image quality in various medical imaging modalities such as magnetic resonance and multi-detector CT. Here, the noisy captured 3D data were first transformed by discrete complex wavelet transform. Using a nonlinear function, they have modeled the data as sum of the clean data plus additive Gaussian or Rayleigh noise. They used a mixture of bivariate Laplacian probability density functions for the clean data in the transformed domain. The MAP and minimum mean-squared error (MMSE) estimators allowed them to efficiently reduce the noise. Furthermore, they have estimated the parameters of the model using local information. Their experiments on CT images show that among their derived shrinkage functions usually BiLapGausMAP produced images with higher peak SNR.

On the basis of correlation between two similar noisy CT images, Borsdorf et al. [15] proposed wavelet based method for noise reduction over the noisy CT images.

Here, The proposed algorithm works on the two input noisy CT images which are similar with CT data but differ with noise. Wavelet coefficients were obtained and by identifying correlation values, thresholding was performed for CT image denoising. They also tested correlation analysis on the basis of gradient approximation. the results indicates that noise reduction of approximately 50 percent is possible without loss of structure information. Further, Borsdorf et al. [13] extended a scheme based on a possibility to compute precise orientation dependent noise estimates for every pixel position. Here, projection noise is estimated using indirect fan-beam FBP reconstruction. Further, denoising process has been performed through bilateral filtering method using estimated noise. With this method, noise is effectively reduced in compare of bilateral filtering method. In another extended work, Borsdorf et al. [14] proposed an image denoising algorithm using wavelet transform. The authors works on two input CT images with the assumptions that both CT images have similar data with uncorrelated noise. Wavelet coefficients are identified of both input CT images and correlation analysis are analyzed. They provide a framework where small correlation values were suppressed which are considered as noise while high correlation values are preserved which are considered as structures or edges. The final noise-suppressed image was reconstructed from the averaged and weighted wavelet coefficients of the input images. The quantitative and qualitative evaluation based on phantom as well as real clinical data showed that high noise reduction rates of around 40 percent could be achieved without noticeable loss of image resolution.

In another approach, Shih et al. [129] proposed a method to reduce the noise from the low-dose computed tomography (LDCT) images using multiresolution total variation minimization (MRTV) method. Here, discrete wavelet transform was performed over the CT images to decompose low and high frequency wavelet coefficients. These high frequency wavelet coefficients were further processed using total variation minimization with suitable tuning parameters. The CT image reconstructed by inverse wavelet transform is the denoised CT image. The results were tested on the Shepp-Logan phantom added with Gaussian white noise and also real head CT images. They concluded that results were improved in terms of signal-to-noise ratio in compare to total variation minimization methods. Similarly, Duan et al. [40] proposed a scheme based on second order total generalized variation mode to remove speckle noise from medical images. Here, FFT-based split Bregman algorithm was incorporated to provide the high computational efficiency. A quantitative evaluation on the synthetic medical data was evaluated and observed that proposed scheme suppresses the noise better than the existing state-of-the-art speckle reduction methods. A cluster based dictionary learning approach has also been combined in wavelet domain such as, Ghadrdan et al. [51] proposed a new scheme based on wavelet transform where denoising was performed using clustering and dictionary learning. They extracted the most suitable features using wavelet and clustering in the CT images to obtain accurate dictionary atoms for the denoising algorithm. Here, a single image noise level estimation was developed to update the cluster by observing higher

PSNRs. In another hybrid approach, Shao et al. [128] proposed a new approach where two or more denoising methods were combined together. They analyzed two methods named: constrained least square filter algorithm and Lucy-Richardson algorithm. In analysis, they concluded that both methods were good and effective for image resolution but not efficient for denoising. Similarly, they perform denoising using Non-local Means filter algorithm and wavelet filter. Here, both approaches work effectively for noise suppression but have less impact to enhance resolution.

Skiadopoulos et al. [133] analyzed a comparative study between multi-scale platelet denoising methods. They applied a Butterworth filter at the stage of pre and postprocessing on image reconstruction. The comparison with and/or without noise was made on cardiac phantom containing two different size cold defects and a pilot-verified clinical dataset of 15 patients with ischemic defects reduction. The authors concluded that denoising by platelet and Butterworth post-processing methods for without noise attenuation conditions outperformed on Butterworth pre-processing for large size defects. In another approach, Vandeghinste et al. [138] proposed an alternative TV minimization based on split-Bregman based algorithm to perform iterative CT reconstruction using shearlet regularization. Shearlet model contained the structure in image using a non-piecewise constant image model which leads to different artifacts than in the case of TV. However, on acquired CT data, the textures are more similar to the reference texture than TV.

1.5 Outline of the Thesis

Chapter 2 consists some background of Wavelet transform, and some necessary concepts which will be used in subsequent chapters.

Chapter 3 presents a technique based on weighted total variation based denoising where split-bergman method is used to denoise the CT images. The results of proposed methodology are also compared with some standard existing schemes. Quantitative and qualitative result evaluations are also discussed in this chapter.

In Chapter 4, two novel and robust approaches have been introduced to reduce the noise in CT images using wiener filtering and wavelet thresholding concept. The results of proposed methodologies are also compared with some similar standard existing schemes. Quantitative and qualitative result evaluations are also discussed in this chapter.

Chapter 5 presents two methodologies for CT image denoising using circular shift based thresholding in wavelet domain. The results of proposed methodologies are also compared with some standard existing schemes. Quantitative and qualitative result evaluations are also given in this chapter.

In Chapter 6, two locally adaptive CT image denoising methods are presented using intra and inter scale dependencies in wavelet domain. The results of proposed methodologies are also compared with some standard existing schemes. Quantitative and qualitative result evaluations are also discussed in this chapter.

In Chapter 7, two CT image denoising methods are developed using extended versions of wavelet transform. The results of proposed methodologies are also compared with some standard existing schemes. Quantitative and qualitative result evaluations are also presented in this chapter.

Finally, the thesis concludes with a critical analysis of the work presented in earlier chapters and the overall concluding observations of this study along with a brief discussion on the scope of future work.

CHAPTER 2

Preliminaries

Chapter 2

Preliminaries

In this chapter, we briefly introduce some background of Wavelet transform and some necessary concepts which will be used in subsequent chapters.

2.1 Introduction to the Wavelet Representation

The Fourier transformation (FT) can be used to determine the frequency content of a signal and it is one of the most important tools in signal analysis. One of its disadvantages is that it only provides a frequency resolution, but no spatial or time resolution. Although all frequencies present in a signal can be identified with the Fourier transformation, no information about the position or time of their presence can be achieved. Consequently, the Fourier transformation is only suitable for global, but not for local signal analysis. One possibility to overcome this problem is to divide the signal into several parts, so called windows or frames, which can then be analyzed separately. This approach leads to the Windowed Fourier Transform (WFT), also referred to as Short-Time Fourier Transform (STFT), which is defined as:

$$STFTfx(t) \equiv STFT(\tau, \omega) = \int f(t)\omega^*(t-\tau)e^{-2\pi i\rho t}dt, \tag{2.1.1}$$

where $\omega^*(t)$ defines the complex conjugate of the window function $\omega(t)$.

The window function $\omega(t)$ is shifted through the signal $f(t)$ and suppresses the signal outside the defined region of interest. This allows the computation of a local spectrum. The problem is that, due to Heisenbergs uncertainty principle, it is not possible to reach a high resolution in time and frequency simultaneously. Due to the limitations of the Fourier Transform (poor time localization) and of the Short-Time Fourier Transform (fixed time and frequency localisation), wavelet transform is introduced.

2.1.1 Wavelet transform

Wavelets are generated from a single real-valued basis function $\Psi(t)$ called mother wavelet by means of scaling and translation:

$$\Psi_{s,\tau} = \frac{1}{\sqrt{s}}\Psi(\frac{t-\tau}{s}), \tag{2.1.2}$$

with $s > 0$.

The scaling factor s is used for expansion and compression of the wavelet. The parameter τ is responsible for the translation. For energy normalization the factor $\frac{1}{\sqrt{s}}$ is needed. The Fourier transformation (Ψ_ρ) of the wavelet $\Psi(t)$ must satisfy the admissibility condition, as given below:

$$C_\Psi = \int_{-\infty}^{+\infty} \frac{|\Psi(\rho)|^2}{|\rho|} < \infty \tag{2.1.3}$$

For $\Psi(0) = 0$, wavelets must have a band-pass like spectrum. Mathematically, the wavelet Ψ is a function of zero average, having the energy concentrated in time:

$$\int_{-\infty}^{+\infty} \Psi(t)dt = 0 \tag{2.1.4}$$

Therefore, it must be oscillatory, which explains the name wavelet.

2.1.2 Continuous Wavelet Transformation

With this definition of wavelets a local signal analysis becomes possible. The continuous wavelet transformation is defined as:

$$WT(s,\tau) = \int_{-\infty}^{+\infty} f(t)\Psi^*_{s,\tau}(t)dt \tag{2.1.5}$$

where $\Psi^*(t)$ is the complex conjugate of $\Psi(t)$. The coefficients $WT(s,\tau)$ specify the similarity of the wavelet $\Psi_{s,\tau}(t)$ to the function around the position τ .

The frequency information is included in the scale s. A low scale s describes a compressed wavelet that can only detect rapidly changing details and, therefore, corresponds to high frequencies; analogously, a high scale corresponds to low frequencies. This is the reason why the wavelet transformation is referred to as a time-scale and not a time-frequency representation. The original continuous function can be reconstructed from its wavelet coefficients by:

$$f(t) = \frac{1}{c_\psi}\int_{-\infty}^{+\infty}\int_{-\infty}^{+\infty} WT(s,\tau)\Psi_{s,\tau}(t)\frac{dsd\tau}{s^2} \tag{2.1.6}$$

The CWT is shift invariant and highly redundant.

2.1.3 Discrete Wavelet Transformation

Because the CWT is very redundant, discrete wavelet transformation (DWT) was introduced. Usually, the discrete wavelet transformation (DWT) is associated with the signal expansion into a (bi-)orthogonal wavelet basis. In contrast to the highly

redundant CWT there is no redundancy included in the DWT representation of a signal. Wavelet transformations, which use this kind of sampling are also called dyadic wavelet transformations where the scales s_x are usually chosen as powers of two and the time sampling is proportional to the scaling, as below:

$$s_x = 2^{-x}; \quad \tau_k = k.s_x = k.2^{-x}, \quad x, k \in Z \tag{2.1.7}$$

The DWT uses the dyadic sampling, which can be expressed as:

$$f(t) = \sum_{x=-\infty}^{+\infty} \sum_{x=-\infty}^{+\infty} d_{x,k} \Psi_{x,k}(t), \tag{2.1.8}$$

where, $\Psi_{x,k}(t) = \frac{1}{\sqrt{|s_x|}} \Psi \frac{t-\tau_k}{s_x} dt; \quad x, k \in Z$. The wavelet coefficients $d_{x,k}$ are given by the inner products of the signal $f(t)$ with the dual basis $\Psi^{\acute{*}}_{x,k}$:

$$d_{x,k} = \int_{-\infty}^{+\infty} f(t) \Psi^{\acute{*}}_{x,k}(t) dt \tag{2.1.9}$$

Multiresolution Analysis

Due to the band-pass-like spectrum of the wavelets, it can be derived that a series of dilated dyadic wavelets shifted through the signal results in a band-pass filter bank. With the constraint of $f(t)$ being band limited, its whole spectrum might be covered by infinitely many scaled versions of the wavelet. Mallat [90] introduced the so-called scaling function $\phi_{x,k}(t)$, which covers the lowpass parts covered by infinitely many dilated wavelets up to a given x. The signal $f(t)$ can then be split into a low frequency approximation part c and its high frequency details d according to:

$$f(t) = \sum_k c_{x,k} \phi_{x,k}(t) = \sum_k c_{x-1,k} \phi_{x-1,k}(t) + \sum_k d_{x-1,k} \Psi_{x-1,k}(t) \tag{2.1.10}$$

On the basis of the two-scale relation

$$\phi(t) = \sqrt{2} \sum_k g_k \phi_{2t-k}(t) \tag{2.1.11}$$

and analogous for the wavelets

$$\Psi(t) = \sqrt{2} \sum_k h_k \phi_{2t-k}(t) \tag{2.1.12}$$

which states that a scaling or wavelet function at a given scale can be expressed in terms of translated scaling functions at the next smaller scale. It can be derived that the coefficients $c_{x,k}$ and $d_{x,k}$ can be computed by filtering with the analysis high-pass h and low-pass g filter followed by downsampling, according to:

$$c_{x,k} = \int f(t)\phi_{x,k}(t)dt \tag{2.1.13}$$

and

$$d_{x,k} = \int f(t)\Psi_{x,k}(t)dt \tag{2.1.14}$$

Hence, forward 1D-DWT coefficients for sequence ($n = 0 \ \ to \ \ M-1$) can be obtained as:

$$W_\phi(x_0, k) = \frac{1}{\sqrt{M}} \sum_n f(n)\phi_{x_0,k}(n), \tag{2.1.15}$$

$$W_\Psi(x, k) = \frac{1}{\sqrt{M}} \sum_n f(n)\Psi_{x,k}(n), \qquad for\ x \geq x_0 \tag{2.1.16}$$

To obtain inverse 1D-DWT, it can be processed as:

$$f(n) = \frac{1}{\sqrt{M}} \sum_k W_\phi(x_0, k)\phi_{x_0,k}(n) + \frac{1}{\sqrt{M}} \sum_{x=x_0}^{\infty} \sum_k W_\Psi(x, k)\Psi_{x,k}(n) \tag{2.1.17}$$

DWT is largely used for one-dimensional discrete signals. If we want apply the discrete wavelet transform to two-dimensional signals (images, for instance), we need to use the DWTs extension to two dimensions, namely the 2D DWT.

2.2 Wavelet based image reconstruction

When dealing with images, the two-dimensional wavelet transformation is required. The one-dimensional transformation can be applied to the rows and columns of an image X successively, which is referred to as separable transformation.

2D-DWT of image $X(i,j)$ of size $M \times N$ is defined as [54]

$$W_{\varphi}(x_0,m,n) = \frac{1}{\sqrt{MN}} \sum_{i=0}^{M-1} \sum_{j=0}^{N-1} X(i,j)\phi_{x_0,m,n}(i,j) \tag{2.2.18}$$

$$W_{\psi}^{i}(x,m,n) = \frac{1}{\sqrt{MN}} \sum_{i=0}^{M-1} \sum_{j=0}^{N-1} X(i,j)\psi_{x,m,n}^{i}(i,j) \tag{2.2.19}$$

where $W_{\varphi}(x_0,m,n)$ defines approximation part of image $X(i,j)$ and $W_{\psi}^{i}(x,m,n)$ defines horizontal, vertical and diagonal parts.

For the given equation (2.2.18) and (2.2.19), inverse 2D-DWT is defined as

$$X(i,j) = \frac{1}{\sqrt{MN}} \sum_{m} \sum_{n} W_{\varphi}(x_0,m,n)\phi_{x_0,m,n}(i,j) + \frac{1}{\sqrt{MN}} \sum_{i=H,V,D} \sum_{x=x_0}^{\infty} \sum_{m} \sum_{n} W_{\psi}^{i}(x,m,n)\psi_{x,m,n}^{i}(i,j) \tag{2.2.20}$$

For obtaining 2-D wavelet decomposition, 1-D DWT can be applied on image first in horizontal and then in vertical direction using different filters. 2-D DWT decomposes the image into two parts: the lowpass approximation image LL, and

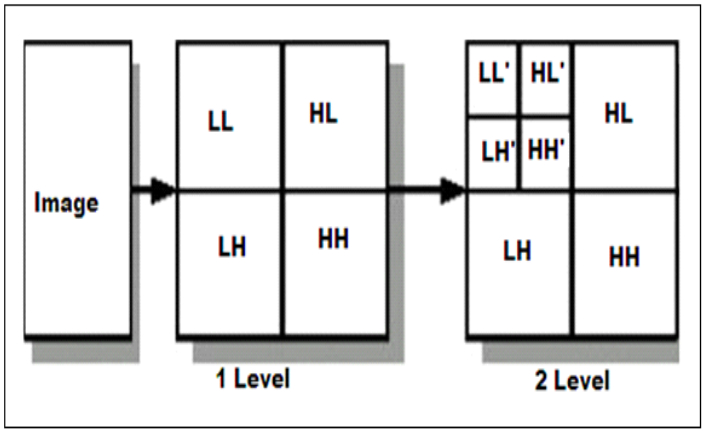

Figure 2.1: Description of two decomposition levels of a 2-D-DWT.

three detail images LH, HL and HH which include high frequency structures in the horizontal (H), vertical (V) and diagonal (D) directions. Figure 2.1 a schematic description of the separable two-dimensional DWT is presented. Like the 1-D case, the 2-D multiresolution wavelet decomposition can be computed iteratively from the approximation coefficients of the previous decomposition level. An example of a 2-D-DWT performed on a CT-image is shown in Figure 2.2. The separable DWT can easily be extended to also work for more than two dimensions.

The performance of Wavelet transform based denoising affects on the basis of Wavelet families such as Haar, DB2 and many more. The wavelet functions [12] of the Haar, Db2 and CDF9/7 are shown in figure 2.3. The Haar wavelet was already introduced in 1909 by Alfred Haar, who was interested in the construction of basis functions for the $L^2(R)$. As illustrated in figure 2.3(a), the Haar wavelet is discontinuous and resembles a step function. This orthogonal and symmetric wavelet is the simplest member of wavelet families. Daubechies wavelets were the first wavelets after

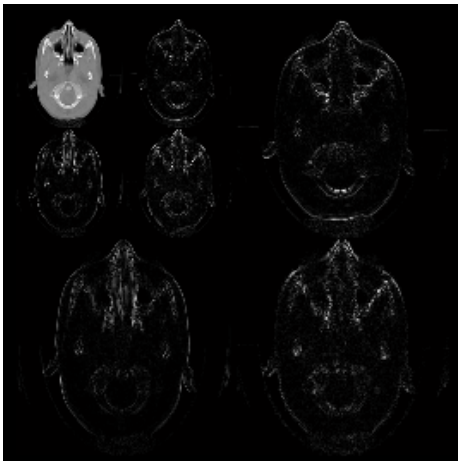

Figure 2.2: Two levels of a 2D-DWT applied to a CT image.

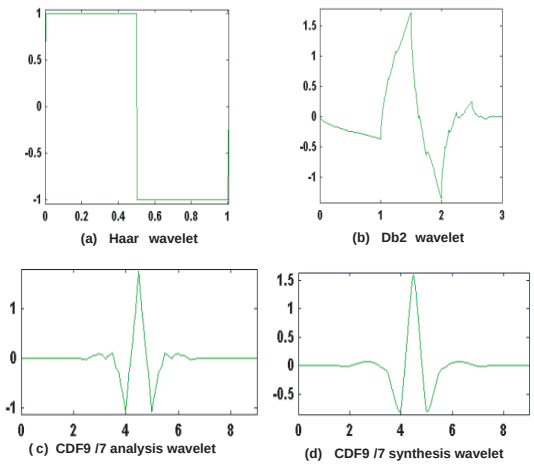

Figure 2.3: Wavelet functions [12] of Haar, Db2 and CDF9/7, which are used for noise suppression.

the Haar wavelet that were found to build an orthonormal basis in $L^2(R)$. Daubechies wavelets are compactly supported and regular. The maximum number of vanishing moments of the wavelet function N is indicated by its name DbN. In figure 2.3(b) the wavelet function $Db2$ is visualized which indicates Daubechies wavelets are not necessarily symmetric. A biorthogonal wavelet is a wavelet where the associated wavelet transform is invertible but not necessarily orthogonal. In the biorthogonal case, there are two scaling functions, which may generate different multiresolution analysis, and accordingly two different wavelet functions. So the numbers of coefficients in the scaling sequences may differ and must satisfy the property of biorthogonality conditions. Cohen-Daubechies-Feauveau (CDF) wavelet are the first family of biorthogonal wavelets. CDF 9/7 wavelet are widely used for noise suppression and image compression. The CDF 9/7 wavelet for analysis and synthesis are displayed in figures 2.3(c) and 2.3(d).

The extended versions of Wavelet transforms also affects the performance on Wavelet based denoising. Some major extended versions of Wavelet transforms which are used in the subsequent chapters, are briefly described.

2.2.1 Tetrolet Transform

The idea of tetrolet transform came from a famous computer game Tetris, where five geometric patterns (as shown in figure 2.4(a)) are used with rotation and reflection properties [76]. These geometric patterns are known as tetrominoes.

Tetrolet transform is a powerful tool for signal and image processing tasks because

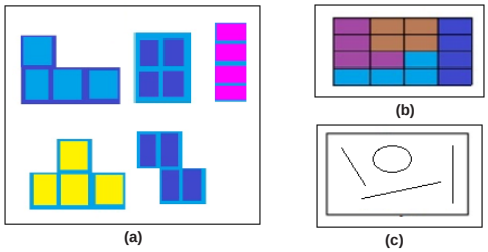

Figure 2.4: Tetromeno patterns with example. (a) five tetromeno patterns. (b) one of the disjoint covering from 117 kind of tilings. (c) corresponding local structure of (b).

of local enhancement through tetrominoes, multi-resolution analysis, sub-banding and localization in both frequency and time domain. All the tetrominoes are connected with a four equal sized squares. In tetrolet transform, an image $X[i,j]_{i,j=1}^{N}$ with $N = 2^P, P \in N$ is divided into 4x4 blocks. Each block is covered with any four free tetrominoes, which is responsible for enhancing the local structure using properties of rotations and reflections. These four tetrominoes (X_o, X_1, X_2, X_3) are mapped in a unique order (0, 1, 2, 3) by applying bijective mapping (L) with their corresponding order. For each tetromino subset (X_v), the discrete basis functions [76] are defined as follows:

$$\phi_{X_v}[i,j] := \begin{cases} 1/2 & ; \quad (i,j) \in X_v \\ 0 & ; \quad otherwise \end{cases}$$

$$\psi^l{}_{X_v}[i,j] := \begin{cases} \in [l,\ L(i,j)] & ; \quad (i,j) \in X_v \\ 0 & ; \quad otherwise \end{cases}$$

for l=1,2,3, $\psi^l{}_{X_v}$ represents tetrolets and ϕ_{X_v} is scaling function. Haar wavelet transform matrix W has four fixed 2x2 squares with 117 solution for disjoint covering of a 4x4 board.

$$W = (\in[m,n])_{m,n=0}^{3} = \frac{1}{2}\begin{pmatrix} 1 & 1 & 1 & 1 \\ 1 & 1 & -1 & -1 \\ 1 & -1 & 1 & -1 \\ 1 & -1 & -1 & 1 \end{pmatrix}$$

There are 117 kinds of tilings for covering of a 4x4 block with any four tetrominoes. Figure 2.4(b) represents one of the covering from 117 kinds of tilings and figure 2.4(c) represents its local structure.

2.2.2 Dual-tree complex wavelet transform

Discrete Wavelet Transform (DWT) has several limitations, some majors are: aliasing, shift sensitivity and poor directional selectivity. Due to large changes in wavelet coefficients and downsampling, aliasing may occurs in DWT. The inverse DWT removes this aliasing only if the wavelet and scaling coefficients are unchanged. Because of shift sensitivity, the small shifts in input signals can cause an unpredictable change in the distribution of energy between DWT coefficients at different scales. DWT cannot distinguish between $+45^{\circ}$ and -45° spectral features because of poor directional selectivity. These limitations of DWT can be resolved using complex wavelet transforms (CWT). CWT use analytic filter that decomposes the complex signals into real and imaginary parts in the transform domain. The real and imaginary coefficients are used to compute the amplitude and phase information. To overcome from the limitations of DWT, Kingsbury [73] proposed the dual-tree complex wavelet transform, which allows perfect reconstruction with the advantages of complex wavelets.

The dual-tree complex wavelet transform is enhanced version of DWT, with important additional properties: shift invariance and good directionality. In DT-CWT, two critically-sampled DWTs are used over the same data and the filters are designed in such a way that the sub bands of upper DWT are interpreted as real part of complex wavelet transform and the lower tree as imaginary part. 2D DT-CWT decomposes an image into two complex-valued low-frequency subbands and six complex-valued high frequency subbands at each level of decomposition. The high frequency subband images are highly oriented at six different directions which are $+75°$, $+45°$, $+15°$, $-15°$, $-45°$ and $-75°$. These directional wavelets of DT-CWT are obtained by taking sum and difference of highpass subbands which have the same pass bands.

2.2.3 Curvelet Transform

Curvelet transform is a multi-scale transform followed by ridglet transform which provides several features such as multi-directional and multi-resolution [48]. The point discontinuity through Fourier transform is not well preserved. This problem was recovered by wavelet transform. But wavelet transform was failed to handles the curve discontinuity. To handle that, Curvelet transform performs well using small number of curvelet coefficients. The curvelet transform is based on the combination of ridgelet and wavelet transform. Here wavelet transform is helpful for spatial partitioning where each scale of wavelet transform is divided into number of blocks. Further these blocks are processed using ridgelet transform to obtain the curvelet coefficients [93].

Therefore, curvelet transform is considered as a localized ridglet transform which gives more sharp edges such as curves. To gain the fine scalability, it also follows the properties of scalable rule.

Discrete curvelet transform have four major steps which can be defined over the function $f(x_1, x_2)$ as below:

a) Subband decomposition: Here, an image f is decomposed into subbands using $\grave{a}$ trous method [93] as given below,

$$f \mapsto (P_0 f, \triangle_1 f, \triangle_2 f, ...) \tag{2.2.21}$$

where $P_0 f$ is a low pass filter bank and $\triangle_1, \triangle_2....$ are the High pass (bandpass) filters.

b) Smooth Partitioning: To gain smooth partitioning, each sub-band is smoothly windowed into a set of dyadic squares.

$$h_Q = (w_Q . \triangle_S f) \tag{2.2.22}$$

where, w_Q is collection of smooth windowing function to localized near dyadic squares Q_S, $Q \in Q_S$ and $S \geq 0$.

c) Re-normalization: Here, re-normalization is performed over the each dyadic square to the unit scale of [0,1]x[0,1] using the following function

$$g_Q = (T_Q^{-1} . h_Q) \tag{2.2.23}$$

where, $(T_Q f)(x_1, x_2) = 2^S f(2^S x_1 - k_1, 2^S x_2 - k_2)$ is the renormalizing operator.

d) Ridgelet analysis: For each $a > 0$, $b \in \Re$ and $\theta \in [0, 2\pi])$ in a given function

$f(x_1, x_2)$, discrete ridgelet coefficients can be obtained as:

$$\Re_f(a, b, \theta) = \int f(x_1, x_2)\Psi_{a,b,\theta}(x_1, x_2)dx_1dx_2 \tag{2.2.24}$$

where, a is a scale parameter, b is a location parameter, θ is the orientation parameter, and Ψ is the wavelet function as, $\Psi_{a,b,\theta}(x) = a^{1/2}\Psi(\frac{x_1\cos\theta+x_2\sin\theta-b}{a})$. Discrete ridgelet transform is obtained through radon transform, can be analyzed as:

$$\Re_f(a, b, \theta) = \int g(t, \theta)a^{1/2}\Psi(\frac{t-b}{a})dt \tag{2.2.25}$$

where, function g represents the Radon transform over the variable t, which can be expressed as below,

$$g(t, \theta) = \int f(x_1, x_2)\delta(x_1\cos\theta + x_2\sin\theta - t)dx_1dx_2 \tag{2.2.26}$$

where, δ is Dirac distribution.

2D fast discrete curvelet transform (2D FDCT) is the version of curvelet transform which can be developed via wrapping methods. 2D FDCT with wrapping method is implemented on the basis of parabolic scaling function, anisotropic concept, tight framing and wrapping.

2.2.4 Nonsubsampled Contourlet Transform

The contourlet transform helps to provide multi-scale decomposition and directional decomposition using laplacian pyramid and direction filter bank. Enhance version of contourlet transform is nonsubsampled contourlet transform (NSCT) which helps to improve the frequency aliasing problem of contourlet transform. NSCT is based on the

contourlet conception which helps to avoid the sampling steps during decomposition and reconstruction stages. The structure of NSCT contains two filter banks: non-subsampled pyramid and non-subsampled directional filter banks. The combination of both filter banks help to provide the features of shift-invariance, multi-resolution and multi-dimensionality for image presentation. The design and reconstruction of NSCT filters (analysis and synthesis)are easy to be realized because it helps to provide better collection of frequency and regularity [31].

After a brief description of wavelet transformations, a short overview of some of the most important methods are described below for the use in CT image denoising, which are used within this thesis.

2.2.5 Image denoising using Wavelet transform

Wavelets transform have been widely used in scientific and engineering fields, traditional wavelets perform well for representing point singularity. The most investigated domain in denoising using Wavelet Transform is the non-linear coefficient thresholding based methods [90]. Thresholding methods have been introduced, which erase insignificant coefficients, but preserve those with larger values. Various thresholding techniques [125] are used for noise reduction. In transform-domain denoising techniques, the input data is decomposed into its scale-space representation and have a property of energy compaction. It is observed form multi resolution based denoising techniques that (i) the noise and clean signal behave differently. (ii) Noise is detected on geometrical components and sharp transitions of images. (iii) Most of the noise

can be de detected from low resolution images.

The noise contains very less value which is embedded with clean pixel value to make a pixel noisy. Thresholding is one of the strategies to clean the pixels in an image. In wavelet based thresholding, small wavelet coefficients are removed in high frequency bands and large wavelet coefficients are preserved. The strategy of calculating value to differentiate between small and large wavelet coefficients are known as threshold estimation.

Threshold estimation:

For CT image denoising, selection of a threshold value is a cumbersome task for edge preservation and noise suppression. By selecting small threshold value, the resultant image may left noisy while large threshold value may produce blurring on the edges of resultant image. To deal with this situation, an appropriate algorithm is to be selected to estimate a threshold value. Three threshold estimation criteria, called VisuShrink, SureShrink and BayesShrink, are described as follows.

VISUShrink proposed by Donoho and Johnstone [39] is a non-adaptive universal threshold, which depends only on the number of pixels in the image (X), defined as:

$$\lambda_{VISU} = \sigma_\eta \sqrt{2LogX} \tag{2.2.27}$$

The same threshold is applied to all levels of decomposition. Although the resulting estimate is very smooth and has a pleasant visual appearance, it is known that VisuShrink tends to oversmooth the signal.

SureShrink is a thresholding scheme that applies a subband adaptive threshold [88]. A separate threshold is computed for each subband based on Steins unbiased risk estimator (SURE), expressed as:

$$\lambda_{SURE} = arg \min_{t \geq 0} SURE(t, Y_S) \tag{2.2.28}$$

which minimizes the risk

$$SURE(t, X_S) = N_S - 2[1 : N_S] + \sum_{i,j=1}^{N_S} [min(|X_{i,j}|, t)]^2$$

where X_S is the wavelet coefficients from subband S and N_S is the number of coefficients in $X_{i,j}$.

BayesShrink [65] uses a Bayesian mathematical framework and assumes generalized Gaussian distribution for the wavelet coefficients in each detail subband to find the threshold that minimizes the Bayesian risk, the threshold value can be expressed as,

$$\lambda = \frac{\sigma_\eta^2}{\sigma_Y} \tag{2.2.29}$$

For the images, the noise variance (σ_η^2) can be estimated from the highest frequency coefficients. A robust estimate of noise variance uses the median absolute value of the wavelet coefficients [65], which is insensitive to isolated outliers of potentially high amplitudes. Generaly this method is known as robust median estimator, defined as:

$$\sigma_\eta^2 = \Big[\frac{median(|X(i,j)|)}{0.6745}\Big]^2 \tag{2.2.30}$$

and variance σ_Y^2 of noiseless image can be extracted as,

$$\sigma_Y^2 = max(\sigma_X^2 - \sigma_\eta^2, 0) \tag{2.2.31}$$

where $\sigma_X^2 = \frac{1}{w}\sum_{i=1}^{w} X_i^2$ and w is the number of wavelet coefficients in respective sub-bands.

Thresholding:

After estimating a threshold value, the process of thresholding is applied by selecting an appropriate algorithm. The shrinkage rule defines how the threshold must be applied. In its basic form, each coefficient in the wavelet transform domain is compared against a threshold. If the coefficient is smaller than the threshold, it is assigned zero; otherwise, it is kept or modified. The motivation is that large coefficients are due to important signal features, while small coefficients can be thresholded without affecting the significant features of the image. Hard thresholding and soft thresholding methods are very popular for thresholding.

Hard thresholding and soft thresholding methods are very popular for thresholding. In hard threshold, each coefficient value is compared with threshold value and less than value is replaced by zero.

$$T_{hard} = \begin{cases} X, & \mid X \mid > \lambda \\ 0, & Otherwise \end{cases} \tag{2.2.32}$$

A disadvantage of the hard thresholding is its abrupt discontinuity, which may cause artifacts in the reconstructed image. On the other hand, the soft thresholding tends to oversmooth the reconstructed image. In Soft threshold, replaced by zero process is same as in hard threshold, additionally rest of coefficients are modified by

subtracting threshold values. Soft thresholding method can be defined as,

$$T_{soft} = \begin{cases} sign(X)(|X| - \lambda), & | X | > \lambda \\ 0, & Otherwise \end{cases} \tag{2.2.33}$$

In comparison of both, Soft thresholding gives better performance for visual appearance of images. But soft thresholding has a limitation with large coefficient values. To overcome those limitations, an optimal linear interpolation (OLI) shrink algorithm [44] is used for thresholding.

An optimal linear interpolation shrink algorithm can be expressed as:

$$T_{(OLI)_s} = \begin{cases} 0; & | X(i,j)_s | \leq \lambda_s \\ X(i,j)_s - \alpha(i,j)_s; & | X(i,j)_s | > \lambda_s \end{cases} \tag{2.2.34}$$

$\alpha(i,j)_s$ can be estimated as:

$$\alpha(i,j)_s = \frac{\sigma^2_{\eta_{(X)_s}}}{\sigma^2_{(X)_s}}(X(i,j)_s - \mu_s) \tag{2.2.35}$$

where, μ_s is the mean value of the respective subband (s).

To avoid the drawbacks of both hard and soft thresholding rules, firm thresholding function [50] was also introduced, which provides less sensitivity to small perturbations in the data and reduces overall mean-squared error which is given by,

$$T_{firm} = \begin{cases} X, & if \mid X \mid > \lambda_2 \\ sign(X)\frac{\lambda_2(|X|-\lambda_1)}{\lambda_2-\lambda_1}, & if \lambda_1 < \mid X \mid \leq \lambda_2 \\ 0, & Otherwise \end{cases} \tag{2.2.36}$$

After performing, image denoising over the CT images, the quality of image denoising performance was measured using some standard performance metrics. Some performance metrics are discussed below, which are used in this thesis.

2.3 Measures of Image Denoising Performance

All experiments in this thesis work are evaluated in MATLAB 7.12 on Pentium Dual Core 2 GHz. To perform implementation, the CT scanned test images are obtained from public access database (https://eddie.via.cornell.edu/cgibin/datac/logon.cgi). In CT image data set, first CT image is denoted as CT1. Similarly, second, third, fourth, fifth and sixth CT images are denoted as CT2, CT3, CT4, CT5 and CT6, respectively. All image denoising schemes in this thesis are applied on several test CT images (size 512x512) corrupted by simulated additive Gaussian noise at four different noise level $\sigma \in [10, 20, 30, 40]$.

The quality of denoised CT image can be analyzed by visual analysis and also by evaluating performance metrics. To measure the visual analysis, there is no mathematical or specific method available. Therefore, we have to evaluate the results with naked eye to determine best filtered image. For better visual inspection, we follow four criteria: (i) visibility of the artifacts; (ii) preservation of edge details; (iii) visibility of low contrast objects, and (iv) preservation of the texture.

To evaluate the performance metrics of CT image denoising, some standard methods are used, which are explained below: To measure the accuracy of proposed algorithm, some standard performance metrics are used, such as: Peak Signal-to-noise Ratio (PSNR), Structural Similarity [146] (SSIM), Image Quality Index (IQI), Entropy Difference (ED) and Difference in Variance (DIV).

Peak Signal-to-noise Ratio (PSNR) is an important factor to evaluate denoising

performance. The high PSNR value represents more similarity between the denoising and original image than lower PSNR values. For clean image (X) and denoised image (R), the PSNR is expressed as:

$$PSNR = 10 \times log_{10}\left(\frac{255\times255}{MSE} \right) \tag{2.3.37}$$

where, Mean Square Error (MSE) is defined as- $MSE = \frac{1}{mn}\sum_{i=0}^{m-1}\sum_{j=0}^{n-1}[X(i,j) - R(i,j)]^2$.
SSIM between two images X and R is defined as

$$SSIM(X,R) = \frac{(2\mu_X\mu_R + C_1)(2\sigma_{XR} + C_2)}{(\mu_X^2 + \mu_R^2 + C_1)(\sigma_X^2 + \sigma_R^2 + C_2)} \tag{2.3.38}$$

where, μ_X, μ_R, σ_X^2, σ_R^2 are the averages and variances of X and R respectively, σ_{XR} is the covariance between X and R, C_1 and C_2 are predefined constants. SSIM provides the accuracy on the basis of structural information. The outcome of SSIM lies between -1 to 1, the value closer to 1 values shows better results.
For input image (X) and denoised image (R), the Image Quality Index (IQI) can be defined as:

$$IQI = \frac{4\sigma_{XR}\bar{X}\bar{R}}{(\sigma_X^2 + \sigma_R^2)[(\bar{X})^2 + (\bar{R})^2)]} \tag{2.3.39}$$

where, $\bar{X} = \frac{1}{N}\sum_{i=1}^{N}X_i$, $\bar{R} = \frac{1}{N}\sum_{i=1}^{N}R_i$, $\sigma_X^2 = \frac{1}{N-1}\sum_{i=1}^{N}(X_i - \bar{X})^2$, $\sigma_R^2 = \frac{1}{N-1}\sum_{i=1}^{N}(R_i - \bar{R})^2$ and $\sigma_{XR} = \frac{1}{N-1}\sum_{i=1}^{N}(X_i - \bar{X})(R_i - \bar{R})$.
The image quality index range lies between 1 to -1. The best value 1 represents an identical values of input image pixels and denoised image pixels.

Entropy is a statistical measure of randomness that can be used to characterize the texture of the input images. Between clean image (X) and denoised image (R),

patch wise Shannon entropy is estimated. The difference of mean value represents as Entropy Difference (ED). Entropy Difference (ED) is calculated as follows:

$$ED = SE(X) - SE(R) \tag{2.3.40}$$

Where, SE represents Shannon entropy. Shannon entropy (SE) is calculated as follows, ([114]):

$$SE = -\sum_i X_i^2 log(X_i^2) \tag{2.3.41}$$

The performance of image denoising can also be measured by estimating DIV, defined as follows:

$$DIV = 1 - \frac{Var(R)}{Var(X)} \tag{2.3.42}$$

where, $Var(R)$ is the variance of denoised image and $Var(X)$ is the variance of clean image. The values closer to 0 indicate better results of ED and DIV.

CHAPTER 3

CT image denoising using Total Variation

Chapter 3

CT image denoising using Total Variation

In this chapter, we present a method based on the Total Variation (TV) to improve the quality of noisy CT images. Here, a new exponentially directional weighted function (EDWF) has been introduced based on the difference of L_1 and L_2 norms. Furthermore, a numerical algorithm has been discussed to solve the minimization problem of EDWF using iterative Split Bregman method.

3.1 Introduction

This chapter is concerned with the suppression of noise from the CT images using the concept of Total Variation method. Recently, various methods have been studied to remove the Gaussian noise by least square fidelity minimization [153, 154, 155, 156]. In least square fidelity minimization, the authors [153] enhanced the TV formulation with the concept of soft shrinkage for image denoising. Further, this work was extended using a power-iterative strategy to provide the smoothness using the discontinuity of the global minimizer concept [154]. Similarly, a weighted TV (WTV) method [156] was also used to denoise the images by estimating the weight value over

the TV regularization function. Some other TV methods [3, 6, 53, 79, 134, 153] are also popular due to enhancing the weight values for image denoising.

The main concept of image denoising is to suppress the noise and preserve the edges from the noisy images. Unfortunately, these methods [3, 6, 53, 79, 134, 153] have not preserved well structures while suppression of noise over the noisy images. Therefore, to suppress the noise with better edge preservation, we presented a method for CT image denoising using total variation method, where an exponentially directional weight function is introduced using $L_2 - L_1$, directional derivatives and exponential function. Two advantages of $L_2 - L_1$ over other nonconvex measures are its Lipschitz regularity, and guarantee of convergence, which is analogous to a convex splitting technique for gradient systems. The directional derivatives and exponential function help to provide better edge preservation and more smoothness over the noisy pixels, respectively. The main contribution of this chapter is to develop an exponentially directional weighted function using the difference between anisotropic and isotropic functions for CT image denoising. Further, Split Bregman method is used to solve the minimization problem of the exponentially directional weighted function.

The organization of this chapter is as follows: Section 3.2 describes a brief introduction on total variation. In section 3.3, the proposed exponentially directional weighted total variation model and its numerical algorithm based on Split Bregman algorithm is described in detail. The Experimental results and comparisons are discussed in section 3.4. Finally, the conclusions are drawn in section 3.5.

3.2 Background of Total Variation

Total variation is one of the popular models to develop the optimization algorithms for solving sparse representation problem which was originally developed for image denoising by Rudin, Osher, and Fatemi (R.O.F.) [121]. A general model for such problem is:

$$R = \min_{Y} TV(Y) + \frac{\mu}{2}\|Y - X\|^2 \tag{3.2.1}$$

where, $TV(Y)$ is the regularization term as a total variation (TV), μ is a positive parameter to control $TV(Y)$, $\|Y - X\|^2$ is the fidelity term, and $||.||$ represents L_2 norm. R is the optimal solution or the reconstructed result. This is a simple and convex optimization model. To solve the optimization problem, firstly, the Gradient projection method [121] has been used to accelerate the convergence using fixed point or variable splitting algorithms. Further, more efficient techniques were also developed such as Newton's method [142], dual formulation based TV denoising method [25][53]. Generally, TV model follows a pair of directions: horizontal and vertical directions. Many authors [66, 6] gave the privilege to the edges along the directions for image denoising, while few authors [6] used the trigonometric functions to reweight the horizontal and vertical directions to smooth the noisy regions of the images. In fidelity term, L_2 norm is the most common norm which was used to reduce the Gaussian noise and it works well in image denoising [107, 156, 79]. However, if some of the pixels are degraded by non-Gaussian type noise, then those pixels are not properly denoised with these methods. Few authors [34] have also used fidelity term with L_1 norm for

non-Gaussian type of noisy images.

TV model is widely used in image processing for various applications such as image deblurring [27], denoising [3], etc. The formulation of TV model can be categorized as: isotropic and anisotropic TV, which are used as a regularization term for sparse representation problems. The total variation (TV) can be defined as the sum of L_1 or L_2 norm of the gradients for all the pixels.

An anisotropic TV model is denoted by $TV^{(A)}$, and can be expressed as:

$$TV^{(A)}(Y) = \sum_{ij}(|\nabla_x Y(i,j)|) + (|\nabla_y Y(i,j)|) \tag{3.2.2}$$

where, $|.|$ represents L_1 norm.

An isotropic TV model is denoted by $TV^{(I)}$, and can be expressed as:

$$TV^{(I)}(Y) = \sum_{ij}\sqrt{(\nabla_x Y(i,j))^2 + (\nabla_y Y(i,j))^2} \tag{3.2.3}$$

where, $\nabla_x Y$ and $\nabla_y Y$ are the horizontal and vertical gradients, respectively.

3.3 Proposed Methodology

Here, with the assumption that the CT images are corrupted by Gaussian noise with zero mean and different variances, the scheme is presented using total variation model. However, TV method has been proven to be quite efficient for suppression of Gaussian noise in images. But it has a tendency to remove certain image details and texture along with the noise. The requirement for the presented scheme is that the regularization function should be an increasing function with respect to the smoothness of

the image. At the same time, considering numerical algorithm of the minimization, it is highly expected that the regularization function should be in its simplest form. Therefore, an exponentially directional weighted function (EDWF) has been introduced using anisotropic and isotropic total variations, which is discussed below in the first subsection. Further, a numerical algorithm is designed to solve the minimization problem of EDWF using Split Bregman method [53] for CT image denoising, discussed in second subsection.

3.3.1 Exponentially Directional Weighted Function (EDWF)

The basic idea of re-weighting of the total variation function is to enhance the sparsity which was originally introduced in [22]. Here, a new exponentially directional weighted function (EDWF) for anisotropic and isotropic TV is introduced.

The directional derivatives ($\nabla_S Y$) are computed as:

$$\nabla_S Y(i,j) = \begin{cases} \nabla_a Y(i,j) = Y(i,j) - Y(i-1,j) \\ \nabla_b Y(i,j) = Y(i,j) - Y(i+1,j) \\ \nabla_c Y(i,j) = Y(i,j) - Y(i-2,j) \\ \nabla_d Y(i,j) = Y(i,j) - Y(i+2,j) \\ \nabla_e Y(i,j) = Y(i,j) - Y(i,j-1) \\ \nabla_f Y(i,j) = Y(i,j) - Y(i,j+1) \\ \nabla_g Y(i,j) = Y(i,j) - Y(i,j-2) \\ \nabla_h Y(i,j) = Y(i,j) - Y(i,j+2) \end{cases} \tag{3.3.4}$$

where $S \in \{a, b, c, d, e, f, g, h\}$.

The mean of the absolute derivatives is calculated as:

$$E(i,j) = \frac{\sum\limits_{i,j} |\nabla_S Y(i,j)|}{K} \tag{3.3.5}$$

where, K is the total number of directional derivatives.

These directional derivatives are responsible to preserve the structures in images such as edges. By using these directional derivatives over the noisy pixels, an exponentially directional weighted function (EDWF) is introduced to suppress the noise from CT images.

The exponentially directional weighted functions (EDWF) are defined, as:

$$\alpha = e^{(-|(|E(i,j)|-\gamma\|E(i+1,j)\|)|)}, \quad \beta = e^{(-|(|E(i,j)|-\gamma\|E(i,j+1)\|)|)} \tag{3.3.6}$$

where, γ is a diagonal dominant weight factor which is used as a control parameter. It can be estimated by obtaining the similarity between horizontal and vertical directions [14], and can be expressed as:

$$\gamma = \frac{2.E(i+1,j).E(i,j+1)}{E^2(i+1,j)+E^2(i,j+1)} \tag{3.3.7}$$

The values of weights (α and β) and diagonal dominant weight factor (γ) are normalized between 0 to 1. According to similarity factor, the weight values (α and β) are attenuated differently. When average value of γ is close to 0, weight values (α and β) behave like $e^{-(|L_1|)}$. If it is close to 1, weight values (α and β) behave like $e^{-(|L_1-L_2|)}$.

In the proposed method, the original oscillation measure ∇Y is modified using exponential weighted function. The motivation of using exponential functional is that, the exponential energy curve emphasizes more on the noisy pixels, because as the value of L_2-L_1 increases, the exponential curve increases faster than the L_2-L_1.

As more energy is penalized, more smoothness of noisy pixels is increased. In addition, when the value of $L_2 - L_1$ is zero, the slope value of the energy curve may become zero or near to zero due to more pixels with the same intensity value. This means as the energy decreases, the difference between pixels becomes smaller, which leads to the blocking effect. Whereas, the exponential function with $L_2 - L_1 = 0$ assures that the pixels can still exchange intensities even when their intensity values are very close to each other which reduces blocking effect up-to a certain degree.

Let, the total variation (TV) be defined with EDWF in horizontal and vertical gradients by $\nabla_x Y$ and $\nabla_y Y$, respectively. An anisotropic TV denoted by $TV^{(A)}_{EDWF}$ can be expressed as:

$$TV^{(A)}_{EDWF}(Y^l) = \sum_{ij} \alpha(i,j)(|\nabla_x Y^l(i,j)|) + \beta(i,j)(|\nabla_y Y^l(i,j)|) \tag{3.3.8}$$

and, isotropic TV denoted by $TV^{(I)}_{EDWF}$ can be expressed as:

$$TV^{(I)}_{EDWF}(Y^l) = \sum_{ij} \sqrt{\alpha(i,j)(\nabla_x Y^l(i,j))^2 + \beta(i,j)(\nabla_y Y^l(i,j))^2} \tag{3.3.9}$$

Where, $\alpha(i,j) > 0$ and $\beta(i,j) > 0$ are the weights which effectively allow to convert the nonconvex total variation into the convex total variation. The major role of exponentially directional weighted function (EDWF) is to keep TV_{EDWF} to convex as long as possible. l is the number of iterations to estimate the re-weighted values for the TV_{EDWF} minimization. Following is the proposed iterative reweighted algorithm to solve the TV minimization problem.

Algorithm 3.1: Iterative reweighted TV minimization

1: Initialize the parameters: μ, l, and set $\alpha(i,j) = \beta(i,j) = 1$.
2: Compute directional derivatives $\nabla_S Y$.
3: For l number of iteration, solve the TV_{EDWF} regularized problem as,
$\min_Y TV_{EDWF}(Y) + \frac{\mu}{2}\|Y - X\|^2$
and update values of $\nabla_S Y$, $\alpha(i,j)$ and $\beta(i,j)$.
4. Repeat step 3 for next iteration.
5. Terminate; When l iterations are completed.

In algorithm 3.1, Step 3 has to solve the minimization problem. To solve the minimization problem for both anisotropic and isotropic TV, Split Bregman iteration method is used which is discussed in the following subsection.

3.3.2 Split Bregman Iteration Method

The Split Bregman method has several good properties such as it can converge very quickly when applied to the L_1 regularization problem and avoid the problem of numerical instabilities [53].

Anisotropic TV denoising

We begin with anisotropic total variation to solve the minimization problem of algorithm 3.1 for CT image denoising, as follows:

$$\min_Y |\nabla_x^{EDWF} Y| + |\nabla_y^{EDWF} Y| + \frac{\mu}{2}\|Y - X\|^2 \tag{3.3.10}$$

where, $\nabla_x^{EDWF} Y = \alpha(i,j)(Y(i,j) - Y(i+1,j))$ and $\nabla_y^{EDWF} Y = \beta(i,j)(Y(i,j) - Y(i,j+1))$.

Here in the equation (3.3.10), first and second terms are the total variation regularizer, third is the fidelity norm and $\mu > 0$ is the weighted function to control the regularizer and fidelity terms. Bregman Splitting method can be applied to solve the above minimization problem. First, $\nabla_x^{EDWF}Y$ and $\nabla_y^{EDWF}Y$ are replaced by d_x and d_y, respectively. This yields the constrained problem as:

$$\begin{aligned} \min_Y |d_x| + |d_y| + \frac{\mu}{2}\|Y - X\|^2, \\ s.t.\ \ d_x = \nabla_x^{EDWF}Y,\ \ d_y = \nabla_y^{EDWF}Y \end{aligned} \tag{3.3.11}$$

By enforcing the constraints, the above equation turns into unconstrained optimization problem, as,

$$\begin{aligned} \min_{d_x,d_y,Y} |d_x| + |d_y| + \frac{\mu}{2}\|Y - X\|^2 + \frac{\lambda}{2}\|d_x - \nabla_x^{EDWF}Y - b_x^l\|^2 \\ + \frac{\lambda}{2}\|d_y - \nabla_y^{EDWF}Y - b_y^l\|^2 \end{aligned} \tag{3.3.12}$$

where, b_x^l and b_y^l are updated through Bregman iteration, as follows:

$$b_x^{(l+1)} = b_x^l + \nabla_x^{EDWF}Y^{(l+1)} - d_x^{(l+1)} \tag{3.3.13}$$

$$b_y^{(l+1)} = b_y^l + \nabla_y^{EDWF}Y^{(l+1)} - d_y^{(l+1)} \tag{3.3.14}$$

To obtain $Y^{(l+1)}$, $d_x^{(l+1)}$ and $d_y^{(l+1)}$, the above equations can be written as follows:

$$\begin{aligned} u^{(l+1)} = \arg\min_Y \frac{\mu}{2}\|Y - X\|^2 + \frac{\lambda}{2}\|d_x^l - \nabla_x^{EDWF}Y - b_x^l\|^2 \\ + \frac{\lambda}{2}\|d_y^l - \nabla_y^{EDWF}Y - b_y^l\|^2 \end{aligned} \tag{3.3.15}$$

$$d_x^{(l+1)} = \arg\min_{d_x} |d_x| + \frac{\lambda}{2}\|d_x^l - \nabla_x^{EDWF}Y^{(l+1)} - b_x^l\|^2 \tag{3.3.16}$$

$$d_y^{(l+1)} = \arg\min_{d_y} |d_y| + \frac{\lambda}{2}\|d_y^l - \nabla_y^{EDWF}Y^{(l+1)} - b_y^l\|^2 \tag{3.3.17}$$

To solve equation (3.3.15), a method suggested in [156] is used to get the first order optimal condition for weighted TV regularization. Therefore, the first order optimal condition for weighted TV regularization can be written as:

$$\{\mu + \lambda(\nabla_x^{EDWF})^T\nabla_x^{EDWF} + \lambda(\nabla_y^{EDWF})^T\nabla_y^{EDWF}\}Y^{l+1}$$
$$= \mu X + \lambda\nabla_x^{EDWF}(d_x^l - b_x^l) + \lambda\nabla_y^{EDWF}(d_y^l - b_y^l) \tag{3.3.18}$$

where, $(\nabla_x^{EDWF})^T$ and $(\nabla_y^{EDWF})^T$ are the adjoint matrices of ∇_x^{EDWF} and ∇_y^{EDWF}. Equation (3.3.18) can be solved by using Gauss-Seidel method because the system is strictly diagonal dominant, therefore,

$$Y^{l+1}(i,j) = \frac{\psi}{\xi} \tag{3.3.19}$$

where, $\psi = \mu X + \lambda\nabla_x^{EDWF}(d_x^l - b_x^l) + \lambda\nabla_y^{EDWF}(d_y^l - b_y^l) + \lambda[\alpha^2(i,j)Y^l(i+1,j)] + \alpha^2(i-1,j)Y^{l+1}(i-1,j) + \beta^2(i,j)Y^l(i,j+1) + \beta^2(i,j-1)Y^{l+1}(i,j-1)$ and $\xi = \mu + \lambda[\alpha^2(i,j) + \alpha^2(i-1,j) + \beta^2(i,j) + \beta^2(i,j-1)]$.

To solve the coupling problem in elements of d_x and d_y, both d_x and d_y are computed using shrinkage rule, as given below:

$$d_x^{l+1} = sgn(\tau_x).max(|\tau_x| - 1/\lambda, 0) \tag{3.3.20}$$

$$d_y^{l+1} = sgn(\tau_y).max(|\tau_y| - 1/\lambda, 0) \tag{3.3.21}$$

where, $\tau_x = \nabla_x^{EDWF}Y^{(l+1)} + b_x^l$ and $\tau_y = \nabla_y^{EDWF}Y^{(l+1)} + b_y^l$.

Isotropic TV denoising

Here, the convex problem is discussed to solve the exponentially directional weighted isotropic TV regularization using Split Bregman method, which can be expressed as:

$$\min_{Y} \sum_{i,j} \sqrt{\{\nabla_x^{EDWF} Y(i,j)\}^2 \ + \{\nabla_y^{EDWF} Y(i,j)\}^2} \ + \frac{\mu}{2}\|Y - X\|^2 \tag{3.3.22}$$

Similarly, as discussed in anisotropic TV denoising, the problem for exponentially directional weighted isotropic TV regularization using Split Bregman strategy can be formulated as:

$$\min_{Y} \sum_{i,j} \sqrt{\{d_x(i,j)\}^2 + \{d_y(i,j)\}^2} \ + \ \frac{\mu}{2}\|Y - X\|^2, \quad s.t. \ d_x = \nabla_x^{EDWF} Y, \ d_y = \nabla_y^{EDWF} Y \tag{3.3.23}$$

By enforcing the constraints, the above equation turns into unconstrained optimization problem, as:

$$\min_{d_x, d_y, Y} \sum_{i,j} \sqrt{\{d_x(i,j)\}^2 + \{d_y(i,j)\}^2} + \frac{\mu}{2}\|Y - X\|^2 + \frac{\lambda}{2}\|d_x - \nabla_x^{EDWF} Y - b_x^l\|^2 + \frac{\lambda}{2}\|d_y - \nabla_y^{EDWF} Y - b_y^l\|^2 \tag{3.3.24}$$

To solve the above equation for l number of iterations, it can be rewritten as:

$$u^{(l+1)} = \arg\min_{Y} \frac{\mu}{2}\|Y - X\|^2 + \frac{\lambda}{2}\|d_x^l - \nabla_x^{EDWF} Y - b_x^l\|^2 + \frac{\lambda}{2}\|d_y^l - \nabla_y^{EDWF} Y - b_y^l\|^2 \tag{3.3.25}$$

$$(d_x^{(l+1)}, d_y^{(l+1)}) = \arg\min_{d_x, d_y} \sum_{i,j} \sqrt{\{d_x(i,j)\}^2 + \{d_y(i,j)\}^2} + \frac{\lambda}{2}\|d_x^l - \nabla_x^{EDWF} Y^{(l+1)} - b_x^l\|^2 + \frac{\lambda}{2}\|d_y^l - \nabla_y^{EDWF} Y^{(l+1)} - b_y^l\|^2 \tag{3.3.26}$$

As, in anisotropic case, the variables d_x and d_y are decoupled, but in anisotropic case, both variables are coupled. To solve this problem, a generalized shrinkage formula is used, as given below:

$$d_x^{(l+1)} = max(s^l - 1/\lambda, 0)\frac{\nabla_x^{EDWF} Y^{(l)} + b_x^l}{s^l} \tag{3.3.27}$$

$$d_y^{(l+1)} = max(s^l - 1/\lambda, 0)\frac{\nabla_y^{EDWF} Y^{(l)} + b_y^l}{s^l} \tag{3.3.28}$$

where, $s^l = \sqrt{|\nabla_x^{EDWF} Y^{(l)} + b_x^l|^2 + |\nabla_y^{EDWF} Y^{(l)} + b_y^l|^2}$

In the proposed method, exponentially directional weighted functions (α and β) are introduced for horizontal and vertical directions. These weighted functions are effectively used to modify the TV method for CT image denoising, as shown in algorithm 3.1. Further, minimization problem of algorithm 3.1 can be solved by using Split Bregman method.

3.4 Numerical Experiments

In this section, the numerical results are presented on some real CT images to verify the efficiency of proposed algorithm. Here in the experiments, two types of noisy CT images are used to analyse the performance of the proposed algorithm. The sample of real CT images shown in figure 3.1 is the first type of CT images. Figure 3.2 represents noisy CT image data set with σ= 20. Another type of CT image is real noisy CT image as shown in figure 3.12(a) which is also used for experimental evaluation.

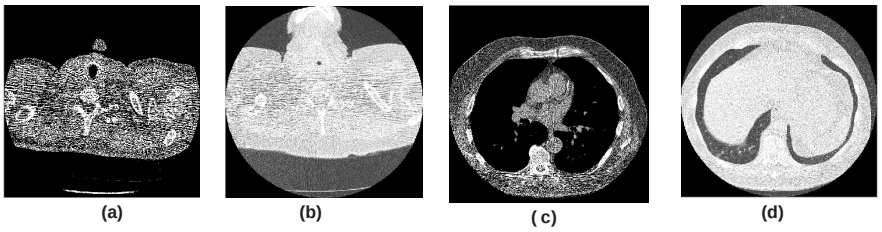

Figure 3.1: Original CT image data set

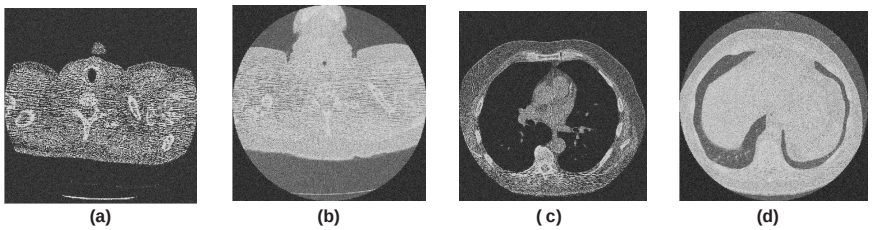

Figure 3.2: Noisy CT image data set σ=20

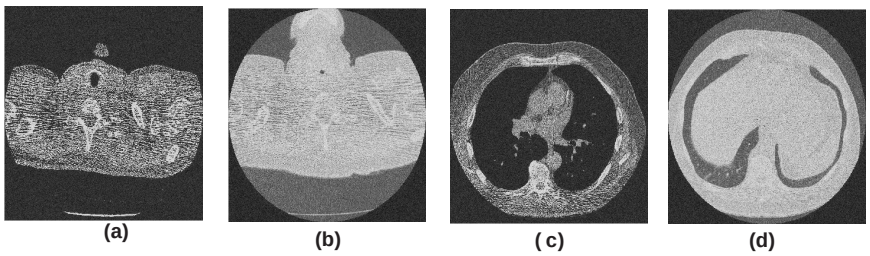

Figure 3.3: Results of DTV

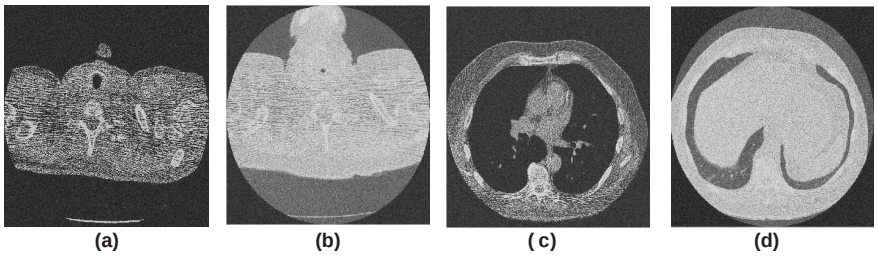

Figure 3.4: Results of CDTV

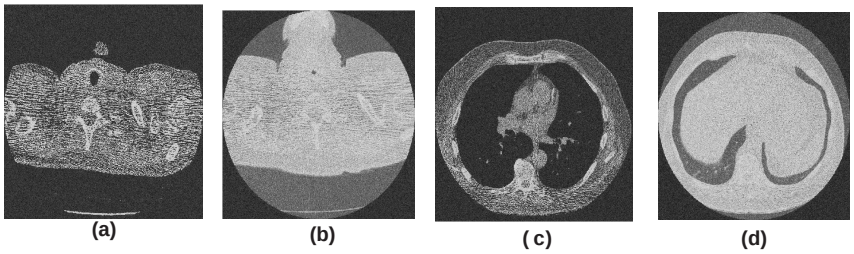

Figure 3.5: Results of NCTV

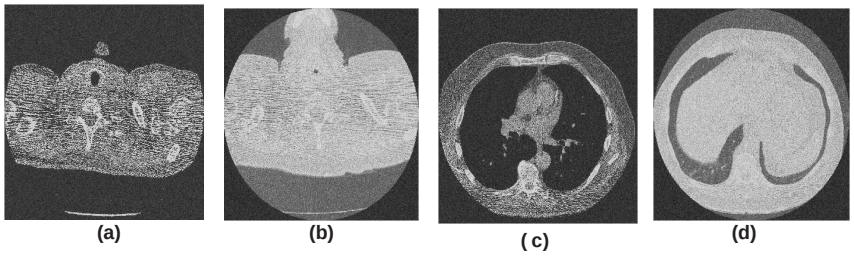

Figure 3.6: Results of SBTV

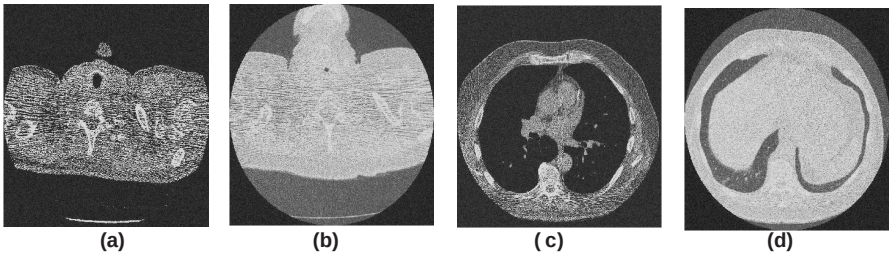

Figure 3.7: Results of IRTV

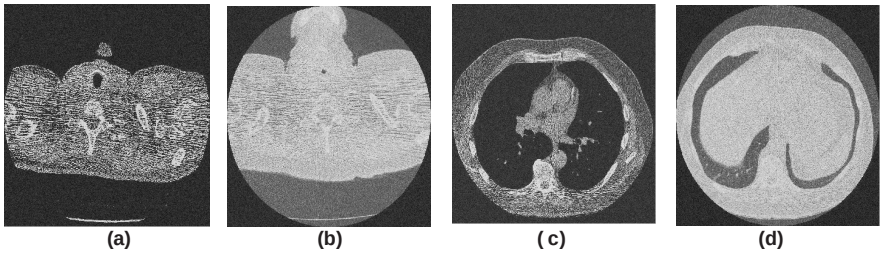

Figure 3.8: Results of ETV

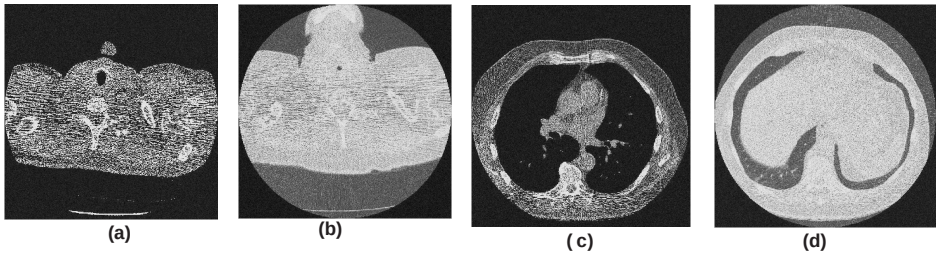

Figure 3.9: Results of proposed (TV_{EDWF}) scheme

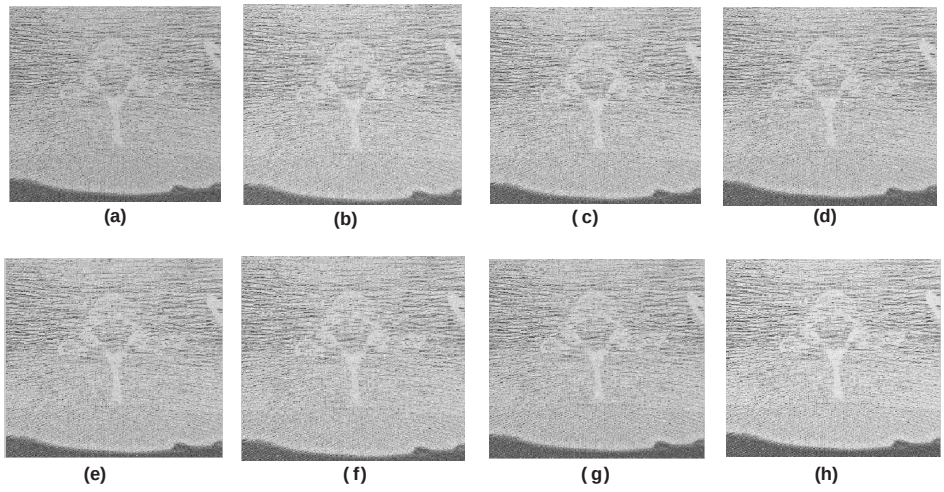

Figure 3.10: Analysis on zoomed image of noisy CT2 image: (a) zoomed image of noisy CT2; (b) result of DTV; (c) result of CDTV; (d) result of NCTV; (e) result of SBTV; (f) result of IRTV; (g) result of ETV; and (h) result of proposed algorithm

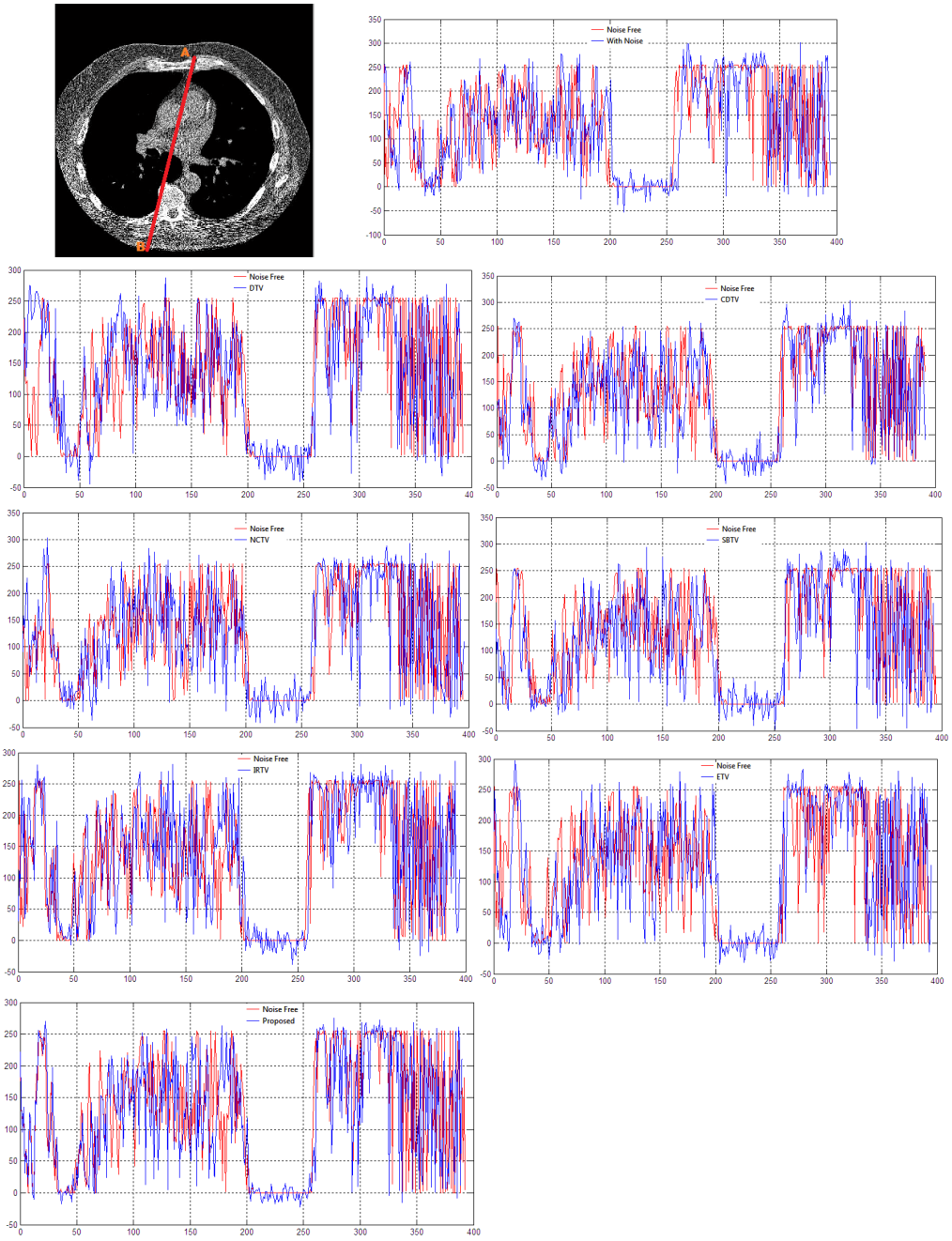

Figure 3.11: Intensity profile of a line on CT3 image. In each plot, the Noise Free intensity profile is plotted in red and filtered profile is plotted in blue.

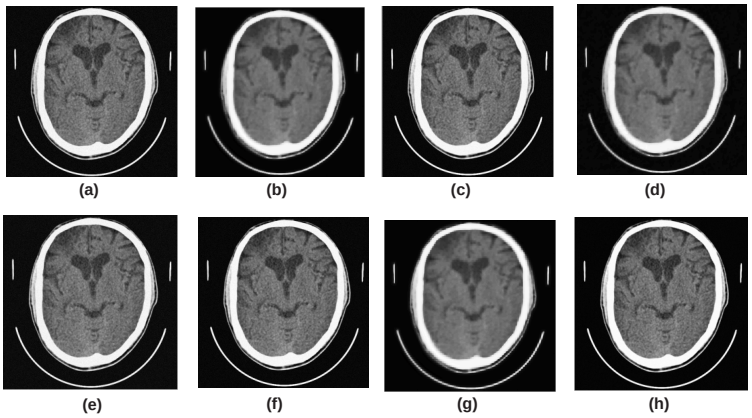

Figure 3.12: Analysis on real noisy CT image: (a) real noisy CT image; (b) result of DTV; (c) result of CDTV; (d) result of NCTV; (e) result of SBTV; (f) result of IRTV; (g) result of ETV; and (h) result of proposed algorithm

From literatures [7, 61] as well as from experimental evaluation, it is observed that in most of the cases anisotropic total variation gives better outcome or sometimes similar in comparison to isotropic TV. With this consideration, here all simulations are reported using anisotropic type of total variation. For all experiments, the maximum number of iterations l is set to 30, μ is .05 and λ is 2μ.

Since the comparative study is also required to show the ability of the proposed algorithm, therefore, some well-known standard methods are chosen for comparison, such as: directional total variation (DTV) [6], coefficients-driven total variation (CDTV) [3], nonnegativity constrained total variation (NCTV) [79], Split Bregman total variation (SBTV) [53], iterative re-weighted TV_p algorithm (IRTV) [153] and Exponential total variation (ETV) [134]. For comparison analysis, the parameter values other than iteration number l, μ and λ are used as reported in corresponding literature, [6], [3], [79], [53], [153], and [134].

To measure the accuracy of the proposed algorithm, some standard performance metrics are used, such as: peak signal to noise ratio (PSNR), Structural Similarity [146] (SSIM), Entropy Difference (ED) and Difference in Variance (DIV).

Table 3.1: PSNR and SSIM of Proposed (TV_{EDWF}) scheme and Existing schemes for CT image denoising

		PSNR				SSIM			
Image	σ	10	20	30	40	10	20	30	40
CT1	DTV	29.8509	22.9115	19.1317	16.5074	0.8822	0.6992	0.6077	0.5592
	CDTV	29.4675	22.7472	19.0078	16.3576	0.8737	0.6963	0.6075	0.5576
	NCTV	28.7581	22.4145	18.7997	16.2564	0.8563	0.6871	0.6020	0.5550
	SBTV	28.1380	22.0987	18.5870	16.1113	0.8429	0.6776	0.5983	0.5519
	IRTV	30.6353	23.2813	19.3408	16.6642	0.8954	**0.7158**	0.6133	0.5634
	ETV	30.1796	23.0866	19.2330	16.5542	0.8879	0.7050	0.6109	0.5608
	Proposed	**31.2315**	**23.5284**	**19.5213**	**16.7543**	**0.9078**	0.7153	**0.6176**	**0.5637**
CT2	DTV	29.8539	22.9272	19.1310	16.5018	0.9385	0.8061	**0.6989**	0.5856
	CDTV	29.4308	22.7662	18.9880	16.4016	0.9344	0.8021	0.6816	0.5788
	NCTV	28.7628	22.4219	18.8004	16.2565	0.9250	0.7926	0.6741	0.5730
	SBTV	28.1481	22.1194	18.5722	16.0855	0.9157	0.7822	0.6659	0.5671
	IRTV	30.6324	23.2822	19.3444	16.6427	0.9471	0.8151	0.6936	0.5882
	ETV	**31.2232**	23.0625	19.2373	16.5475	0.9422	0.8102	0.6886	0.5861
	Proposed	30.1670	**23.5287**	**19.5095**	**16.7653**	**0.9534**	**0.8230**	0.6976	**0.5938**
CT3	DTV	29.8411	22.9201	19.1163	16.5092	0.8702	0.6649	0.5480	0.4788
	CDTV	29.4595	**23.5497**	18.9883	16.3875	0.8618	0.6567	0.5468	0.4767
	NCTV	28.7274	22.4204	18.7901	16.2338	0.8411	0.6457	**0.5597**	0.4722
	SBTV	28.1256	22.1220	18.5845	16.1000	0.8258	0.6395	0.5343	0.4692
	IRTV	30.6330	23.2785	19.3486	16.6475	0.8869	0.6785	0.5568	0.4824
	ETV	30.1490	23.0714	19.2376	16.5473	0.8774	0.6674	0.5528	0.4798
	Proposed	**31.2272**	22.7271	**19.5047**	**16.7670**	**0.8988**	**0.6858**	0.5588	**0.4872**
CT4	DTV	29.8542	22.9476	19.1196	16.4963	0.9361	0.7952	0.6608	0.5480
	CDTV	29.4288	22.7422	19.0063	16.4156	0.9306	0.7897	0.6570	**0.5560**
	NCTV	28.7928	22.4103	18.8110	16.2462	0.9207	0.7776	0.6450	0.5412
	SBTV	28.1205	22.1312	18.6235	16.0812	0.9121	0.7702	0.6393	0.5305
	IRTV	30.6432	23.2788	**19.4924**	16.6792	0.9450	0.8025	0.6680	0.5557
	ETV	30.1645	23.0779	19.2071	16.5582	0.9396	0.7987	0.6653	0.5494
	Proposed	**31.2347**	**23.5212**	19.3333	**16.7741**	**0.9519**	**0.8105**	**0.6735**	0.5498

Figures 3.3, 3.4, 3.5, 3.6, 3.7, 3.8 and 3.9 are showing the results of DTV, CDTV, NCTV, SBTV, IRTV, ETV and proposed algorithm, respectively. For real noisy CT image, figures 3.12(b), 3.12(c), 3.12(d), 3.12(e), 3.12(f), 3.12(g) and 3.12(h)

Table 3.2: ED and DIV of Proposed (TV_{EDWF}) scheme and Existing schemes for CT image denoising

Image	σ	ED				DIV			
		10	20	30	40	10	20	30	40
CT1	DTV	0.6618	0.5657	0.5396	0.5233	1.4230	3.2890	5.0488	6.9309
	CDTV	0.6547	0.5681	0.5367	0.5228	1.4849	3.1835	4.8124	6.4410
	NCTV	0.6436	0.5619	0.5368	0.5222	1.5318	3.5606	5.0399	6.7116
	SBTV	0.6276	**0.5572**	0.5359	0.5227	1.6782	3.4186	5.4367	6.9713
	IRTV	0.6771	0.5707	0.5375	0.5236	1.4013	**2.8137**	4.5955	6.6144
	ETV	0.6691	0.5674	0.5368	0.5237	1.4874	3.1870	4.9947	6.5835
	Proposed	**0.6213**	0.5739	**0.5313**	**0.5219**	**1.2270**	2.9833	**4.7102**	**6.4088**
CT2	DTV	0.2160	0.1866	0.1917	0.2122	2.0167	4.3235	7.0097	9.7046
	CDTV	0.2129	**0.1846**	0.1904	0.2165	2.0869	4.6213	7.0424	9.2240
	NCTV	0.2105	0.1862	0.1930	0.2170	2.2377	4.8857	7.1624	10.1340
	SBTV	0.2045	0.1858	0.1962	0.2190	2.4397	5.0360	7.5028	9.8770
	IRTV	0.2226	0.1872	0.1880	0.2115	1.8326	4.2262	6.7563	9.4507
	ETV	0.2184	0.1869	0.1899	0.2139	1.9644	4.3427	7.0746	9.6899
	Proposed	**0.2037**	0.1885	**0.1878**	**0.2099**	**1.7305**	**4.3030**	**6.4731**	**9.0947**
CT3	DTV	0.6924	0.5971	0.5737	0.5686	3.7617	8.7158	13.5662	18.4269
	CDTV	0.6865	0.5950	0.5755	0.5698	4.0448	8.9458	13.6403	17.8657
	NCTV	**0.6739**	0.5928	0.5726	0.5675	4.3108	9.2104	14.0623	18.8141
	SBTV	0.6810	0.5879	0.5792	0.5683	4.7438	9.0988	14.0902	19.3326
	IRTV	0.7080	0.5991	0.5735	0.5667	3.6907	8.2033	12.1909	17.6931
	ETV	0.6987	0.5997	0.5738	0.5664	3.8453	8.7534	13.2321	18.1521
	Proposed	0.6940	**0.5846**	**0.5716**	**0.563**6	**3.1779**	**7.9014**	**13.1541**	**16.8782**
CT4	DTV	0.2180	0.1853	0.1852	0.2040	1.8633	4.3152	6.5716	8.5008
	CDTV	0.2139	0.1855	0.1867	0.2037	2.0693	4.2925	6.8359	8.9685
	NCTV	0.2087	0.1856	0.1881	0.2073	2.1010	4.3883	6.8031	9.2242
	SBTV	0.2176	0.1852	0.1886	0.2087	2.4249	4.7364	7.0283	9.2779
	IRTV	0.2229	**0.1840**	0.1859	0.2025	1.8446	4.1105	6.3610	8.4685
	ETV	0.2185	0.1863	0.1860	0.2027	1.8374	4.2139	6.6262	8.8953
	Proposed	**0.2049**	0.1849	**0.1842**	**0.2017**	**1.6181**	**3.8725**	**6.3447**	**8.4888**

are showing the results of DTV, CDTV, NCTV, SBTV, IRTV, ETV and proposed algorithm, respectively. To measure the visual comparison, there is no mathematical or specific method available. Therefore, the results need to be evaluated with naked eye to determine the best filtered images. For better visual inspection, we follow four criteria: (i) visibility of the artifacts; (ii) preservation of edge details; (iii) visibility of low contrast objects, and (iv) preservation of the texture.

Table 3.3: Execution time for different denoising methods (in seconds)

Method	DTV	CDTV	NCTV	SBTV	IRTV	ETV	Proposed
Time	15.4976	3.3612	3.3125	.5667	2.9831	6.7121	3.0195

The performance metrics (PSNR, SSIM, ED and DIV) are also computed using various noise levels and shown in table 3.1 and table 3.2. The best values among all the methods are shown in bold. The results shown in tables 3.1 and 3.2 demonstrate that in most of the cases, the proposed method is superior to all other compared methods.

The results of DTV, NCTV and ETV are good in terms of noise reduction from noisy CT images. However, DTV method gives satisfactory results to reduce the Gaussian noise from CT images but failed to preserve the edges over the strong noisy edges. The DTV method gives better SSIM values only over the CT2 image with noise level 30. The ETV method provides smooth edges over the homogeneous regions. However, as noise increases, the edges get blurred. The ETV method gives better PSNR values only over the CT2 image with noise level 10. The NCTV method is also helpful to reduce the Gaussian noise from CT images, but, visually texture is not as good as required for clinical purpose. However, the NCTV method gives better SSIM value only over the CT3 image with noise level 30 and Entropy Difference (ED) value only over the CT3 image with noise level 10. The results of CDTV, IRTV and SBTV methods indicate that the noise from CT images is effectively reduced. From experimental analysis, it was analyzed that the results of CDTV method do not

sufficiently reducing the higher noise. However, the CDTV method gives some better results such as PSNR values over the CT3 image with noise level 20, SSIM value over the CT4 image with noise level 40, and ED value over the CT2 image with noise level 20, as shown in tables 3.1 and 3.2. The SBTV and IRTV methods failed to provide the smoothness over the homogeneous regions, which can be analyzed from figures 3.6 and 3.7. As noise increases, SBTV method also fails to preserve the textures. However, the SBTV method gives better ED value over the CT1 image with noise level 20. While, the IRTV method also gives some better results such as ED values over the CT4 image with noise level 20, SSIM and DIV values over the CT1 image with noise level 20, PSNR values over the CT4 image with noise level 30. The results of the proposed scheme provide better outcome for effective noise reduction on the CT images. The edges and texture are well-preserved without over-smoothing or generating the unwanted denoising flaws. In most of the cases, the proposed method gives better PSNR, SSIM, ED and DIV values over given CT image dataset, as shown in tables 3.1 and 3.2. For more sophisticated CT images, physicians generally prefer original noisy images more willingly in comparison to over-smoothed images. The proposed algorithm provides less smoother results with preserved edges and reduced noise which can be helpful for clinical purpose.

A zoom cropped object of low contrast noisy CT2 image as shown in figure in 3.10(a) is also used to verify the performance of the proposed algorithm. Figures 3.10(b), 3.10(c), 3.10(d), 3.10(e), 3.10(f), 3.10(g) and 3.10(h) are the results of DTV,

CDTV, NCTV, SBTV, IRTV, ETV and the proposed method, respectively. Visually, it can be analyzed that the proposed method gives better outcomes in terms of noise reduction and better edge preservation. For more critical analysis of noise reduction from noisy CT image, the profile of CT3 image is also obtained to compute the intensity values along a line. The analysis of the profiles of denoised CT image as shown in figure 3.11 indicates that the proposed scheme is better in comparison to existing denoising schemes.

The computation time is also an important factor to measure the performance of the proposed methods. The average computation time in second(s) of proposed method and compared methods is shown in table 3.3. From table 3.3, it can be observed that the proposed method takes relatively less computation time in comparison to DTV, CDTV, NCTV and ETV methods but slightly more time in compare to SBTV and IRTV methods. As the number of iterations is increased, the time cost is proportionally increased. However, the proposed method still takes relatively less computation time in comparison to DTV, CDTV and ETV methods. Hence, there is tradeoff between the performance and computation time in the proposed scheme. The major difficulty of deriving the results is to find the optimum values of the inner parameters (α, β, μ). However, it can be resolved by setting default values of inner parameters to perform the proposed algorithm iteratively. The results can slightly vary by changing the inner parameter values of the proposed scheme.

3.5 Conclusions

In this chapter, a new exponentially directional weighted function (EDWF) for anisotropic and isotropic TV is discussed to denoise the computed tomography medical images. The performance of the proposed method is evaluated with various factors such as visual inspection of real CT image (added noisy and real noisy). The performance metrics such as PSNR, SSIM, ED and DIV are also computed and compared. From comparison and result analysis, it can be clearly said that the proposed method recovers visually accepted image by preserving most of the structures with less computation time. It also preserves the small image details and generates no visually artifacts. However, the performance of the proposed algorithm has a great potential to serve for denoising the computed tomography images. But the features of denoised CT images can be more preserved with Wavelet domain in compare to spatial domain. Therefore, in the next chapter, a novel and robust approach is presented for CT image denoising in Wavelet domain.

CHAPTER 4

CT image denoising using Wiener filtering in Wavelet domain

Chapter 4

CT image denoising using Wiener filtering in Wavelet domain

In previous chapter, the CT images were denoised by using modified total variation (TV) method in spatial domain. Spatial domain methods works directly over the pixels. However, Wavelets allow multi-resolution analysis at different scales or resolution. It permits us to deal an image in terms of frequencies in the images. It captures both frequency and location information thus the temporal resolution is a key advantage over the spatial domain. Therefore, this chapter presents Wavelet based noise reduction techniques for CT image denoising where Wiener filtering and wavelet thresholding methods are used.

4.1 Introduction

Wavelet transform is a powerful tool for signal and image processing tasks because of multi-resolution analysis, subbanding and localized in frequency and time domain. Wavelet packet method provides richer range of possible information for image and signal analysis. Wavelet packet transform decomposes the images into low and high frequencies. The further decomposition of low and high frequencies is helpful to

obtain detail characteristics of images. In wavelet packet analysis, both the detail and approximation part can be split. However in DWT only approximation part can split. The main strength of Wavelet thresholding is to estimate the true signals using estimation technique and process on different frequency components of the image.

Various articles have been published to improve the quality of images using denoising techniques, as discussed in [125]. Among these methods, Wiener filter is one of the most popular methods for image denoising because of its simplicity and effectiveness. However, the wavelet based denoising using the concept of wiener filtering methods also achieved good results for image denoising. In [97, 98], the variance of wavelet coefficients are obtained by using an approximate maximum a posteriori probability rule and then denoising is performed using the local Wiener filter. However in these methods, variance estimation of wavelet coefficients is an important factor for image denoising. Further, the variance estimation method [71] is improved using thresholding operation. In another approach [42], the multiple variances of wavelet coefficients are estimated from differently shaped windows from the noisy image and a weighted average is obtained which is further used for image denoising. In [130], the directional window is used to improve the performance of local Wiener filter.

Wang et al. [144] introduced Wiener filter parallel denoised model algorithm based on wavelet transform. Wavelet transform has a capability to decompose into several different direction sub-images. These different directions based sub-images are filtered

by auto-adapted Wiener filter. The experimental evaluation indicates that proposed algorithm, can not only enhance the detailed characteristics of CT image such as edges, but also reduce the noise more effectively than the traditional algorithms. In extended method, Ke et al. [72] presented a novel CT image denoising method based on multi-scale Wiener filtering. Firstly, they analyze noise from the CT images then performed denosing process. For denoising, they performed two times wiener filtering over different decomposition level in wavelet domain. The result analysis indicates that obtained results are good qualitatively and quantitatively in compare to conventional wiener filtering. Silva et al. [132] introduced denoising methods for tumor discrimination in high-resolution Computed Tomography images. They studied several denoising methods: geometric mean filter, Wiener filtering, and wavelet denoising. The performance of each method was analyzed on brain and thoracic phantoms, as well as several real thoracic HRCT images through visual inspection, profile region intensity analysis, and global figures of merit. They concluded that wavelet denoising performs well for denoising but it is hard to conclude that wavelet denoising works well for all CT reconstructed images. Yasuda et al. [158] introduced a method based on nonlinear wavelet-based edge preservation de-noising using trimmed-thresholding over the low-dose chest Multidetector-row computed tomography (MDCT) images. They also examined the impact of denoising for reducing the radiation dose. The results indicate that their algorithm is helpful for dose reduction and provides the denoised image. However, for higher noise, it fails to preserve the small edges.

Although the above mentioned Wiener filter methods achieved good results, but the performance is limited. Therefore in this chapter, two schemes are presented to improve the performance of CT image denoising. In first proposed algorithm (WF-WPT), a Wavelet based noise reduction technique has been presented to improve the image quality where adaptive Wiener filtering and Wavelet Packet Threshold (WPT) algorithm are used. In second proposed algorithm (WFWT-MN), another new approach has been presented by using the concepts of Wiener filtering and method noise in wavelet domain. Experimental results show that the both proposed algorithms are perform better to achieve CT denoised images.

The rest of the chapter is organized as follows. In section 4.2, Wiener filter is briefly discussed. The proposed methodologies are expressed in section 4.3, where both (WF-WPT and WFWT-MN) methods are discussed. In Section 4.4, the experimental evaluations, including comparison with existing techniques, are described. Finally, the conclusion is summarized in Section 4.5.

4.2 Wiener filter

Wiener filter is founded on considering images and noise as random processes and the objectives is to find an estimate of the uncorrupted image such that the mean square error between them can be minimized, i.e. Wiener filter can be regarded as a linear estimating method. Wiener filter works as a linear estimating method over desired signals such as noisy images, so that mean square error can be minimized. The local

Wiener filter can be expressed as:

$$R_1(i,j) = \frac{E\{Y^2(i,j)\}}{E\{Y^2(i,j)\} + E\{\eta^2(i,j)\}}.X(i,j) \tag{4.2.1}$$

where, $E\{\eta^2(i,j)\}$ is the noise variance. In above equation, $E\{Y^2(i,j)\}$ can be estimated as:

$$E\{Y^2(i,j)\} = max(E\{X^2(i,j)\} - E\{\eta^2(i,j)\}, 0) \tag{4.2.2}$$

Further, $E\{X^2(i,j)\}$ can be obtained as:

$$E\{X^2(i,j)\} = \frac{1}{w}\sum_{i,j=1}^{w} X^2(i,j) \tag{4.2.3}$$

where, w is the size of specified window of image neighborhood pixels.

4.3 Proposed Methodologies

In this section, two (WF-WPT and WFWT-MN) schemes are presented for CT image denoising. In WF-WPT scheme, a Wavelet based noise reduction technique has been presented using adaptive Wiener filtering and Wavelet Packet Thresholding (WPT). Further WF-WPT scheme is modified and extended for better edge preservation and noise suppression. In extended (WFWT-MN) scheme, the concepts of Wiener filtering and method noise in wavelet domain are used for CT image denoising. In this work, a discrete wavelet transform (DWT) is performed over the noisy CT images. The high frequency wavelet coefficients are modified using local Wiener filtering. The first intermediate result is obtained using inverse discrete wavelet transform (IDWT). For better edge preservation, first intermediate result is subtracted from the input

noisy image and processed using wavelet packet thresholding. The outcome of wavelet packet thresholding is the second intermediate result. Both intermediate results are added to gain the final denoised CT image.

In both (WF-WPT and WFWT-MN) schemes, Wavelet decomposition is performed based on a cost function. A cost value is generated for each subband in top down approach manner. Various types of cost function are used such as shannon entropy; wiener based cost function; and etc. Here, cost function for each subband s is chosen as log energy (LE) [44]. After defining cost function, the wavelet packet decomposition is performed with following steps:

i) Set the maximum number of decomposition levels.

ii) For each level, decompose the image into four subbands (child nodes).

iii) Compute cost value for each subband for each level.

iv) In top down approach manner, check the cost value.

- If the cost of parent node is greater than total cost of child nodes, the decomposition will continue.
- Otherwise; eliminate children nodes.

v) End the process, if there is no node to decompose.

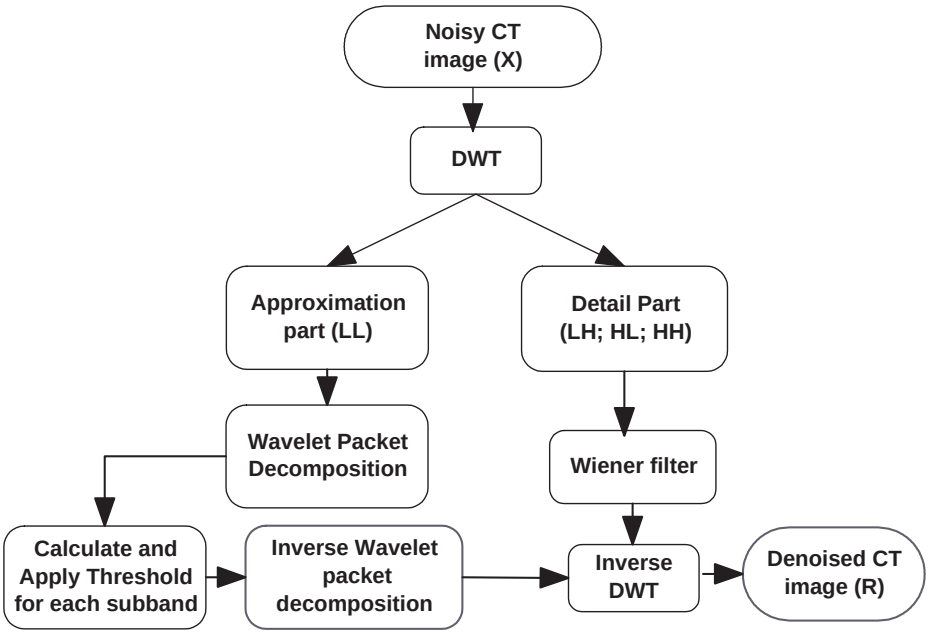

Figure 4.1: WF-WPT scheme

4.3.1 Wiener Filtering with Wavelet Packet Thresholding (WF-WPT) scheme

Here, in this subsection, CT image denoising method is presented with the approach of wiener filtering and wavelet packet thresholding. The complete overview of proposed denoising (WF-WPT) scheme as shown in figure 4.1 can be summarized by the following steps:

Step 1: Perform discrete wavelet transform (DWT) of CT image corrupted by Gaussian noise to obtain approximation and detail parts.

Step 2: Apply adaptive Wiener filtering over the detail parts.

Step3: Apply Wavelet Packet Decomposition over approximation part obtained from step 1 and estimate decomposition level by using log energy function.

Step 4: Compute the threshold value for each sub-band in all levels using equation 2.2.29 (discussed in chapter 2).

Step 5: Apply threshold to all sub-bands coefficients using the optimum linear interpolation function (equation 2.2.34).

Step 6: Perform the wavelet packet reconstruction to get denoised approximation part.

Step 7: perform inverse discrete wavelet transform (IDWT), where step 6 has approximation part and step 2 has detail part.

In WF-WPT scheme, the noisy images are decomposed using 2D-DWT to obtain the approximation and detail parts. Initially, wiener filter is performed over the detail parts. In parallel, wavelet packet transform is performed over the approximation part to get the richer detail parts where an optimal linear interpolation (OLI) shrink algorithm [44] is performed. To obtain denoised CT image, inverse wavelet packet transform and inverse 2D-DWT operations are performed. However, this scheme gives better results with some similar existing schemes but edges are not strongly preserved. Therefore, this scheme is further extended for more strongly edge preservation which is discussed in following subsection.

4.3.2 Wiener Filtering and Wavelet Thresholding using method noise (WFWT-MN) scheme

The complete overview of proposed denoising (WFWT-MN) scheme as shown in figure 4.2 and the steps can be is summarized as follows.

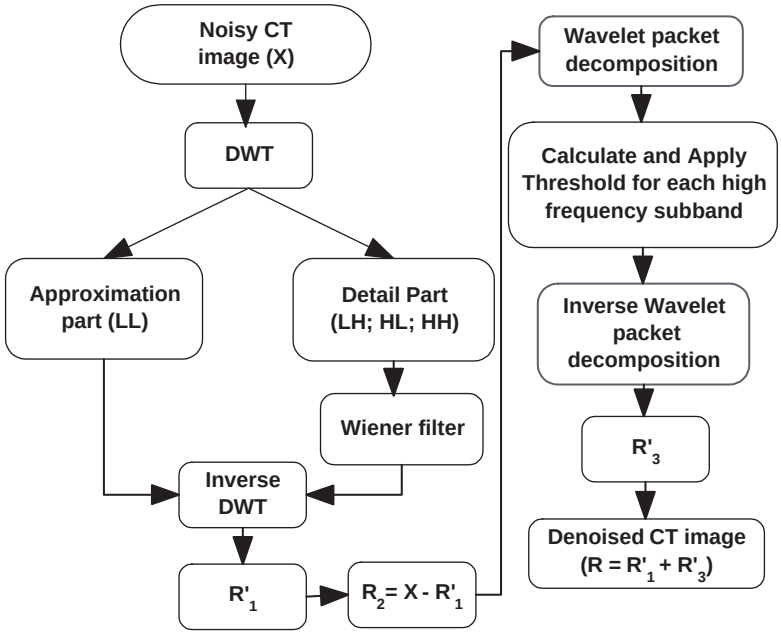

Figure 4.2: WFWT-MN scheme

Step 1: Apply 2D-DWT on noisy input CT image (X) to decompose into approximation (A) and detail (D) parts.

Step 2: Perform local Wiener filtering on detail parts (wavelet coefficients).

Step 3: Apply inverse discrete wavelet transform (IDWT) to get first intermediate result (R_1').

Step 4: Perform subtraction between noisy input image (X) and first intermediate result (R_1'), as:

$$R_2 = X - R_1' \tag{4.3.4}$$

Step 5: Apply wavelet packet transform on R_2 to get the detail parts.

Step 6: Perform an optimal linear interpolation (OLI) shrink algorithm on detail parts (wavelet coefficients) using equations 2.2.29 and 2.2.34.

Step 7: Apply inverse wavelet packet transform to get second intermediate result (R_3').

Step 8: Perform addition between both intermediate results to get final denoised CT image, as:

$$R = R_1' + R_3' \tag{4.3.5}$$

Here in WFWT-MN scheme, 2D-DWT is performed on the noisy CT image (X). Over the detail part, wiener filter is applied. By inverse 2D-DWT, the first intermediate result (R_1') is obtained. For better edge preservation, method noise concept is used where, noisy image is suppressed with first intermediate result. Over the subtracted image (R_2), wavelet packet transform is applied and an optimal linear interpolation (OLI) shrink algorithm on detail parts (wavelet coefficients) is performed to suppress the noise. Further, inverse wavelet packet transform is performed to obtain the second intermediate result (R_3'). The final outcome can be obtained by adding both intermediate results.

4.4 Experimental results and Discussion

In this section, the experimental results are evaluated on some CT images shown in figure 4.3. Figure 4.4 represents noisy CT image data set with σ= 20. The comparative study is also required to show the ability of proposed algorithm, some well-known standard methods are chosen for comparison, such as adaptive wavelet packet thresholding (AWPT) [44] and multi-scale Wiener filtering (MWF) [72].

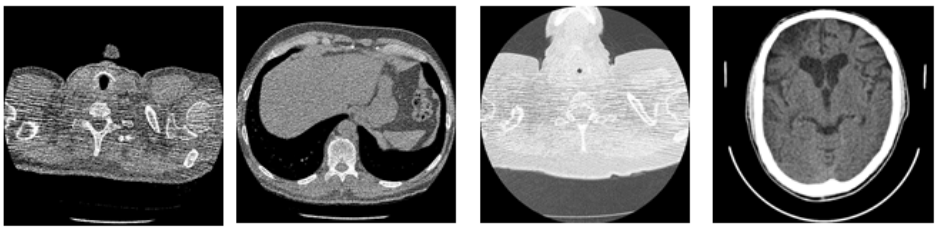

Figure 4.3: Original CT test images

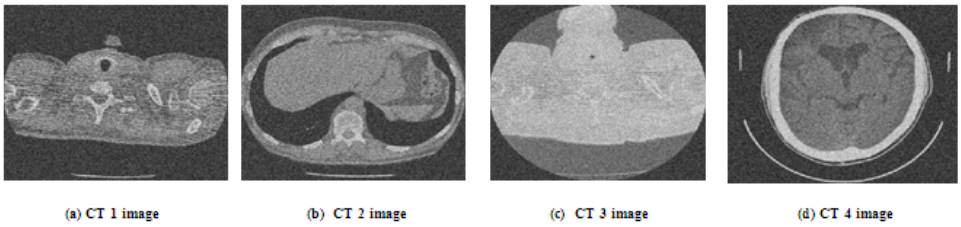

Figure 4.4: Noisy CT test images σ=20

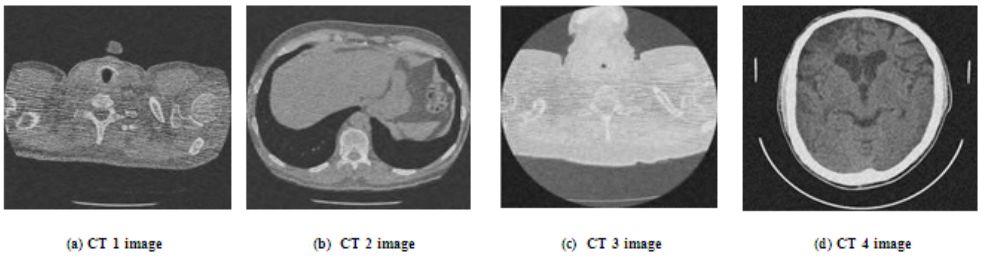

Figure 4.5: Results of adaptive wavelet packet thresholding (AWPT)

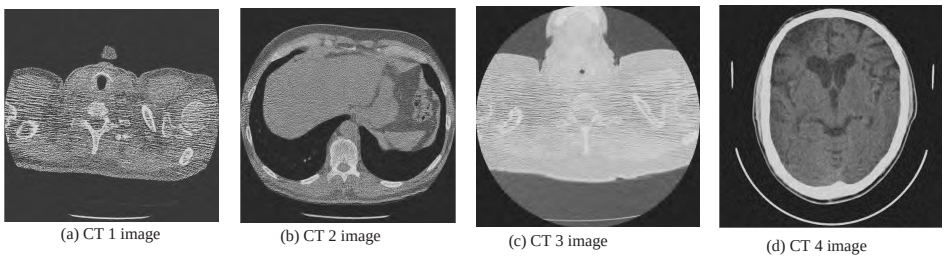

Figure 4.6: Results of multi-scale Wiener filtering (MWF)

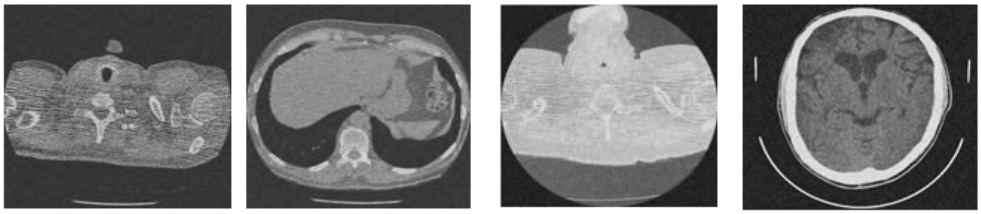

Figure 4.7: Results of Wiener Filtering with Wavelet Packet Thresholding (WF-WPT) scheme

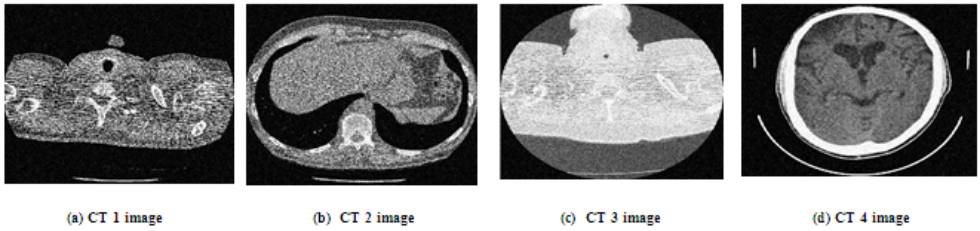

Figure 4.8: Results of Wiener Filtering and Wavelet Thresholding using method noise (WFWT-MN) scheme

To examine the performance of proposed method, some standard performance metrics are used, such as: peak signal to noise ratio (PSNR) and image quality index (IQI).

Figures 4.5, 4.6, 4.7 and 4.8 are showing the results of AWPT [44], MWF [72], WF-WPT and WFWT-MN scheme, respectively. From the visual comparison, it can be analyzed that both proposed methods are giving better results in terms of edge preservation and noise reduction in compare to existing schemes. Other than visual comparison, PSNR and IQI values are also calculated for existing and proposed methods, as shown in table 4.1. The best values for denoising are shown in bold in their respective tables. From table 4.1, it can be analyzed that most of the cases, the both proposed schemes are giving better results in comparison to existing schemes. However in compare to both proposed schemes, it is also analyzed

Table 4.1: PSNR and IQI of Proposed (WF-WPT and WFWT-MN) and Existing schemes for CT image denoising

		PSNR				IQI			
Image	σ	10	20	30	40	10	20	30	40
CT1	AWPT [44]	31.09	26.51	23.02	21.17	0.9927	0.9013	0.8802	0.8547
	MWF [72]	30.11	27.14	23.38	20.91	0.9933	0.9112	0.8932	0.8511
	WF-WPT	31.12	27.56	23.39	21.11	0.9939	0.9121	0.8941	0.8551
	WFWT-MN	**31.58**	**27.96**	**23.95**	**21.93**	**0.9947**	**0.9132**	**0.8951**	**0.8612**
CT2	AWPT [44]	30.14	25.40	22.18	19.89	0.9907	0.9096	0.8889	0.8448
	MWF [72]	29.57	26.12	22.34	19.84	0.9924	0.9103	0.8915	0.8497
	WF-WPT	30.67	26.71	22.45	20.05	0.9931	0.9110	0.8926	0.8498
	WFWT-MN	**30.83**	**26.84**	**22.63**	**20.31**	**0.9942**	**0.9127**	**0.8935**	**0.8502**
CT3	AWPT [44]	30.13	26.42	22.89	20.15	0.9913	0.9002	0.8803	0.8471
	MWF [72]	30.21	26.14	22.17	20.32	0.9925	0.9101	0.8933	0.8513
	WF-WPT	30.52	26.51	22.91	20.41	0.9932	0.9119	0.8939	0.8525
	WFWT-MN	**30.63**	**26.74**	**22.95**	**20.53**	**0.9942**	**0.9125**	**0.8945**	**0.8558**
CT4	AWPT [44]	30.13	26.22	22.87	20.77	0.9912	0.9006	0.8809	0.8469
	MWF [72]	30.21	26.41	22.34	20.53	0.9931	0.9017	0.8952	0.8439
	WF-WPT	30.58	26.74	22.46	20.89	0.9936	0.9091	0.8974	0.8481
	WFWT-MN	**30.83**	**27.06**	**22.91**	**21.03**	**0.9941**	**0.9102**	**0.8991**	**0.8501**

that Wiener Filtering and Wavelet Thresholding using method noise (WFWT-MN) schemes are giving better outcomes in terms of visually, PSNR and IQI.

4.5 Conclusions

In this chapter, CT image denoising is performed based on the two proposed (WF-WPT and WFWT-MN) schemes. WF-WPT scheme is based on the Wiener Filtering with Wavelet Packet Thresholding. Second proposed scheme (WFWT-MN) is the modified version of the WF-WPT scheme using method noise concept. Both proposed methods are giving better outcomes in comparison to existing schemes. However in compare to both proposed schemes, it is also analyzed that WFWT-MN scheme giving better outcomes in comparison to WF-WPT scheme. Due to the impact of method

noise, WFWT-MN scheme is giving visually better results in comparison to other schemes. Apart from visual analysis, the PSNR and IQI values are also calculated to measure the performance of the denoising schemes. The performance of WFWT-MN scheme is also better in terms of PSNR and IQI. From comparison and result analysis, it can be clearly said that WFWT-MN scheme recovers visually accepted image by preserving structures. It also preserves the small image details and generates no visually artifacts. Due to the concept of method noise and Bayes shrinkage rule in wavelet domain, the edges are well preserved. Therefore in the next chapter, two CT image denoising schemes are performed for better noise suppression and edge preservation using locally adaptive Bayes shrinkage rule in Wavelet domain.

CHAPTER 5

CT image denoising using Circular shift thresholding in Wavelet domain

Chapter 5

CT image denoising using Circular shift thresholding in Wavelet domain

In the previous chapter, thresholding concept has been used for CT image denoising. However, the results of CT image denoising are good in terms of noise suppression and edge preservation, but the performance of thresholding is depends upon the selected threshold value. Therefore, this chapter devotes two CT image denoising schemes based on the thresholding using circular shifting concept. In circular shifting concept, the pixel values of image are circularly rotated in horizontal and vertical directions and then further operations can be processed. In first proposed framework for CT image denoising, a new technique has been developed to denoise the CT images with edge preservation in tetrolet domain (Haar-type wavelet transform) where a locally adaptive shrinkage rule is performed by using circular shift on high frequency tetrolet coefficients in such a way that noise can be reduced more effectively. In second proposed framework for CT image denoising, a new technique has been developed to denoise the CT images with edge preservation where Non-local means (NLM) filter and circular shifting based wavelet packet thresholding is performed.

5.1 Introduction

This chapter is devoted to CT image denoising using circular shifting based thresholding in wavelet domain. Several linear and nonlinear filtering methods for noise reduction in the projection data have been proposed. Linear filters such as Wiener filter [72], [105] in the wavelet domain gives optimal results when the signal distortion is estimated by Gaussian approximation and the accuracy is measured by calculating Mean Square Error (MSE). Most of the techniques like nonlocal means (NLM) denoising [17] and local linear SURE based edge-preserving image filtering (LLSURE) [116] take an advantage of statistical properties of objects in image space and preserve clinical structures such as sharp edges, similarities between neighboring pixels, etc. In spatial domain, non-local means (NLM) [17] filter has been used for edge preserving noise reduction. NLM filter was proposed by Buades [17] in which each pixel is replaced by a weighted average of the most similar pixels where similarity is measured by comparisons of neighboring pixels within a specified search window. Recently in [33], both the sparse representation and non-local averaging operations are also integrated to denoise the images. Similarly in [87], nonlocal method is also integrated with soft thresholding to denoise the images. In spatial domain filtering, small structures of medical images can be treated as noise and these may be lost while denoising. Filters in spatial domain are efficient inefficient for noise reduction but inefficient for preserving the edges especially in small structures [72]

Various thresholding techniques for noise reduction have been introduced with

wavelet such as efficient image denoising method based on a new adaptive wavelet packet thresholding function [44], ideal spatial adaptation via wavelet shrinkage [26], SURE-LET approach for image denoising [11], etc. Other thresholding schemes have also been proposed, which take the advantages of both soft and hard thresholding. Some well-known shrinkage rules are hyperbola function [141], firm thresholding [50], garrote thresholding [49] and SCAD thresholding [5]. The idea of shrinkage with geometric wavelets methods such as tetrolet based thresholding [76] is also popular for image denoising.

Recently, many researchers extended the idea of shrinkage for better structure preservation in image denoising such as Non-local means filter and its method noise thresholding (NLFMT) [77]. The NLFMT cleans the edges without losing too many fine structures but for sophisticated CT images, fine structures may suffer. For more sophisticated CT images, physicians generally prefer original noisy image than smoothed versions because smoothed images may loss some relevant important details. CT image denoising is a challenging task because of finding correct noise variation, relationship between coefficients and achieving an optimal tradeoff between denoising and blurring or artifacts. With these challenges, we proposed two CT image denoising schemes. The first proposed scheme is based on the circular shift based thresholding in tetrolet domain. The second proposed scheme is based on NLM filter and circular shift based wavelet packet thresholding.

This chapter is organized as follows. Section 5.2 gives a brief overview of NLM

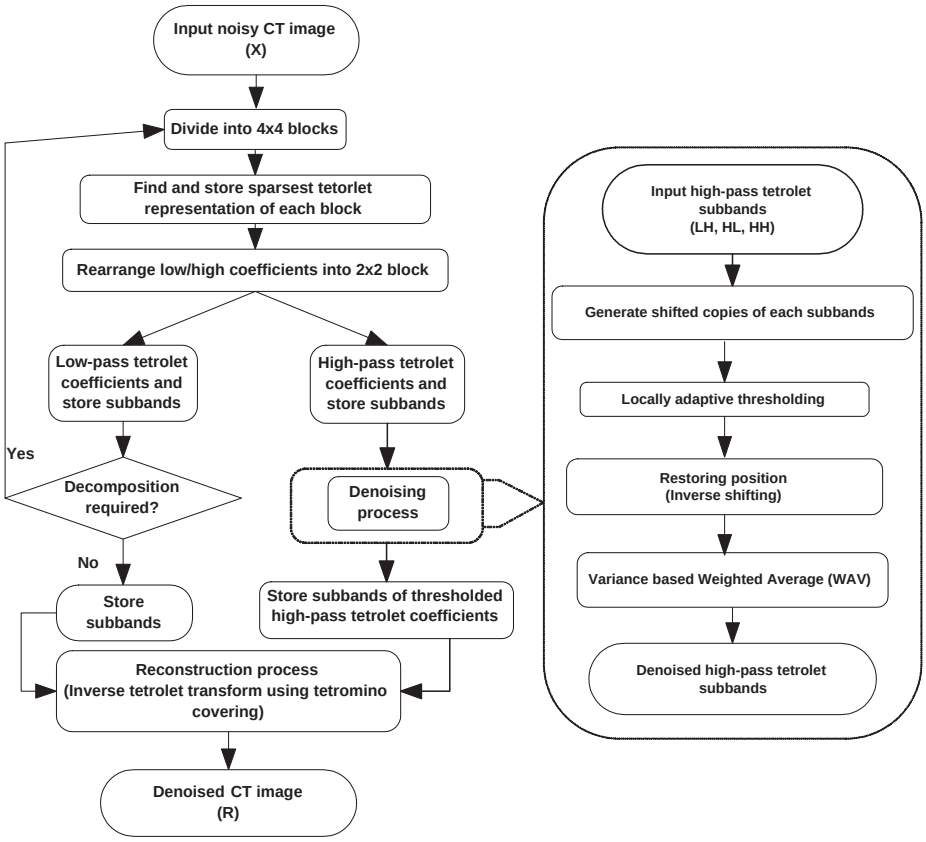

Figure 5.1: Circular shift based tetrolet thresholding (CSBT) scheme

filter. In section 5.3, the proposed methods are presented in details. Experimental results, including a comparison with other denoising methods, are given in section 5.4. Finally, some discussions and conclusions are summarized in section 5.5.

5.2 Nonlocal Means

The Nonlocal Means (NLM) method proposed by Buades [17] is based mainly on the redundancy of patches in images. In this method, each pixel can be denoised by a weighted mean of pixels in a fixed region. These weights are calculated using Euclidean distance to measure the similarity between a central patch and neighboring

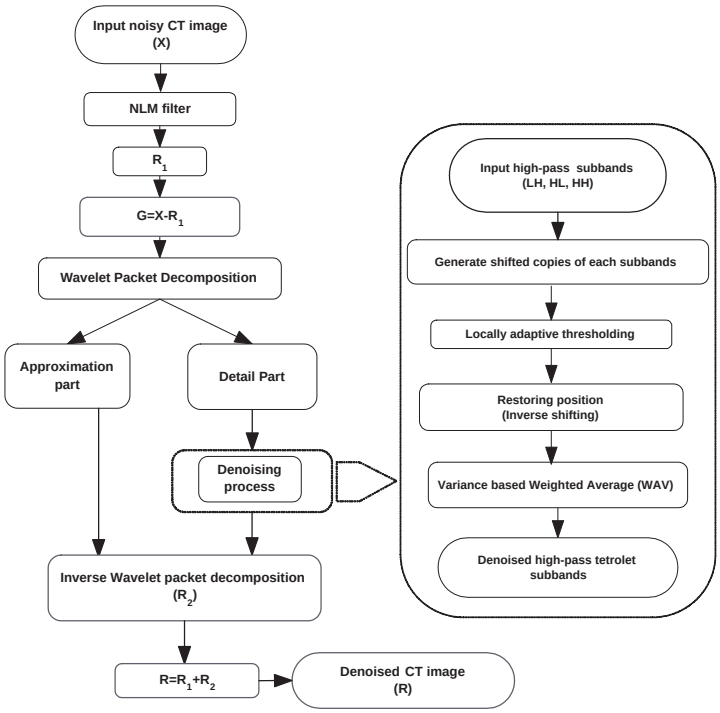

Figure 5.2: NLM and circular shift based wavelet packet thresholding (NLM-WPT) scheme

patches in a search window. For each pixel i of image, the non-local means can be formulated as:

$$NLM[X(i)] = \sum_{j \epsilon X} w(i,j)X(j) \tag{5.2.1}$$

where, X is the noisy image and $w(i,j)$ is a weighting function. The weighting function meet the following conditions:

(1) $0 \leq w(i,j) \leq 1$

(2) $\sum_{j} w(i,j) = 1$

The weights are based on the similarity between the pixels i and j. The weighting

function can be written as:

$$w(i,j) = \frac{1}{z(i)} e^{\frac{-\|X(N_i)-X(N_j)\|^2}{h^2}} \tag{5.2.2}$$

where $z(i) = \sum_j e^{\frac{-\|X(N_i)-X(N_j)\|^2}{h^2}}$ and h is a weight control parameter.

If the value of h is very small, the enough noise may not be removed and if it is very high, the image may become blurry. $X(N_i)$ and $X(N_j)$ denote similarity windows or patches. If similarity window is too large, no similar neighborhoods will be found. Therefore, noise is not effectively reduced. However, if similarity window is too small, too many similar neighborhoods will be found and blurring problem can occur. A fixed search area is needed to compute the similarity between two neighborhoods and the weighted sum of squares difference between the two neighborhoods is used.

5.3 Proposed methodologies

In this section, the proposed schemes for CT image denoising are discussed in below subsections.

5.3.1 Circular shift based tetrolet thresholding (CSBT) scheme

For denoising of noisy CT scanned images, tetrolet transform plays a major role to enhance the local information of an image because of its multi-scale geometric property. The block diagram of the first proposed scheme is shown in figure 5.1.

In circular shift based tetrolet thresholding (CSBT) scheme, tetrolet transform is used to decompose input noisy CT image into low (LL) and high (LH, HL, HH)

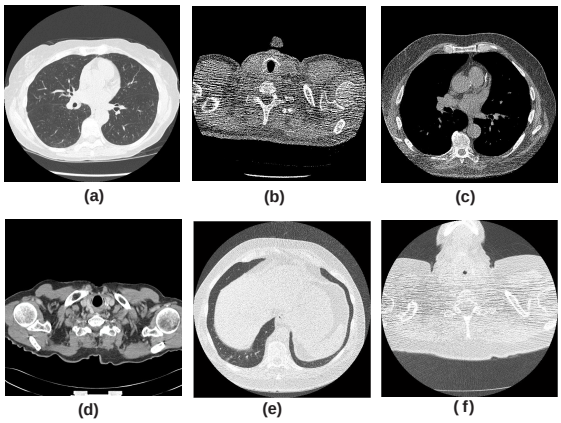

Figure 5.3: Original computed tomography image data set

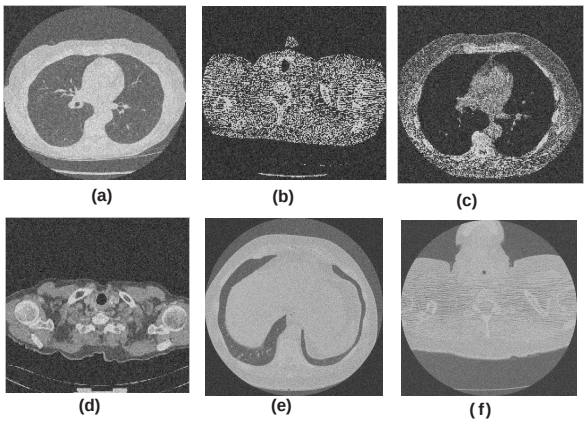

Figure 5.4: Noisy computed tomography image data set σ=20

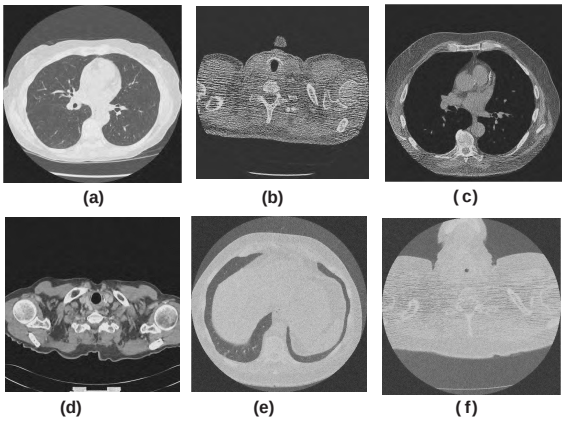

Figure 5.5: Results of LLSURE

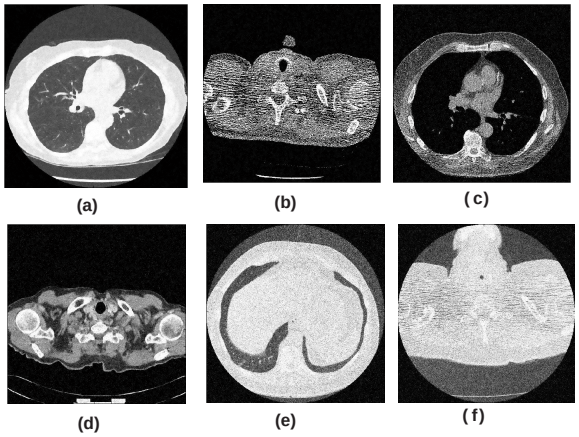

Figure 5.6: Results of NLM filtering

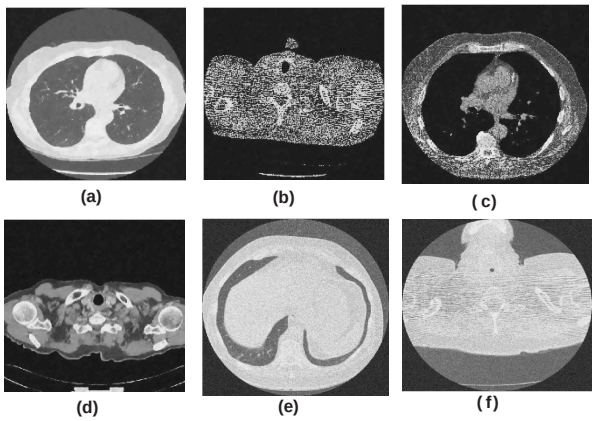

Figure 5.7: Results of NLFMT

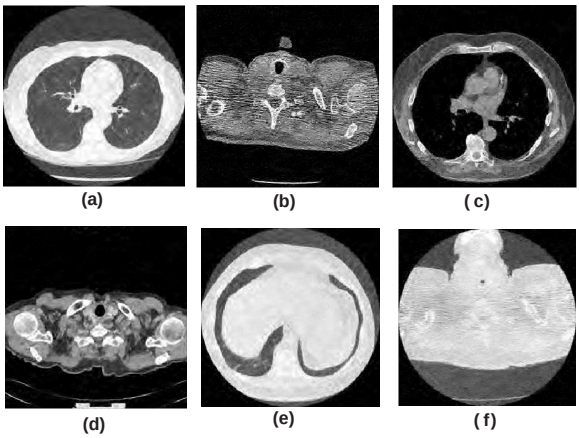

Figure 5.8: Results of SURELET

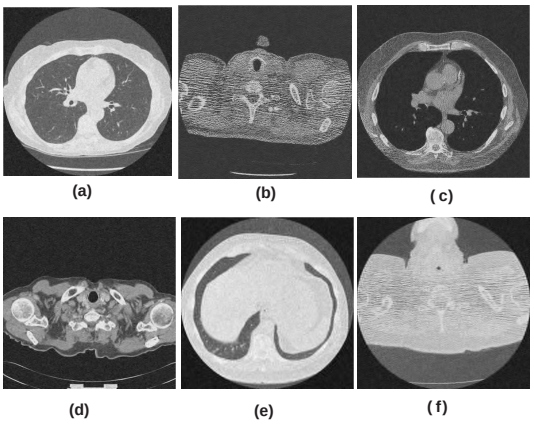

Figure 5.9: Results of Bayes thresholding

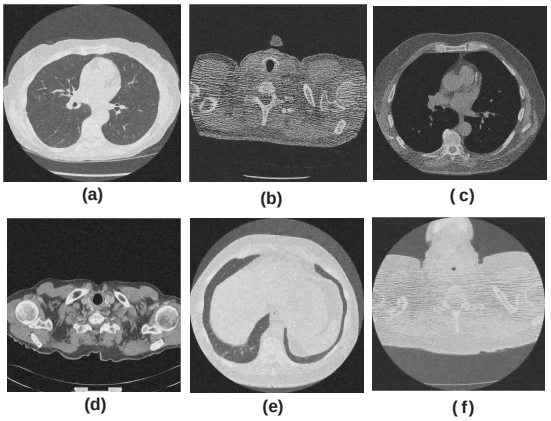

Figure 5.10: Results of Biorthogonal wavelet thresholding

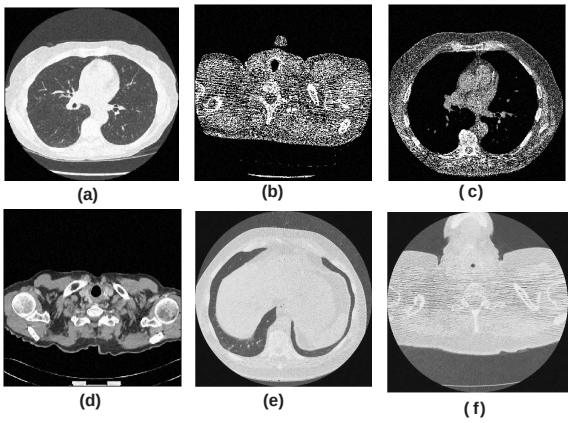

Figure 5.11: Results of CSBT scheme

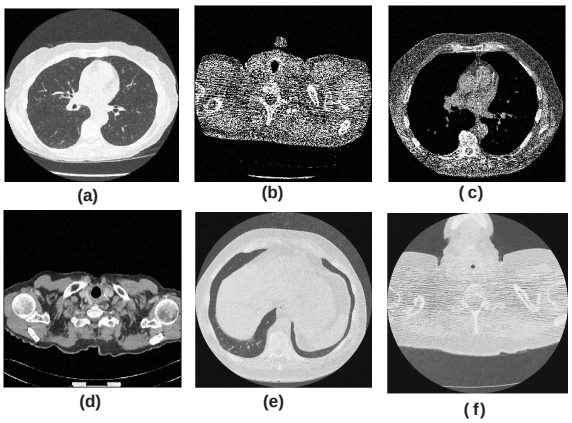

Figure 5.12: Results of NLM-WPT scheme

frequency subbands. The perfect optimization for estimating a threshold value is an almost impossible task for image denoising. Thus as an alternative, an iterative method [56] is used to get an optimum threshold value for each coefficient. To accomplish this, we made several high-frequency tetrolet subbands by shifting the coefficient position in the direction of x- and/or y-axis circularly which are known as shifted copies of respective high-frequency tetrolet subbands. These shifted high frequency subbands are thresholded separately by applying locally adaptive shrinkage rule using estimated threshold value and averaged to get the final denoised coefficients.

In circular shift based tetrolet thresholding (CSBT) scheme, a thresholding shrinkage rule [50] has been used to denoised high frequency tetrolet subbands which helps to avoid the limitations of both hard and soft thresholding. This function also helps to minimize the overall mean-squared error. To estimate the threshold value, BayesShrink method is applied using equation 2.2.29 and firm thresholding has been performed using equation 2.2.36 (discussed in chapter 2). After thresholding

process, all shifted copies of high frequency tetrolet subbands are restored by shifting coefficients into their original position and patch wise variance based weighted average is performed to get final thresholded high frequency tetrolet subbands. Finally, inverse tetrolet decomposition has been performed to obtain final denoised CT image.

The CSBT scheme comprises the following steps:

Step 1: Apply tetrolet decomposition on noisy input CT image to obtain low and high frequency subbands as follows:

a) Divide the image into 4x4 blocks.

b) Set the decomposition level and tetromino covering values (default, 117).

c) Find and store sparsest tetorlet representation of each block.

d) Rearrange low/high coefficients into 2x2 blocks and obtain low and high frequency subbands .

e) Decomposition on low frequency subband:

- Decomposition on low frequency subbands are performed. Decomposed subbands are known as child node for respective parent node.
- Calculate the entropy as a cost function [131] of each child nodes as well as parent nodes.
- In top down approach manner, check the cost value. If the cost of parent node is greater than total cost of child nodes; continue further decomposition. Otherwise; Stop decomposition and eliminate children nodes.

Step 2: Prepare k number of shifted copies of high frequency tetrolet subbands by shifting the coefficient positions in the direction of the x- and/or y-axis circularly.

$$X'(i,j)_{s^\gamma} = circular\_shift\{X(i,j)_s, [i_{shift}, j_{shift}]\} \tag{5.3.3}$$

where $\gamma = 1....k$, the value of k depends on the length of respective high frequency tetrolet subband.

Step 3: For each decomposition level (L):

(a) Calculate local noise variance using equation (2.2.30)

(b) For each tetrolet coefficients in each subbands (s):

(i) Compute threshold value λ_1 using equation (2.2.29)

(ii) Compute threshold value λ_2, by setting $\lambda_2 = 0.9.\lambda_1$

(iii) Apply shrinkage rule using equation (2.2.36)

Step 4: After thresholding on each subbands, perform the inverse shift. The resulting thresholded high frequency tetrolet coefficients ($\hat{X}'(i,j)_{s^\gamma}$) are shifted back to the original position and store the multiple high frequency tetrolet modified subbands.

$$X''(i,j)_{s^\gamma} = circular\_shift\{\hat{X}'(i,j)_{s^\gamma}, [-i_{shift}, -j_{shift}]\} \tag{5.3.4}$$

Step 5: To get final denoised high frequency tetrolet subbands, perform patch wise variance based weighted average on multiple high frequency tetrolet modified subbands [63], as given below:

$$\hat{X}(i,j)_s = \sum_{\gamma=1}^{k} \alpha_{s^\gamma}.X''(i,j)_{s^\gamma} \tag{5.3.5}$$

where, $\alpha_{s^\gamma} = \frac{var^{-1}(X''_{w,s^\gamma})}{\sum_{\gamma=1}^{k} var^{-1}(X''_{w,s^\gamma})}$, $var^{-1}(.)$ represents inverse of the variance, $\hat{X}(i,j)_s$ is the final thresholded value for the coefficient at position (i,j) in the subband s and w is local neighborhood which is used to calculate the local variance.

Step 6: Perform inverse tetrolet decomposition, to get the final denoised CT image.

5.3.2 NLM and circular shift based wavelet packet thresholding (NLM-WPT) scheme

In NLM and circular shift based wavelet packet thresholding (NLM-WPT) scheme, the NLM filter is used to suppress the noise from noisy input CT images. In NLM filter, the images are denoised using weight values which are obtained using similar local patches. However on noisy image, the NLM filter provides sharp and smooth image, but it blurs the edges as the noise level increases. Due to blurring, some sophisticated image details may be removed. Therefore, the method noise concept is used in the proposed framework to recover the missing details from the noisy images. Hence, the difference of input noisy CT image (X) and NLM filtered image (R_1) is obtained. The difference image (G) consists of noise as well as image details along with some edges. Hence, the difference image (G) can be considered as a combination of noise and sharp image details.

Now, the approach suppresses the noise from the difference image (G) and preserve the edges that are removed by NLM filter. The wavelet packet thresholding is performed over the difference image (G). Here, Bayes estimation method is used to

select the threshold value. The thresholding has been performed using soft thresholding function. The block diagram of NLM and circular shift based wavelet packet thresholding (NLM-WPT) scheme is shown in figure 5.2.

The main steps of second proposed framework are summarized, as follows:

Step 1: Apply NLM filter on noisy input CT image to get sharp and smooth image (R_1).

Step 2: Subtract NLM filtered image (R_1) from noisy input CT image (X), and get the difference image G.

Step 3: Apply wavelet packet decomposition on G to get the low and high frequency subbnads for noise suppression and missing structure preservation. Here, low frequency component is not processed.

Step 4: Prepare k number of shifted copies of high frequency wavelet subbands by shifting the coefficient positions in the direction of the x- and/or y-axis circularly as shown in equation (5.3.3).

Step 5: For each decomposition level (L):

(i) Compute threshold value λ using equation (2.2.29)

(ii) Apply soft thresholding using equation (2.2.33)

Step 6: After thresholding on each subbands, perform the inverse shift as defined in equation (5.3.4).

Step 7: To get denoised high frequency wavelet subbands, perform patch wise variance based weighted average on multiple high frequency wavelet modified subbands

as defined in equation (5.3.5)

Step 8: Perform the inverse wavelet packet decomposition to get the filtered difference image (R_2).

Step 9: Perform addition on NLM filtered image (R_1) and filtered difference image (R_2) to get the denoised CT image.

5.4 Experimental results and Discussion

The proposed schemes (CSBT and NLM-WPT) are applied on several test CT images as shown in figure 5.3. Figure 5.4 is showing noisy test image data set with $\sigma = 20$.

With the motivation that in most of the cases, denoising is dependent on the neighbourhood pixels or coefficients, our scheme is designed where high frequency tetrolet coefficients are thresholded by changing neighbourhood coefficients using circular shifting and multiple thresholded high frequency subbands are obtained as discussed in proposed methodologies section. In CSBT scheme, two threshold values (λ_1 and λ_2) are used in thresholding function. The threshold value (λ_1) can be obtained using Bayes estimation method. Another threshold value (λ_2) is used to provide less sensitivity for small variations in the large coefficient values [99]. The value of (λ_2) should be between zero to λ_1. In first proposed scheme, all experimental results are obtained by setting the threshold value (λ_2) as $\lambda_2 = 0.9\lambda_1$. The results may slightly vary by setting different value of λ_2. The variation between multiple thresholded high frequency subbands can be observed by correlation values.

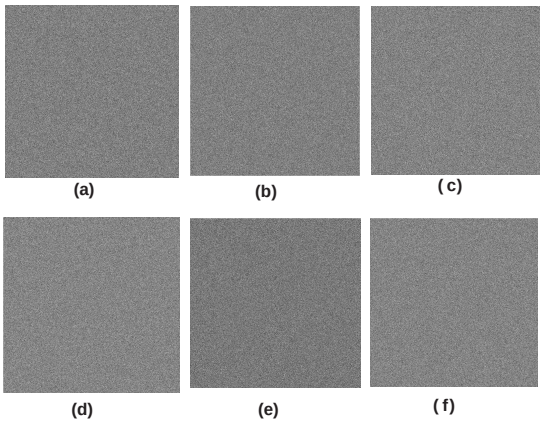

Figure 5.13: Difference between original and noisy image

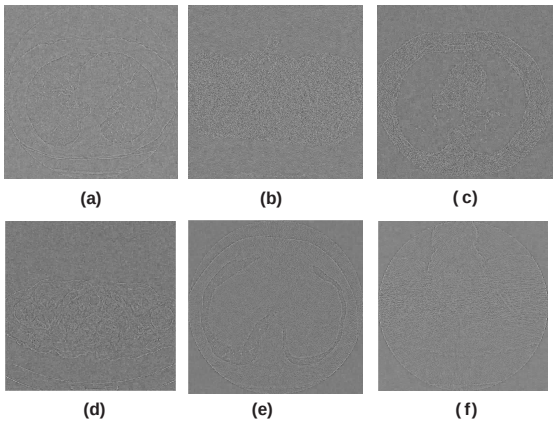

Figure 5.14: Difference between original and LLSURE filtered image

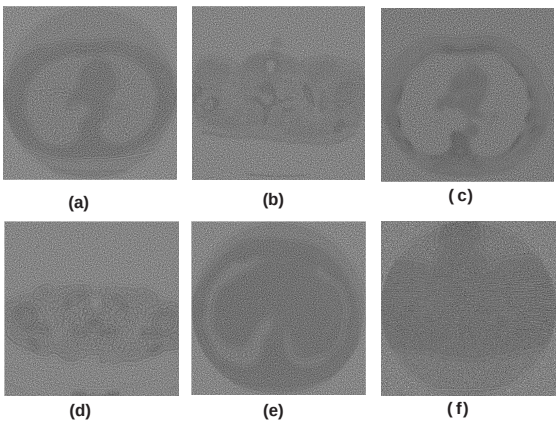

Figure 5.15: Difference between original and NLM filtered image

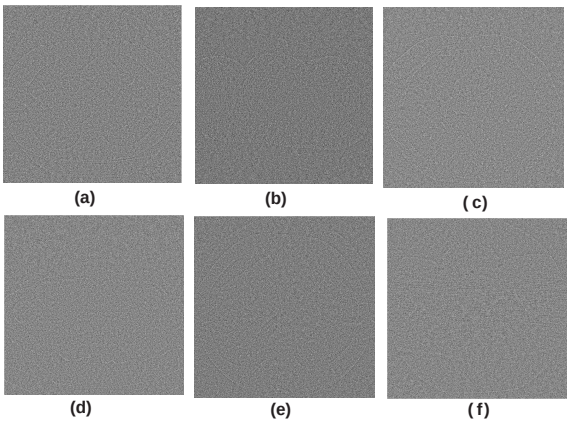

Figure 5.16: Difference between original and NLFMT denoised image

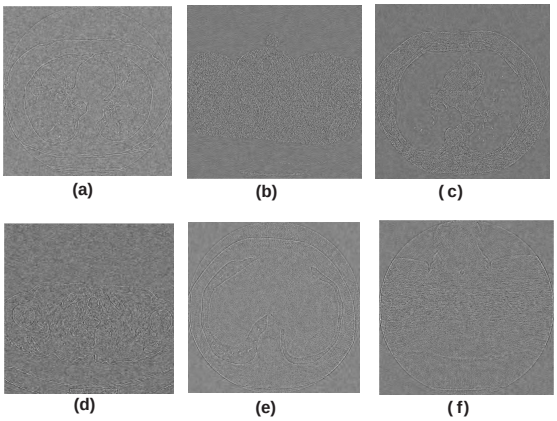

Figure 5.17: Difference between original and SURELET filtered image

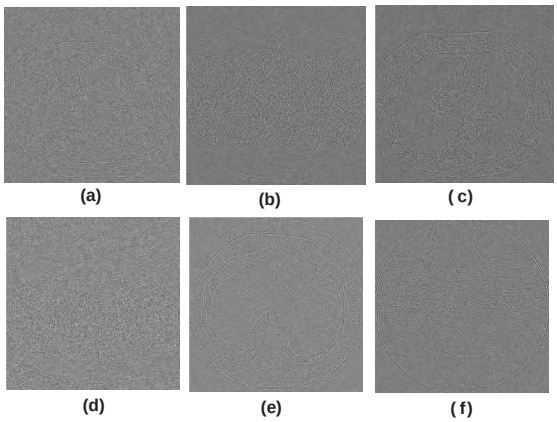

Figure 5.18: Difference between original and Bayes denoised image

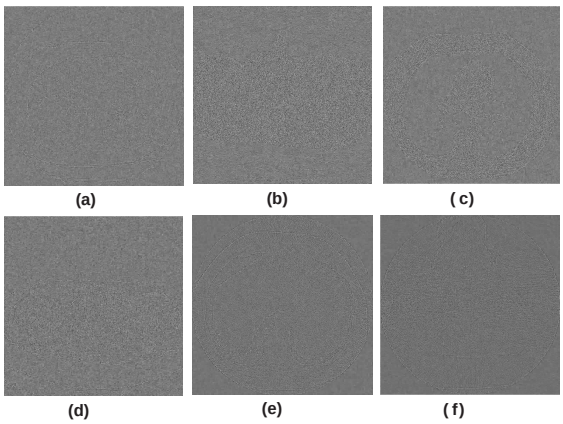

Figure 5.19: Difference between original and biorthogonal wavelet based denoised image

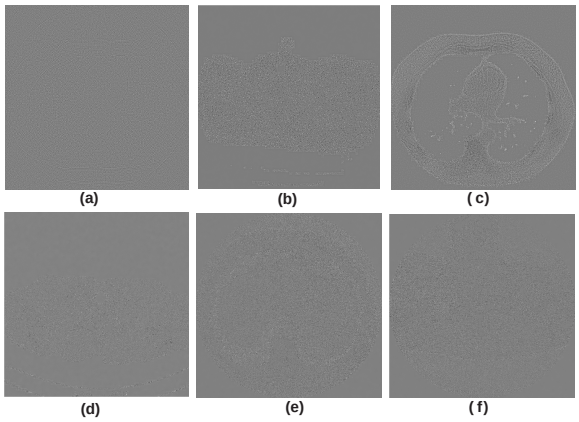

Figure 5.20: Difference between original and CSBT scheme based denoised image

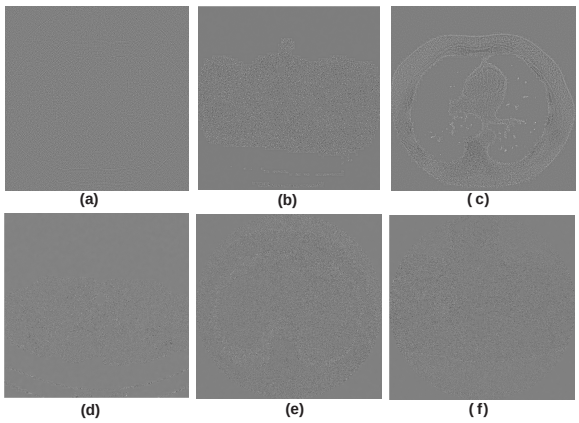

Figure 5.21: Difference between original and NLM-WPT scheme based denoised image

To achieve maximum edge preserving and effective noise reduction, patch wise variance based weighted average is performed on multiple thresholded high frequency subbands where the patch size is used as 3x3. Using inverse tetrolet decomposition, final denoised image is obtained.

In NLM-WPT scheme, several parameters are used for NLM filtering such as patch size (7x7) and window search size (21x21). Here, the parameter $h = .45\sigma_\eta$ is used for the experimental evaluation. The main concepts of NLM is to reduce the noise as much as possible and preserve the information of structures. From experimental analysis, it has been observed that the results are good for noise reduction and preserving the clinically relevant information using NLM but in view of original input image (noise-less image), some information seems to be lost. Figure 5.16 shows the difference between original input image (noise-less image) and NLM filtered image, which is indicating noise with small structures. These small structures indicate that further processing is required to obtain the complete structure with reduced noise. For further processing, method noise is one of the best concepts to reduce the noise and recover the missing structures. For better noise reduction and edge preservation, wavelet packet thresholding has been performed on the difference image (G) by using circular shifting. The concept of circular shift helped to obtain an optimum threshold value.

To validate the superiority of the proposed schemes, its performance is compared in terms of visual quality, MSE, PSNR and Image Quality Index (IQI) of the denoised

images using some standard existing methods. For strong comparison, both wavelet and non-wavelet based existing standard methods are used. The existing methods used for comparison are LLSURE [116], NLM filtering [17], NLFMT [77], SURELET [11], wavelet based Bayes thresholding using Daubechies 8 (DB8)[26] and medical image denoising based on soft thresholding using bi-orthogonal 1.3 (bior 1.3) multiscale wavelet transform [115].

Figures 5.5-5.12 are showing the results of LLSURE [116], NLM [17] filtering, NLFMT [77], SURELET [11], wavelet based Bayes thresholding [26], medical image denoising based on soft thresholding using biorthogonal multiscale wavelet transform [115], CSBT scheme and NLM-WPT scheme respectively. The image quality is measured by visual inspection as there is no generally accepted objective way to judge the image quality of a denoised image. There are two criteria widely used in the literature are: (1) visibility of the artifacts and (2) preservation of edge details. The performance of LLSURE method as shown in figure 5.5, is not satisfactory, specially in homogenous regions and near the edges. The method of NLM filtering as shown in figure 5.6, provides smoother edge preserved results in homogenous regions. For higher noise level, edge preservation of small detail parts are not satisfactory for clinical purpose. The results of NLFMT denoising as shown in figure 5.7, give edge preserved smooth denoised images but texture is not as good as for clinical purpose. The results of SURELET, wavelet based denoising using Bayes thresholding and Biorthogonal wavelet thresholding as shown in figures 5.8-5.10 respectively are providing smoother edge preserved

results in homogenous regions. As the noise level increases, Bayes and Biorthogonal wavelet thresholding methods failed to provide the smooth data over the homogenous regions. SURELET also get failed to provide satisfactory results on the edges over the higher noise level.

The proposed schemes (CSBT and NLM-WPT) perform several intermediate results using variation and averaging on high frequency coefficients to get final denoised image. The proposed denoising method employs a locally adaptive thresholding where all coefficients of each high-frequency subbands are thresholded using the coefficients in their local neighborhoods. It is observed that the results of proposed schemes (CSBT and NLM-WPT) provide better outcomes for effectively noise reduction and edge preservation of the CT images. Figure 5.13 shows the difference between the original and noisy images. Figures (5.14-5.21) show the results as the difference between the original images and the filtered ones for each method where visually it can be observed that proposed scheme gives better outcomes in most of the cases. Table 5.1 shows PSNR (in dB) and IQI values of the denoised images relative to their original images for proposed (CSBT and NLM-WPT) and existing methods. The best values amongst all the methods are represented in bold. The results shown in table 5.1 demonstrate that in most of the cases, the NLM-WPT scheme is superior to all other methods.

Table 5.1: PSNR and IQI of Proposed (CSBT and NLM-WPT) and Existing schemes for CT image denoising

		PSNR				IQI			
Image	σ	10	20	30	40	10	20	30	40
CT1	LLSURE [116]	32.09	27.45	25.01	23.64	0.9968	0.9019	0.8864	0.8670
	NLM [17]	31.11	28.02	26.25	24.49	0.9952	0.9174	0.8942	0.8711
	NLFMT [77]	32.05	28.30	26.49	24.01	0.9976	0.9175	0.8831	0.8540
	SURELET [11]	31.41	28.01	26.12	24.57	0.9951	0.9168	0.8941	0.8702
	Bayes [26]	32.19	28.28	26.51	24.01	0.9971	0.9147	0.8832	0.8521
	Bior [115]	32.23	28.41	26.54	24.33	0.9973	0.9139	0.8812	0.8510
	CSBT	**32.78**	28.61	27.85	24.89	**0.9995**	0.9292	**0.8969**	0.8838
	NLM-WPT	32.72	**28.67**	**27.36**	**24.97**	0.9993	**0.9298**	0.8949	**0.8841**
CT2	LLSURE [116]	32.12	28.32	26.20	24.01	0.9971	0.9028	0.8953	0.8669
	NLM [17]	31.69	28.19	26.28	23.51	0.9975	0.9050	0.8721	0.8611
	NLFMT [77]	32.04	28.48	26.50	24.42	0.9973	0.9061	0.8801	0.8506
	SURELET [11]	31.07	28.12	26.21	24.71	0.9952	0.9168	0.8962	0.8712
	Bayes [26]	32.09	28.29	26.47	24.09	0.9976	0.9154	0.8851	0.8552
	Bior [115]	32.21	28.13	26.39	24.31	0.9961	0.9148	0.8863	0.8521
	CSBT	32.78	**29.23**	27.18	24.87	0.9991	**0.9181**	0.8993	0.8871
	NLM-WPT	**32.87**	29.09	**27.20**	**24.96**	**0.9993**	0.9081	**0.8999**	**0.8875**
CT3	LLSURE [116]	31.01	28.13	26.32	24.11	0.9941	0.8801	0.8781	0.8649
	NLM [17]	31.22	29.07	26.29	23.87	0.9979	0.9080	0.8832	0.8642
	NLFMT [77]	32.01	28.01	26.29	24.01	0.9984	0.8960	0.8728	0.8572
	SURELET [11]	31.41	29.03	27.14	24.89	0.9950	0.8920	0.8705	0.8613
	Bayes [26]	31.89	28.21	26.52	24.41	0.9947	0.9073	0.8837	0.8609
	Bior [115]	31.78	28.39	26.87	24.59	0.9933	0.9061	0.8828	0.8660
	CSBT	**32.11**	29.41	27.07	24.88	**0.9987**	0.9084	0.8872	0.8657
	NLM-WPT	32.08	**29.48**	**27.16**	**24.97**	0.9961	**0.9089**	**0.8879**	**0.8663**
CT4	LLSURE [116]	30.39	28.01	26.10	24.51	0.9942	0.8998	0.8709	0.8553
	NLM [17]	31.43	28.78	26.21	24.01	0.9943	0.9031	0.8789	0.8601
	NLFMT [77]	30.62	28.09	26.61	24.46	0.9962	0.8914	0.8682	0.8565
	SURELET [11]	31.01	28.04	26.24	24.21	0.9953	0.9012	0.8869	0.8659
	Bayes [26]	30.72	28.47	26.45	24.25	0.9976	0.9023	0.8843	0.8636
	Bior [115]	30.93	28.61	26.53	24.59	0.9978	0.9043	0.8813	0.8661
	CSBT	**31.78**	28.81	26.65	24.71	**0.9983**	0.9052	0.8889	0.8691
	NLM-WPT	31.43	**28.89**	**26.68**	**24.78**	0.9979	**0.9059**	**0.8892**	**0.8693**
CT5	LLSURE [116]	31.61	28.48	26.64	23.84	0.9971	0.8812	0.8633	0.8567
	NLM [17]	31.12	27.98	25.19	23.91	0.9934	0.8966	0.8712	0.8533
	NLFMT [77]	30.72	28.11	26.32	23.97	0.9932	0.8734	0.8609	0.8598
	SURELET [11]	31.21	28.31	26.73	24.16	0.9953	0.9012	0.8769	0.8619
	Bayes [26]	31.65	28.75	26.32	24.21	0.9960	0.8912	0.8873	0.8610
	Bior [115]	31.69	28.60	26.54	24.31	0.9967	0.8971	0.8867	0.8601
	CSBT	**31.96**	**28.83**	**26.93**	24.31	**0.9981**	**0.9099**	**0.8896**	0.8623
	NLM-WPT	31.93	28.79	26.88	**24.37**	0.9979	0.9097	0.8812	**0.8625**
CT6	LLSURE [116]	31.11	28.81	26.44	23.56	0.9965	0.8909	0.8616	0.8407
	NLM [17]	31.32	28.97	26.75	23.71	0.9943	0.9078	0.8702	0.8653
	NLFMT [77]	32.14	28.91	26.21	24.33	0.9961	0.9017	0.8714	0.8575
	SURELET [11]	31.31	28.45	26.66	24.67	0.9948	0.9013	0.8709	0.8617
	Bayes [26]	31.22	28.71	26.52	24.34	0.9977	0.9064	0.8811	0.8672
	Bior [115]	31.17	28.68	26.73	24.49	0.9971	0.9001	0.8898	0.8688
	CSBT	32.18	**29.17**	26.76	24.65	0.9969	**0.9118**	0.8901	0.8681
	NLM-WPT	**32.23**	28.67	**26.81**	**24.71**	**0.9971**	0.9108	**0.8903**	**0.8691**

5.5 Conclusions

In this chapter, two (CSBT and NLM-WPT) schemes have been discussed for CT image denoising. In CSBT scheme, thresholding is performed based on the Bayes shrinkage rule in tetrolet domain using circular shift concept. In NLM-WPT scheme, NLM filtering and circular shift based wavelet packet thresholding is performed using method noise concept. However, CSBT scheme is performed well in comparison to existing methods. But most of the times, NLM-WPT scheme is giving better PSNR and IQI values in comparison to CSBT and other existing schemes. Apart from PSNR and IQI, the visual quality of proposed scheme over the CT images is better in terms of clinically relevant details. Due to the dependency on neighborhood pixels, the locally adaptive Bayes shrinkage rule in wavelet domain is performed well in terms of noise suppression and edge preservation. Therefore, in the next chapter, two CT image denoising schemes are performed for better noise suppression and edge preservation using inter and intra scale dependencies based shrinkage rule.

CHAPTER 6

Inter and intra scale dependencies based CT image denoising

Chapter 6

Inter and intra scale dependencies based CT image denoising

In the previous chapter, the visual quality of CT image is not very pleasant, especially for higher noise level. To resolve that, in this chapter, two CT image denoising schemes have been presented based on the dependency of the pixels where the first proposed work is based on intra-scale dependency and the second proposed work is based on inter-scale dependency.

6.1 Introduction

This chapter is devoted for CT image denoising based on the concept of inter-scale and intra-scale dependencies in wavelet domain. Transform based denoising has achieved good results over the last few decades. Wavelet shrinkage algorithms can be generally summarized into three steps: i) apply a wavelet transform on the input noisy image; ii) modify the wavelet coefficients; iii) apply inverse wavelet transform on the modified coefficients. Therefore, there are mainly two areas which affect the performance of the denoising under the wavelet domain framework. First is to find more appropriate wavelet transform and the other is to design better modification strategies for wavelet

coefficients.

In existing literature [37, 139], it can be found that directional wavelet transforms have successfully boosted the denoising performance where as two-dimensional separable wavelet transforms are not upto the mark to represent other discontinuities such as contours and edges in images [139]. Many other directional transforms have also been developed such as tetrolet [76], dual-tree complex wavelet [105], curvelet [35], contourlet [37] and directionlet [139]. From various directional transforms, the dual-tree complex wavelet transform has also received a great deal of attention in denoising since it offers directionality and shift invariance with low computational complexity [118]. For the modification of wavelet coefficients, numerous strategies have been presented to improve denoising performance. These strategies can be broadly categorized into two categories: i) intra-scale dependency based denoising, and ii) inter-scale dependency based denoising. In intra-scale dependency based denoising [106], the wavelet coefficients are modified with in same scale. SureShrink, BayesShrink and VisuShrink are the popular methods [39] of intra-scale dependency based denoising where SureShrink and BayesShrink provide better performance than the VisuShrink. The inter-scale dependence defines that if parent coefficients are large, then its child coefficients are also large. With this consideration, the wavelet coefficients are modified across the scale. The dependency between parent and child coefficients provides better denoising performance. Sendur et al. [127] have developed a wavelet shrinkage

technique based on Maximum a-Posteriori (MAP) estimator to estimate the bivariate prior of a coefficient and its parent as a circularly symmetric Laplacian model. Wavelet transform based thresholding shows remarkable results and outperform those derived from the independent assumption. The main concept of shrinkage based noise reduction using the wavelet transform is to compute the wavelet decomposition of the noisy image and modify the obtained wavelet coefficients. Coefficients that are below the threshold value are replaced by zero. The resulting denoised image can be achieved using inverse wavelet transform.

In image denoising, CT images can be denoised directly without access to raw data. CT image denoising is a challenging task because of finding correct noise variation, relationship between coefficients and achieving an optimal trade-off between denoising and blurring or artifacts. To surmount these challenges, we proposed two CT image denoising schemes using dependency on the wavelet coefficients. However, it has been analyzed that each wavelet coefficients are affected with different patch size. With different patch sizes, the estimated threshold value may not be the same and may affect images in terms of local features and noise. With this consideration, the first scheme of this chapter is proposed based on the intra-scale dependency where threshold value is estimated by using different patch sizes of the image. The second scheme is proposed based on the concept of the inter-scale dependency where CT image denoising is performed using dual-tree complex wavelet transform, which combines the advantages of Bivariate shrinkage and Bilateral filter.

This chapter is organized as follows. Section 6.2 gives a brief overview of Bilateral filtering. In section 6.3, the proposed methods are presented in details. Experimental results, including a comparison with other denoising methods, are given in section 6.4. Finally, some discussions and conclusions are summarized in section 6.5.

6.2 Bilateral filtering

Bilateral filter is a local, non-linear and non-iterative edge preserving filter, introduced by Tomasi and Manduchi [136]. It has two filter kernels, first is a spatial filter kernel which behaves like a classical low-pass filter and other is an edge stoping function which attenuates the filter kernel when the intensity difference between the pixels is large. In Bilateral method, spatial filter kernel is used to get the geometric closeness between two pixels. Similarly, edge stoping function is used for gray level similarity between two pixels. Both filter kernels are based on Gaussian distribution, where the weights of filter depend on not only Euclidean distance but also on the distance in gray space. The advantage of Bilateral filter is that it provides smooth and edge preserved images using neighboring pixels. The Bilateral filter output $B_f(p)$ at a pixel location p is calculated as follows:

$$B_f(p) = \frac{1}{W}\sum_{q\in w} E_{\sigma_w}(\|p-q\|).E_{\sigma_r}(\mid B(p)-B(q)\mid)B(q) \tag{6.2.1}$$

where, $E_{\sigma_w}(\|p-q\|) = e^{-\frac{\|p-q\|^2}{2\sigma_w^2}}$ is a geometric closeness function,

$E_{\sigma_r}(\mid B(p)-B(q)\mid) = e^{-\frac{|B(p)-B(q)|^2}{2\sigma_r^2}}$ is a gray-level similarity/ edge-stopping function,

$W = \sum_{q \in w} E_{\sigma_w}(\|p-q\|).E_{\sigma_r}(\mid B(p) - B(q) \mid)$ is a normalization constant, $\|p-q\|$ is the Euclidean distance between p and q, w is a spatial neighborhood of p, σ_w and σ_r control the behaviour of Bilateral filtering. The value of σ_w is chosen based on desired amount of low-pass filtering. Similarly, the value of σ_r is chosen based on desired amount of an edge to be preserved.

6.3 Proposed Methodologies

In this section, two algorithms are discussed for CT image denoising. In first proposed algorithm, a novel edge preserving image denoising technique using wavelet transform has been presented. This work is divided into two phases. In first phase, an input CT image is separately denoised using different patch size where denoising is performed based on thresholding and its method noise thresholding. The outcome of first phase provides more than one denoised images. In second phase, block wise variation based aggregation is performed in wavelet domain. In second proposed algorithm, a new edge-preserving image denoising scheme has been developed based on Dual-tree Complex Wavelet Transform (DT-CWT), bilateral filtering and a locally adaptive thresholding method. In this scheme, the noisy image is decomposed into Complex Wavelet coefficients through DT-CWT. Low-pass subbands are modified using bilateral filter. High pass subbands are modified using locally adaptive thresholding based on inter scale statistical dependency, where the noise variance of noisy wavelet coefficients are estimated using a robust median estimator.

6.3.1 CT image denoising using locally adaptive patch-wise thresholding (LAPT) scheme

In thresholding, threshold value may be varying according to different patch sizes. With the consideration that the small variation of neighborhood size will not much affect the threshold estimated value, a new locally adaptive different patch size based thresholding (LAPT) scheme is proposed using an intra-scale dependency, where some limited patch sizes are selected. The patch sizes can be extracted as: If (m, n) is the size of image X, then for high frequency subbands first patch size will be $(i/2, j/2)$. Similarly, $(k-1)$ numbers of patch size of respective subbands can be generated by dividing previous patch size by 2. The LAPT scheme can be summarized as:

Step 1: Select the maximum size of input noisy CT image as, (m, n) where $m = 2^k$ and $n = 2^k$.

Step 2: Apply DWT on input image to obtain low frequency (A) and high frequency (D) subbands.

Step 3: Perform thresholding (T) separately using different patch size $(for \;\; i = 1 \;\; to \;\; k-1)$ on respective high frequency subbands, as below:

$$G_i = T(D_i, \lambda) \tag{6.3.2}$$

where, thresholding function T and threshold λ can be estimated using equations 2.2.33 and 2.2.29, respectively.

Step 4: Apply method noise using input high frequency (D) subband and thresholded high frequency subbands (G_i) as:

i) Subtract G_i from D and get F_i, as:

$$F_i = D - G_i \tag{6.3.3}$$

ii) Apply patch wise thresholding on F_i, as:

$$E_i = T(F_i, \lambda) \tag{6.3.4}$$

iii) Add G_i and E_i and get C_i, as:

$$C_i = G_i + E_i \tag{6.3.5}$$

Step 5: Apply inverse DWT, using low frequency (A) and modified high frequency (C_i) subbands. The output (R_i) comes in the form of $k-1$ denoised images.

Step 6: To obtain final denoised image, perform the following steps:

a) Separately apply DWT on R_i images to obtain their approximation (S_i) and detail parts (V_i).

b) Estimate the variance at each pixel of (S_i) using blocks of size 3x3.

c) Estimate the variance (Var) difference between all approximation parts of R_i, as below:

$$\tau = \frac{1}{k-2} \sum_{j=1}^{k-2} \alpha_j \tag{6.3.6}$$

where, $\alpha_j = Var(S_j) - Var(S_{j+1})$. The value of τ is normalized in the range [0 1] and used as a weight factor for the next process.

d) Variance difference based aggregation process is performed on approximation part using following relationship:

$$B_{final} = H + Q \tag{6.3.7}$$

where, $H = \frac{1}{k-1} \sum_{f=1}^{\frac{k-1}{2}} \frac{\tau}{f} S_f$, and $Q = \frac{1}{k-1} \sum_{g=\frac{k-1}{2}+1}^{k-1} (1 - (\frac{\tau}{k-g}))S_g$.

e) Variance based aggregation using correlation ($Corr$) is performed on detail parts using following relationship:

$$C_{final} = \begin{cases} \sum_{i=1}^{k-1} \beta^w V_m^w, & if, \quad corr(V_i, V_{i+1}) < T_h \\ V_1^w, & otherwise \end{cases} \tag{6.3.8}$$

Where, $\beta^w = \frac{Var^{-1}V_1^w}{\sum_{i=1}^{k-1} Var^{-1}V_i^w}$, V_i represents detail part of all first intermediate results (R_i), w represents block size and T_h represents a defined threshold value to differentiate between correlated and uncorrelated coefficients. The function Var^{-1} can be estimated as inverse variance.

Step 7: Apply inverse DWT using B_{final} and C_{final} to obtain final denoised image R.

In LAPT scheme, noisy CT image is denoised in wavelet domain where noise on high frequency coefficients of each subband in L level has been suppressed using Bayes shrink and method noise thresholding with different patch sizes. In method noise, the thresholded patch is subtracted with original patch. The outcome of subtraction is again thresholded and added into the thresholded original patch. This method noise thresholding process is used to observe, how much local features of clinical details are missing at the time of thresholding and can be recovered as shown in Step 4. With different patch size, separate multiple denoised images are obtained. To get final denoised image, DWT is separately performed on all denoised images. In approximation part of all denoised images, a weight value τ is estimated using variance difference between different denoised images. This weight value is incorporated into

denoised images and aggregation relationship has been performed as given in Step 6(iv). In detail part, patch wise correlation coefficient values are obtained between all denoised images. Correlation value lies in the interval [-1; 1], where 1 means perfect correlation, 0 no correlation, and -1 perfect anti-correlation. To find correlated and uncorrelated values, correlation values are normalized in the range of [0; 1]. The correlation values closer to 1 indicate that the similarity structure is present between the images. The lower values (near to 0) indicate that the corresponding value includes only noise and, therefore, can be suppressed. If correlation value is greater with a defined threshold (T_h) value then keep the largest patch size denoised coefficient value of subband, otherwise, perform variance based weighted average between all denoised coefficients of subband as given in Step 6(v). Thus, final denoised CT image can be obtained using inverse wavelet transform.

6.3.2 CT image denoising using Bilateral filtering and bivariate shrinkage rule (BFBS) scheme

In BFBS scheme, an inter-scale dependency based CT image denoising is performed where DT-CWT is used to decompose the input image into low and high frequency subbands. Low frequency subbands are denoised using Bilateral filtering. To denoise high frequency subbands, a locally adaptive thresholding is performed using bivariate shrinkage function.

To denoise the high frequency subbands, a local adaptive thresholding is performed using Bivariate shrinkage function. Let, Y_{2k} represents the parent of Y_{1k} (Y_{2k} is

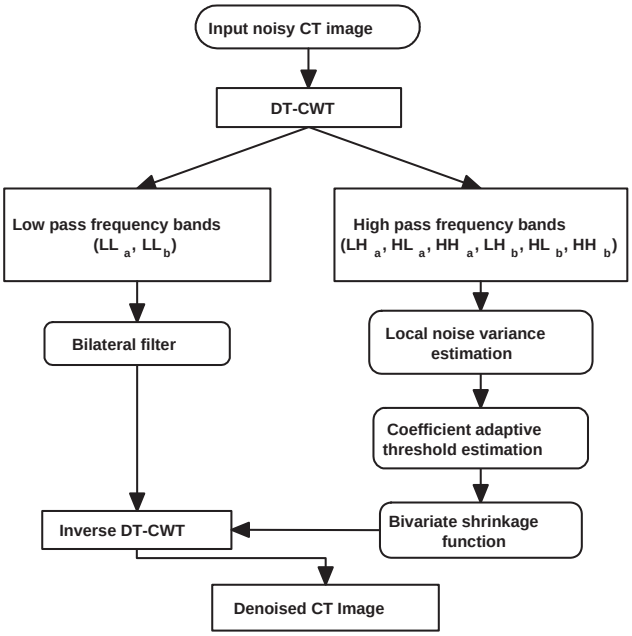

Figure 6.1: BFBS scheme

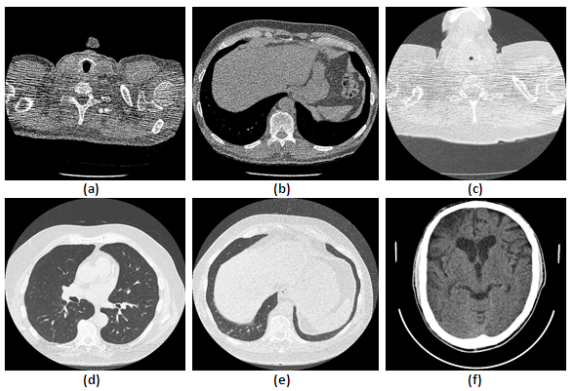

Figure 6.2: Data set of original CT images

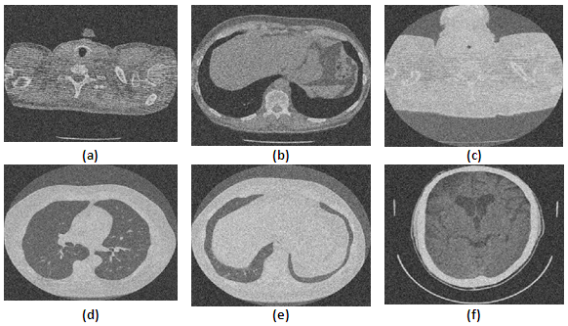

Figure 6.3: Data set of noisy CT images σ=20

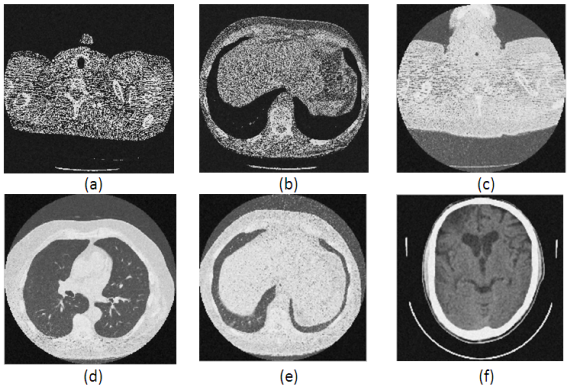

Figure 6.4: Results of Bilateral filtering method(BFM)

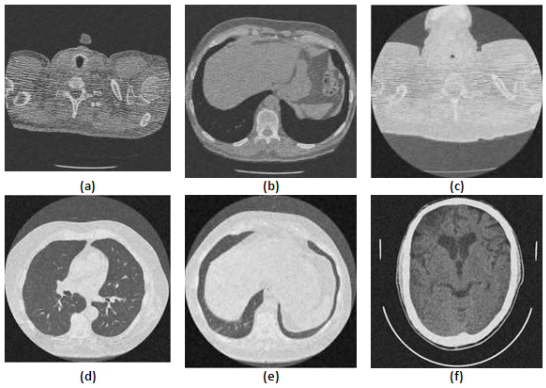

Figure 6.5: Results of wavelet based Bayes thresholding (WBT)

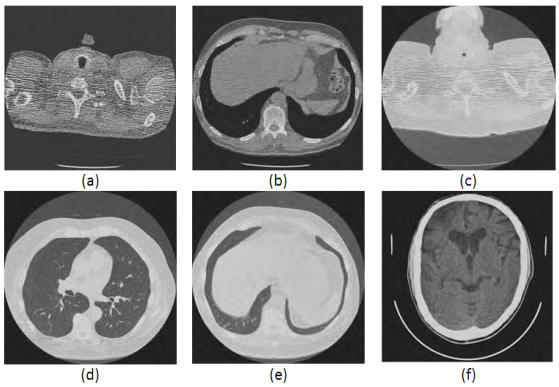

Figure 6.6: Results of wavelet based Bivariate thresholding (WBIV)

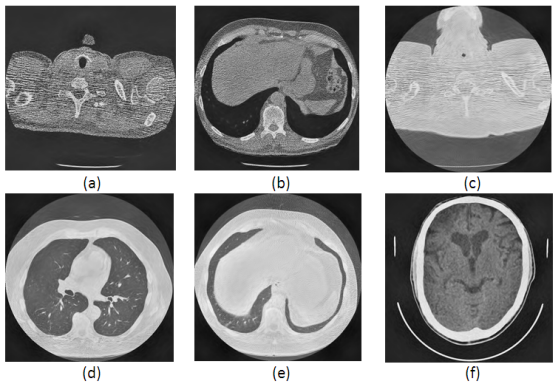

Figure 6.7: Results of LAPT scheme

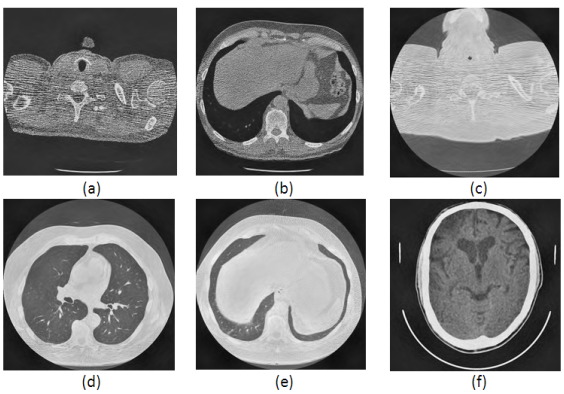

Figure 6.8: Results of BFBS scheme

the complex wavelet coefficient at the same position as the k-th complex wavelet coefficient Y_{1k}, but at the next coarser scale). Then

$$\begin{aligned} X_{1k} &= Y_{1k} + \eta_{1k} \\ X_{2k} &= Y_{2k} + \eta_{2k} \end{aligned} \tag{6.3.9}$$

where X_{1k} and X_{2k} are noisy complex wavelet coefficients, Y_{1k} and Y_{2k} are noiseless complex wavelet coefficients and η_{1k} and η_{2k} are additive noise coefficients. Equation (6.3.9) can be re-written as:

$$X_k = Y_k + \eta_k \tag{6.3.10}$$

where $Y_k = (Y_{1k}, Y_{2k})$, $X_k = (X_{1k}, X_{2k})$ and $\eta_k = (\eta_{1k}, \eta_{2k})$.

To denoise the coefficients of high frequency subbands, Bivariate shrinkage function [127] can be expressed as:

$$\hat{Y}_{1k} = \frac{(\sqrt{X_{1k}^2 + X_{2k}^2} - \lambda_k)_+}{\sqrt{X_{1k}^2 + X_{2k}^2}} . X_{1k} \tag{6.3.11}$$

The function $(a)_+$ is defined as:

$$(a)_+ := \begin{cases} 0, & if \quad a < 0 \\ a, & if \quad a > 0 \end{cases} \tag{6.3.12}$$

The term λ_k in eqn. (6.3.11) is the threshold for the k-th coefficient, computed as:

$$\lambda_k = \frac{\sqrt{3}\sigma_\eta^2}{\sigma_k} \tag{6.3.13}$$

In above equation, σ_η^2 and σ_k can be computed using equations 2.2.30 and 2.2.31 respectively.

The BFBS scheme as shown in figure 6.1 is summarized in the following steps.

Step 1: Perform the Dual Tree Complex Wavelet Transform (DT-CWT) on the noisy

CT image to get low and high frequency subbands.

Step 2: For each decomposition level, apply Bilateral filtering over the low frequency subbands.

Step 3: For each decomposition level

a) Calculate local noise variance σ_η^2 using equation (2.2.30)

b) For each coefficients of each high pass subbands

i) Compute the threshold λ_k using equation (6.3.13)

ii) Perform thresholding on each coefficient using equation (6.3.11)

Step 4: Apply inverse DT-CWT to get denoised image using filtered low and high frequency subbands .

6.4 Results and Discussion

The proposed (LAPT and BFBS) schemes are applied on several test CT images as shown in figure 6.2. Figure 6.3 is showing noisy test image data set with $\sigma = 20$. To evaluate the LAPT scheme, we can evaluate the total number of patch sizes as $k - 1$ i.e 8 and patch size can be expressed as: 256x256, 128x128, 64x64, 32x32, 16x16, 8x8, 4x4 and 2x2. Using these patch sizes, 8 denoised images are obtained separately. Hence, the aggregation is processed to get final denoised image using multiple denoised images. To aggregate the denoised images, correlation values are measured on high frequency subbands using block size 3x3 for all test images where a threshold value

(T_h) is set as 0.96. The value above the threshold can be considered as similarity, therefore large patch sizes of denoised coefficients are opted. For below than threshold value, variation based weighted average is used with block size 3x3. Similarly, variance

Table 6.1: PSNR and IQI of Proposed (LAPT and BFBS) and Existing schemes for CT image denoising

		PSNR				IQI			
Image	σ	10	20	30	40	10	20	30	40
CT1	BFM [136]	32.31	29.63	25.92	21.20	0.9947	0.9519	0.9013	0.8771
	WBT [106]	33.01	29.16	24.13	20.92	0.9953	0.9591	0.9191	0.8709
	WBIV [118]	32.11	28.56	26.31	21.43	0.9972	0.9838	0.9376	0.8848
	LAPT	32.91	29.56	**26.91**	21.64	0.9969	0.9802	**0.9412**	0.8902
	BFBS	**33.23**	**29.77**	26.31	**22.36**	**0.9989**	**0.9819**	0.9398	**0.8928**
CT2	BFM [136]	31.27	28.30	24.44	21.87	0.9952	0.9871	0.9722	0.8871
	WBT [106]	32.24	28.94	25.14	21.04	0.9912	0.9821	0.9691	0.8932
	WBIV [118]	31.46	28.62	24.81	21.63	0.9954	0.9812	0.9796	0.8981
	LAPT	32.36	28.96	**25.61**	21.43	0.9987	0.9895	**0.9812**	0.8992
	BFBS	**32.74**	**29.01**	25.31	**21.95**	**0.9991**	**0.9916**	0.9798	**0.9065**
CT3	BFM [136]	32.49	28.24	25.37	21.44	0.9961	0.9765	0.9081	0.8602
	WBT [106]	32.99	29.68	25.32	21.49	0.9934	0.9673	0.9172	0.8631
	WBIV [118]	32.37	29.92	26.63	22.21	0.9914	0.9826	0.9563	0.8610
	LAPT	32.97	29.76	26.73	22.32	0.9981	0.9856	0.9610	0.8723
	BFBS	**33.09**	**30.06**	**26.91**	**22.56**	**0.9971**	**0.9866**	**0.9683**	**0.8789**
CT4	BFM [136]	31.69	28.33	24.23	20.64	0.9982	0.9591	0.9111	0.8494
	WBT [106]	32.48	28.41	24.24	20.32	0.9916	0.9713	0.9425	0.8592
	WBIV [118]	32.40	28.21	25.37	20.45	0.9986	0.9791	0.9493	0.8602
	LAPT	32.56	28.06	24.87	20.39	0.9979	0.9789	0.9590	0.8791
	BFBS	**32.95**	**28.36**	**24.92**	**20.87**	**0.9991**	**0.9796**	**0.9597**	**0.8813**
CT5	BFM [136]	30.12	28.36	24.38	20.31	0.9908	0.9771	0.9461	0.8754
	WBT [106]	31.49	28.41	24.02	20.12	0.9961	0.9603	0.9365	0.8792
	WBIV [118]	31.11	28.77	24.21	20.61	0.9975	0.9811	0.9492	0.8804
	LAPT	31.05	28.35	24.11	20.87	0.9973	0.9819	0.9580	0.8918
	BFBS	**31.39**	**28.61**	**24.39**	**20.96**	**0.9982**	**0.9866**	**0.9591**	**0.8821**
CT6	BFM [136]	32.31	29.57	25.14	21.22	0.9971	0.9883	0.9703	0.8709
	WBT [106]	33.24	29.75	24.81	21.54	0.9912	0.9871	0.9690	0.8879
	WBIV [118]	32.61	28.93	25.72	21.78	0.9981	0.9891	0.9723	0.8813
	LAPT	33.15	29.13	25.09	21.69	0.9986	0.9897	0.9801	0.8968
	BFBS	**33.42**	**29.38**	**25.43**	**21.91**	**0.9993**	**0.9906**	**0.9865**	**0.8995**

difference based aggregation is performed on low frequency subband. Final output comes in the form of single denoised image. In BFBS scheme, several parameters for bilateral filtering are used such as patch size is 10x10, σ_w is 1.2 and σ_r is 0.13.

Instead of having one threshold for whole high frequency subbands, the threshold is computed for all the noisy coefficients in the respective subbands using Bivariate shrinkage function. The results may vary for different parameters.

To validate the superiority of LAPT and BFBS schemes, the performance of both schemes are compared in terms of visual quality, PSNR, and Image Quality Index (IQI) of the denoised images using the various methods available in literature such as Bilateral filtering method (BFM) [136], adaptive wavelet based denoising using Bayes shrinkage (WBT) [106] and wavelet based denoising using Bivariate shrinkage function (WBIV) [118]. Figures 6.4-6.8 are showing the results of Bilateral filtering method (BFM), Wavelet based denoising using Bayes shrinkage (WBT), wavelet based denoising using Bivariate shrinkage function (WBIV), LAPT and BFBS schemes, respectively. In Wavelet based thresholding methods, three levels of decomposition are used for fair comparison. Table 6.1 shows the PSNR (in dB) and IQI values of the denoised images relative to their original images using proposed and existing methods. Both, WBT and WBIV methods are providing smoother results in homogenous regions. But, as the noise level increases, WBT method fails to provide smoothed data over the homogenous regions and WBIV also fail to provide satisfactory results over the noisy edges. Both LAPT and BFBS schemes are giving better results in compare to WBT and WBIV methods. The best values amongst all the methods are represented in bold. The results shown in table 6.1 demonstrate that in most of the cases, the BFBS scheme is superior to all other methods. The results of LAPT

and BFBS schemes indicate improved texture, noise suppression and sharp preserved edges.

6.5 Conclusions

In this chapter, two (LAPT and BFBS) schemes are discussed for CT image denoising. In LAPT scheme, thresholding has been performed based on the Bayes shrinkage rule in DWT. In BFBS scheme, the Bivariate shrinkage rule and bilateral filtering has been used in dual-tree complex wavelet transform. However, LAPT scheme is performed well in comparison to existing methods. But most of the times, BFBS scheme is giving better PSNR and IQI values in comparison to LAPT and other existing schemes. Apart from performance metrics (PSNR and IQI), the visual quality of LAPT and BFBS schemes over the CT images is also better in terms of clinically relevant details. Due to more directions in wavelet transform, and simplicity of Bayes shrinkage rule, the image denoising is well performed. Therefore, in the next chapter, two new schemes are presented using bayes shrinkage rule with extended versions of wavelet transform.

CHAPTER 7

CT image denoising using extended versions of Wavelet transform

Chapter 7

CT image denoising using extended versions of Wavelet transform

From previous chapters, it can be analyzed that the impact of bilateral filter gives better quality images in terms of sharpness and smoothness. It has also been analyzed that more directions in wavelet transform gives better denoising performance over the CT images. Therefore in this chapter, two CT image denoising schemes are presented where first work is based on Wavelet and Curvelet transforms. While, the second work is based on Curvelet and Non-subsampled Contourlet transforms.

7.1 Introduction

This chapter is focused on CT image denoising method based on the combination with extended versions of Wavelet transforms. Currently, transform domain is one of the popular way to denoise the images such as Wavelet thresholding. The main strength of Wavelet thresholding is to estimate the true signals using estimation techniques and process on different frequency components of the image, separately.

To improve the problem of shift invariance, aliasing and poor directionality in traditional discrete wavelet transform, many other directional transforms have also

been used in image denoising. In the recent years a lot of research has been carried out to improve the treatment of geometric image structures. Curvelets [21], contourlets [37], shearlets [55], and directionlets [139] are wavelet systems with more directional sensitivity. From various directional transforms, curvelet and nonsubsampled contourlet transforms has received a great deal of edge-preservation and noise reduction because of it offers directionality and shift invariance with low computational complexity [35, 112]. However, Wavelet transform has a limitation of directions, which reflects as a less efficiency in sharp transitions such as line and curve singularities. To enhance this limitations, ridgelet transform has been proposed which provides the orientation of the linear edges but it fails to represent the two dimensional singularities. To overcome that, Curvelet transform has been come with smooth curves and better edge preservation. The Contourlet transform also provides better results for noise reduction and edge preservation but it has less directional features than Curvelets. From various directional transforms, curvelet and nonsubsampled contourlet transforms have received a great deal of interest in edge preservation and noise reduction because of it directional and shift invariance properties with low computational complexity.

For less computation time, Hanzouli et al. [57] introduced an improved robustness and an effective interpretational framework for image denoising on CT and PET images by using Hidden Markov Tree (HMT) model. This method is further extended with the combination of wavelet and contourlet transforms where outcomes

are visually better than wavelet based denoising and contourlet based denoising. For more sharp and smooth denoised images, the extended versions of wavelet transform is also used such as, Deng et al. [35] proposed a new scheme for CT image denoising in curvelet domain where Monte-Carlo algorithm is utilized to estimate the noise variance. Using estimated noise variance, a hard thresholding function was performed to get the denosied CT image. The result analysis indicates that edges are well preserved in denoised CT images.

To find a single transform that efficiently represents all such structural details is the demand of today. Many hybrid methods have been introduced that combine the features of more than one transform to create a denoised image that can better preserve the structural details. The combined transform based methodology is also introduced for better image enhancement such as, Pogam et al. [82] introduced a method for edge preservation based image denoising over the medical images. To overcome the limitations of wavelet, they combined wavelet and curvelet based denoising where noise suppression and edge preservation are improved. The results indicate that signal to noise ratio is increased and preservation of both mean intensity and local contrast are also improved. By combining two methods, Bhadauria et al. [9] also presented an efficient denoising scheme for CT images to enhance brain hemorrhage segmentation. They suggested a denoising approach which not only enhanced the visibility but also improved the hemorrhage detection capabilities from brain CT images. This approach utilizes the concept of both TV and curvelet transform-based

methods. The suggested scheme reduces the staircase effects using TV method and visual distortion by curvelet transform in the homogeneous region of the image. Further, Bhadauria et al. [10] also presented a noise reduction based on fusion concept for both computed tomography (CT) and magnetic resonance imaging (MRI). Both images are separately denoised by total variation (TV) method and denoised by curvelet based method. The edge information is also extracted from the noise residual of TV method by processing it through curvelet transform. Both denoised images are fused by using extracted edge information. The performance of the this approach is evaluated on real brain CT and MRI images and results show significant improvement not only in noise suppression but also in edge preservation.

Nonsubsampled contourlet transform (NSCT) based image denoising also proved more effective results over the wavelet based denoising methods. Xiao [45] proposed a method Steins unbiased risk estimate with a linear expansion of thresholds (SURELET) approach based image denoising using nonsubsampled contourlet transform (NSCT). Similarly, Ouyang et. al [112] proposed a method where noise deviation of the different sub-band are estimated based on the coefficients of different directional in NSCT domain, and the thresholds of every sub-band is estimated by Bayes threshold estimation method. After choosing the thresholds, a nonlinear thresholding function was chosen for image denoising where it was analyzed that NSCT domain generated better results than in compare to the wavelet domain.

With different shrinkage rules and different transforms, it cannot be surely

predicted that which one is better in terms of preserving edge, local features and noise reduction specially in case of medical images. With this consideration, this chapter discuss a new hybrid method for reduction of pixel noise with structure preserving using wavelet, Nonsubsampled Contourlet and curvelet transforms which combines the advantages of hard and soft thresholdings.

This chapter is organized as follows. In section 7.2, the proposed methods are presented in details. Experimental results, including discussions and comparison with other denoising methods, have been given in section 7.3. Finally, conclusions have been summarized in section 7.4.

7.2 Proposed Methodologies

In this section, two methods are discussed to denoise the CT images. The first proposed method is divided into two phases. In first phase, wavelet transform based denoisng is performed using bilateral filtering and thresholding. In second phase, a method noise thresholding based on Curvelet transform is performed using the outcome of first phase. In second proposed method, we developed a new edge preserving image denoising where noisy CT images are denoised using Non-subsampled Contourlet Transform (NSCT) and curvelet transform separately. By estimating variance difference on both denoised images, final denoised CT image has been achieved using a variance based weighted aggregation.

7.2.1 CT image Denoising based on Wavelet and Curvelet (WCurv) scheme

In this section, a scheme of CT image denoising is presented which combines the advantages of Wavelet and Curvelet transforms. The block diagram of the WCurv scheme is shown in figure 7.1. In WCurv scheme, wavelet transform is used to decompose an input image into low and high frequency subbands. The low frequency subband is filtered using Bilateral filtering. To denoise high frequency subbands, a threshold value is estimated and thresholding is performed. To estimate the threshold value, Bayesian method is used. Further, thresholding is performed using soft thresholding method. By using inverse wavelet transform, the first intermediate result is obtained. This first intermediate result is further processed to extract the missing edge information of the input noisy image. The noisy CT image (X) is subtracted from first intermediate result (G). To recover the maximum details such as edges, curvelet transform based thresholding is performed over subtracted image (F). Inverse curvelet transform gives an outcome of curvelet denoised image (H) which is added with first intermediate result (G) to get maximum extracted edges and denoised image (R).

Curvelet based thresholding

To denoise the noisy CT images (X), a shrinkage rule is performed using curvelet transform. Before performing shrinkage rule over the curvelet coefficients, the noise variance (σ_γ^2) of respective coefficients must be estimated. The noise estimation [10]

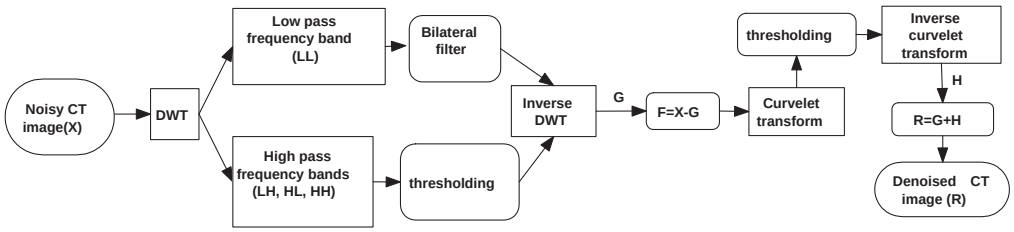

Figure 7.1: WCurv scheme

can be described as below:

$$\sigma_{\gamma}^{2} = \sqrt{\frac{\sum_{i=1}^{N}\sum_{j=1}^{N} X_{\gamma}^{Curvelet}.X_{\gamma}^{Curvelet^{*}}}{N^{2}}} \tag{7.2.1}$$

Using noise estimation, a hard thresholding function is performed over the curvelet coefficients, as given below:

$$R_{\gamma}^{Curvelet} := \begin{cases} X_{\gamma}^{Curvelet}, & \mid X_{\gamma}^{Curvelet} \mid \geq K\sigma\sigma_{\gamma} \\ 0, & Otherwise \end{cases} \tag{7.2.2}$$

where, $X_{\gamma}^{Curvelet^{*}}$ is a complex conjugate of $X_{\gamma}^{Curvelet}$, σ^{2} is estimated noise variance of (X) and K is the noise control parameter.

The WCurv scheme can be summarized with the following steps:

Step 1: Perform discrete wavelet transform (DWT) on input noisy CT image (X) to obtain approximation and detail parts.

Step 2: For each decomposition level, apply Bilateral filtering over the low frequency subband.

Step 3: Denoise the image using following steps:

i) Estimate noise variance using equation (2.2.30)

ii) Estimate threshold value using equation (2.2.29)

iii) Apply soft thresholding on detail parts using equation (2.2.33)

Step 4: Apply inverse discrete wavelet transform (Inverse DWT) to obtain denoised image (G).

Step 5: Subtract input noisy CT image (X) to denoised image (G) as, $F = X - G$

Step 6: Apply curvelet transform on F and perform following steps:

i) Calculate noise variance (σ_γ^2) using equation (7.2.1)

ii) Perform thresholding using equation (7.2.2)

Step 7: Apply Inverse curvelet transform to achieve the output image (H).

Step 8: Perform $R = G + H$, to achieve the final denoised image with improved edges.

7.2.2 CT image Denoising based on Nonsubsampled Contourlet and curvelet (NSCTCurv) scheme

In this section, a new scheme is presented to denoise the noisy CT images by combining the advantages of Nonsubsampled Contourlet Transform (NSCT) based thresholding and Curvelet transform based thresholding.

NSCT based thresholding

Due to the non-orthogonal property of NSCT, the noise variance contains different values for each direction on respective subbands [112]. Therefore, the noise is estimated independently for their respective subbands. In this work, the noise from

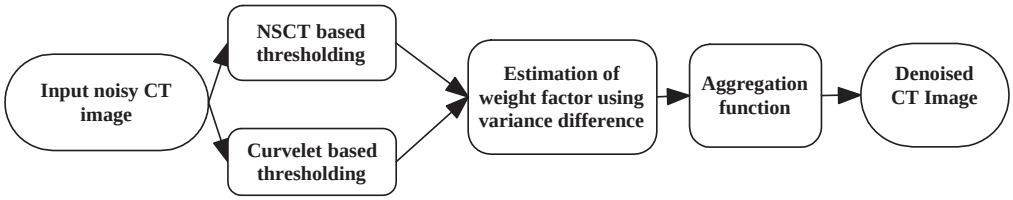

Figure 7.2: NSCTCurv scheme

each NSCT coefficients is estimated for each levels and directions. Further, denoising process is performed using a threshold value. For respective level L and direction D, a threshold value can be estimated using Bayes estimation method. To apply thresholding in NSCT domain, soft thresholding function is used.

The block diagram of the NSCTCurv scheme is shown in figure 7.2 and can be outlined with the following steps:

Step 1: Denoise the input noisy CT image by NSCT based thresholding (R_1) as well as curvelet transform based thresholding (R_2) separately, as given below:

a) For NSCT based thresholding:

i) Estimate noise variance using equation (2.2.30)

ii) Estimate threshold value using equation (2.2.29)

iii) Apply soft thresholding on detail parts using equation (2.2.33)

b) For curvelet transform based thresholding:

i) Calculate noise variance (σ_γ^2) using equation (7.2.1)

ii) Perform thresholding using equation (7.2.2)

Step 2: Estimate patch wise variance (Var_{R_1} and Var_{R_2}) at each pixel of denoised images R_1 and R_2.

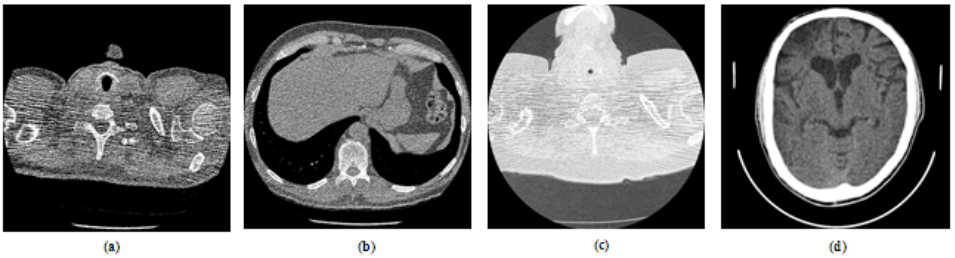

Figure 7.3: Data set of original computed tomography images

Step 3: Estimate the weight value using variance difference of both R_1 and R_2 images:

$$\alpha = \sqrt{(Var_{R_1})^2 - (Var_{R_2})^2} \tag{7.2.3}$$

Normalize α in the range [0,1].

Step 4: Apply aggregation function using an adaptive weight factor α, as shown the following equation:

$$R = \alpha.R_1 + (1 - \alpha).R_2 \tag{7.2.4}$$

where, R is denoised CT image.

7.3 Results and Discussion

The results of both (WCurv and NSCTCurv) schemes are evaluated on the noisy CT images as shown in figure 7.3. Figure 7.4 is the noisy CT image dataset where (σ)= 20.

In WCurv scheme, 2D DWT is performed to get low and high frequency subbands over the noisy input images. Low frequency subband is filtered using Bilateral method. In our results, several parameters for bilateral filtering are used such as

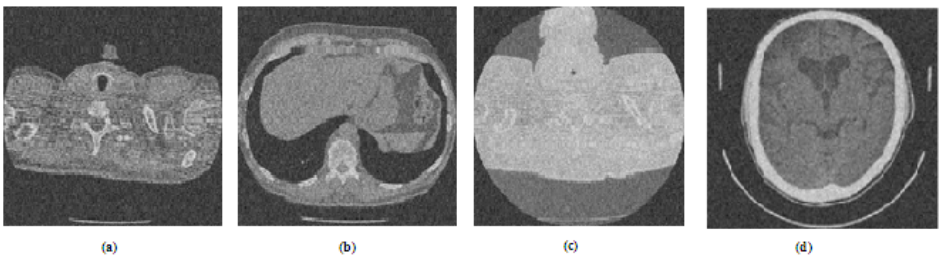

Figure 7.4: Data set of noisy computed tomography images(σ=20)

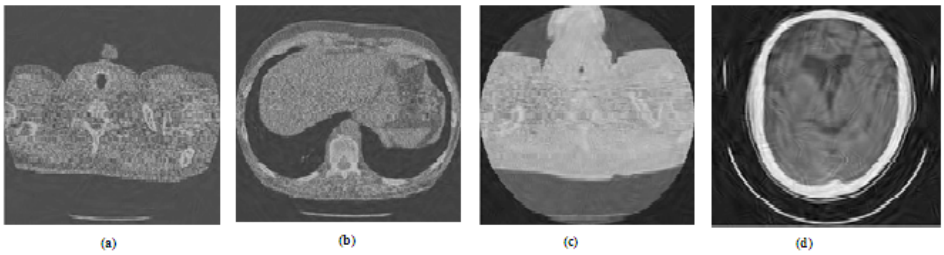

Figure 7.5: Results of curvelet based denoising (CBT)

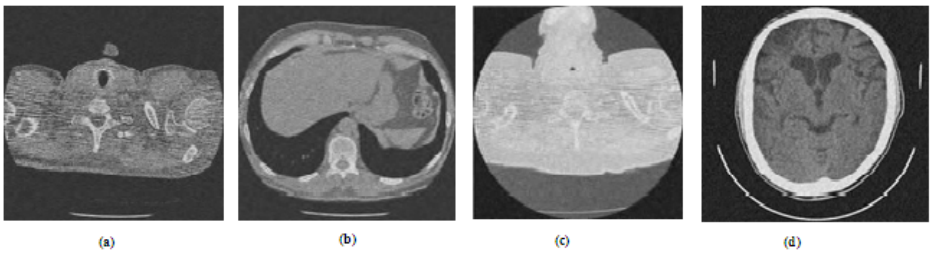

Figure 7.6: Results of dual-tree complex wavelet transform based bivariate thresholding (DTCWTBT)

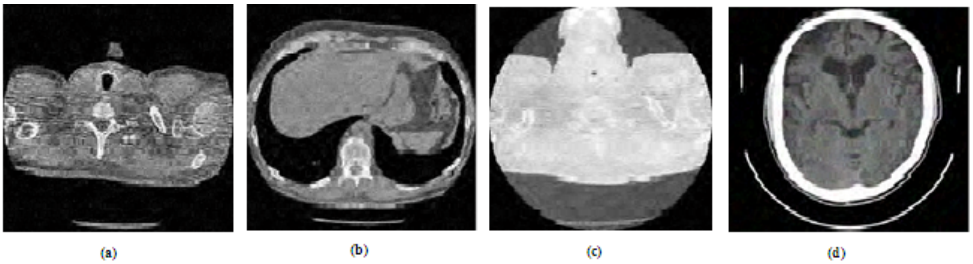

Figure 7.7: Results of NSCT based thresholding (NSCTBT)

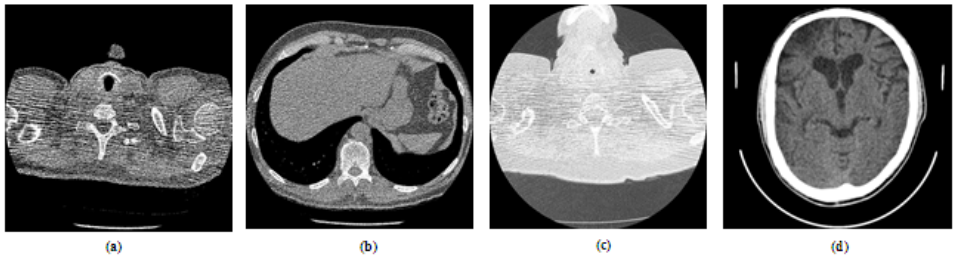

Figure 7.8: Results of WCurv scheme

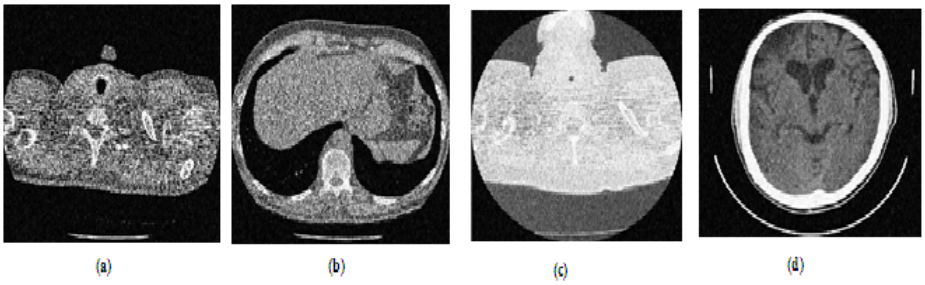

Figure 7.9: Results of NSCTCurv scheme

patch size is 10x10, σ_S is 1.2 and σ_r is 0.13. In high frequency subbands, threshold value is estimated and thresholded for their respective subbands as discussed in proposed methodologies. Inverse DWT, gives an reconstructed denoised image. But from experimental evaluations, it is observed that the edges are missing as the level of noise increases. To resolve that, curvelet transfrom is used via wrapping to extract more edge information. Over the subtracted image (F), curvelet based denoising as discussed in proposed methodologies have been performed. To obtain final denoised image (R), subtracted denoised image (H) and denoised image (G) are added.

In NSCTCurv scheme, the input noisy CT image is denoised using Nonsubsampled Contourlet Transform (NSCT) based thresholding and Curvelet transform based thresholding separately. To achieve maximum edge preservation and noise reduction,

Table 7.1: PSNR and IQI of Proposed (WCurv and NSCTCurv) and Existing schemes for CT image denoising

Image	σ	PSNR				IQI			
		10	20	30	40	10	20	30	40
CT1	DTCWTBT [127]	32.31	27.51	25.02	23.91	0.9972	0.9031	0.8871	0.8682
	NSCTBT [112]	31.11	28.14	26.38	24.91	0.9964	0.9181	0.8977	0.8715
	CBT [10]	32.12	28.34	26.56	24.11	0.9981	0.9161	0.8854	0.8556
	WCurv	32.59	28.51	**27.39**	**24.93**	0.9989	0.9194	**0.8988**	**0.8809**
	NSCTCurv	**32.98**	**28.62**	27.33	24.89	**0.9990**	**0.9197**	0.8984	0.8801
CT2	DTCWTBT [127]	32.19	28.52	26.22	24.01	0.9985	0.9035	0.8969	0.8678
	NSCTBT [112]	31.73	29.12	26.34	23.61	0.9981	0.9080	0.8712	0.8634
	CBT [10]	32.12	28.52	26.55	24.67	0.9989	0.9067	0.8802	0.8512
	WCurv	**32.88**	**29.21**	27.01	24.91	**0.9992**	**0.9087**	0.8994	0.8867
	NSCTCurv	32.81	29.11	**27.12**	**24.97**	0.9990	0.9083	**0.8998**	**0.8871**
CT3	DTCWTBT [127]	32.09	28.15	26.43	24.13	0.9942	0.8911	0.8791	0.8652
	NSCTBT [112]	32.23	29.11	26.33	23.91	0.9990	0.9081	0.8934	0.8745
	CBT [10]	32.16	28.05	26.31	24.02	0.9990	0.9062	0.8833	0.8575
	WCurv	**32.81**	**29.43**	**27.12**	**24.96**	**0.9991**	**0.9189**	**0.8999**	**0.8879**
	NSCTCurv	32.01	29.33	27.09	24.87	0.9981	0.9185	0.8992	0.8873
CT4	DTCWTBT [127]	33.39	28.05	26.12	24.91	0.9982	0.9013	0.8919	0.8695
	NSCTBT [112]	33.02	29.21	26.43	23.01	0.9989	0.9068	0.8923	0.8781
	CBT [10]	32.86	28.05	26.63	24.80	0.9990	0.9086	0.8830	0.8571
	WCurv	33.41	**29.42**	**27.81**	**24.98**	0.9989	**0.9189**	**0.8992**	**0.8883**
	NSCTCurv	**33.81**	29.39	27.71	24.91	**0.9991**	0.9185	0.8990	0.8879

a weight value is estimated using variance difference of both denoised images R_1 and R_2 where the patch size is used as 3x3. Using this weight factor, both images are fused using aggregated function and final denoised image has been obtained.

To validate the superiority of both (WCurv and NSCTCurv) schemes, the performance is compared by existing methods. The existing methods for comparison are adaptive dual-tree complex wavelet transform based bivariate thresholding (DTCWTBT) [127], NSCT based thresholding (NSCTBT) [112] and curvelet based denoising (CBT) [10]. Figures 7.5-7.9 are showing the results of DTCWTBT [127], NSCTBT [112], CBT [10], WCurv and NSCTCurv schemes respectively. Here for fair comparison, three levels of decomposition are used to obtain the denoised image.

Visually, the CBT and DTCWTBT results are not impressive for some images. However, NSCTBT results are slightly improved over the CBT and DTCWTBT methods. Due to the concept of method noise, the results of WCurv are improved in comparison to CBT, DTCWTBT and NSCTBT. However, NSCTCurv results also equally impressive in comparison to WCurv. But, as the noise level increases, WCurv scheme gives better outcomes in comparison to NSCTCurv and existing WCurv schemes.

Table 7.1 shows the PSNR (in dB) and IQI values of the denoised images relative to their original images using proposed and existing methods. Both WCurv and NSCTCurv schemes are giving better results in comparison to CBT, DTCWTBT and NSCTBT methods. The results shown in table 7.1 demonstrate that in most of the cases, the WCurv scheme is superior to all other methods. The best values amongst all the methods are represented in bold. The results of WCurv and NSCTCurv schemes indicate improved texture, noise suppression and sharp preserved edges.

7.4 Conclusions

In this chapter, two (WCurv and NSCTCurv) schemes are presented for CT image denoising. In WCurv scheme, a new approach is investigated to reduce noise in CT images and extracted more edge information by taking the advantage of wavelet and curvelet transforms. To provide smooth and edge preserved image, adaptive bilateral based wavelet thresholding is used. Using method noise concept, more edges have been extracted using curvelet based thresholding. In NSCTCurv scheme, another

new approach has been introduced to reduce noise from the CT images using Non-subsampled Contourlet and Curvelet transforms based thresholding. An aggregation concept is used to obtain the weight value which helps to improve the signal to noise ratio. The outcomes of both (WCurv and NSCTCurv) schemes indicates that the visually results are good, especially in terms of edge preservation. The performance metrics (IQI and PSNR) also indicate that results are good in most of the cases. These experiments indicate that noise is suppressed effectively and clinically relevant details are well preserved. However due to the concept of method noise, WCurv scheme gives better outcomes in comparison to NSCTCurv scheme.

CHAPTER 8

Conclusions and Future scope

Chapter 8

Conclusions and Future scope

8.1 Contributions

This thesis gives a brief introduction of CT imaging and literature review of some of the salient works done in CT image denoising. In this thesis, various schemes have been developed to denoise the CT images. The aim of this thesis is to design and develop denoising techniques with edge and other feature preservation, for CT images corrupted with additive white Gaussian noise.

Image denoising of CT images is a well researched topic. Initially, the first work of the thesis starts from CT image denoising in the spatial domain. Here, total variation based CT image denoising is performed by introducing a new exponentially directional weighted function (EDWF) where anisotropic and isotropic TV methods are modified to denoise the CT images. However the results of this work are good in terms of edge preservation and noise reduction. But textures of denoised images are not as good as required for clinical purpose.

Image denoising based on multi resolution analysis using wavelet transform has received considerable attention in recent years. Therefore, WF-WPT scheme in wavelet domain has been designed for CT image denoising. Here, Wiener filter and

optimum linear interpolation thresholding method were used to suppress the noise from CT images. Experimental results demonstrated that WF-WPT scheme improves the image visual quality in respect to noise removal and edge preservation. However, it was also analyzed that as noise level increases, the quality of edges is decreased. Therefore, this scheme is extended and WFWT-MN scheme is designed by modifying the WF-WPT scheme using the concept of method noise. Here initially, wiener filter has been performed in wavelet domain, and first outcome is obtained. The first outcome is subtracted from input noisy image which shows the missing structures and noise also. Hence, an optimum linear interpolation thresholding in wavelet domain is performed over the subtracted image to preserve the edges and suppress the noise, and second outcome has been obtained. By performing addition of both outcomes, the final denoised CT images are obtained. The experimental evaluations indicated that most of the cases WFWT-MN scheme gives better visual qualities. However the results of WFWT-MN scheme are improved, but still challenging for higher noise CT images.

From literature, it was also analyzed that in most of the cases, image denoising performance depends on the neighboring pixels. If the neighboring pixel is changed, the performance of image denoising is also changed. With this approach two new schemes have been designed: CSBT and NLM-WPT schemes. In CSBT scheme, tetrolet transform based denoising scheme has been developed using circular shift based thresholding. where Bayes estimation method was used to estimate the value

and firm thresholding has been performed to suppress the noise from CT images. However, the results are visually more improved because of rotation and reflection properties in tetrolet transform but sharp features are missing. Therefore in NLM-WPT scheme, CT images have been designed to get sharp and smooth denoised images using NLM and circular shift based wavelet packet thresholding. The results for higher noise CT images have been improved.

The performance of image denoising can also changed by intra and inter scale dependencies. With this motivation, two LAPT and BFBS schemes have been presented. In LAPT scheme, image denoising is performed by choosing different patch sizes in wavelet domain. Using method noise and many intermediate steps, wavelet based thresholding has been performed. However, the results are improved but contrast of denoised images are slightly reduced due to many intermediate steps where Bayes estimation method is used to suppress the noise. In BFBS scheme, a bilateral filter and bivariate shrinkage rule have been performed using Dual-tree Complex Wavelet Transform (DT-CWT). The Bilateral filter helps to give sharp and smooth images with less computation time in comparison to NLM. While, bivariate shrinkage rule is used to suppress the noise based on the dependencies on parent-child wavelet coefficients. Due to the shift invariance property and good directionality in Dual-tree Complex Wavelet Transform (DT-CWT), BFBS scheme gives more enhanced results near to noisy edges.

The extended versions of wavelet transform have more additional properties

which are helpful to improve the image denoising performance. Therefore, WCurv and NSCTCurv schemes have been designed for CT image denoising. In WCurv scheme, Curvelet and Wavelet transform based CT image denoising is performed using Bayes shrinkage rule. Here, bilateral filter, method noise and curvelet transform have been used which help to provide sharp and smooth denoised CT images. In NSCTCurv scheme, Non-subsampled Contourlet transform and Curvelet transform has been performed using Bayes shrinkage rule for more obtaining sharp features. Due to the directional features of Non-subsampled Contourlet transform and Curvelet transform, the results are excellent in terms of sharp and smooth images.

The code for the entire work of simulation studies described in this thesis have been developed using MATLAB in Windows environment. In this thesis work, the experimental results of proposed schemes are excellent in terms of visual as well as performance metrics (PSNR, SSIM, etc). Experimental results demonstrate that the thesis work: (i) Effectively eliminate the noise in CT images, (ii) Preserve the edge and geometrical structures, and (iii) Retain clinically relevant details.

8.2 Future Scope

Scope of this research is still open in terms of speed and extension of the CT image denoising techniques. Several aspects of the proposed algorithms can still be improved. Total variation based CT image denoising in spatial domain can be further modified by improving the complexity of weighted function. Wavelet thresholding

based work using Wiener filtering can also be improved by modifying the thresholding algorithm. The complexity of circular shifting can be reduced and improved for CT image denoising. Circular shifting method for CT image denoising can also be improved by applying the circular shifting over the inter scale coefficients. There is also a scope of improvements in patch variation based CT image denoising by enhancing the intermediate steps. Furthermore, the extended versions of Wavelet transform based schemes such as Shearlet transform, directionlet transform can also be used to improve the image denoising performance.

A more complex spatial segmentation, which is capable of extracting the dominant directions in images with more flexibility may improve the performance of the proposed schemes. Based on the local dominant directions, the wavelet transform based denoising can be further improved. Other types of dependencies in transform domain such as inter-inter scale dependency, inter-intra scale dependency, intra-inter scale dependency and intra-intra scale dependency can be further used and improved the performance of CT image denoising.

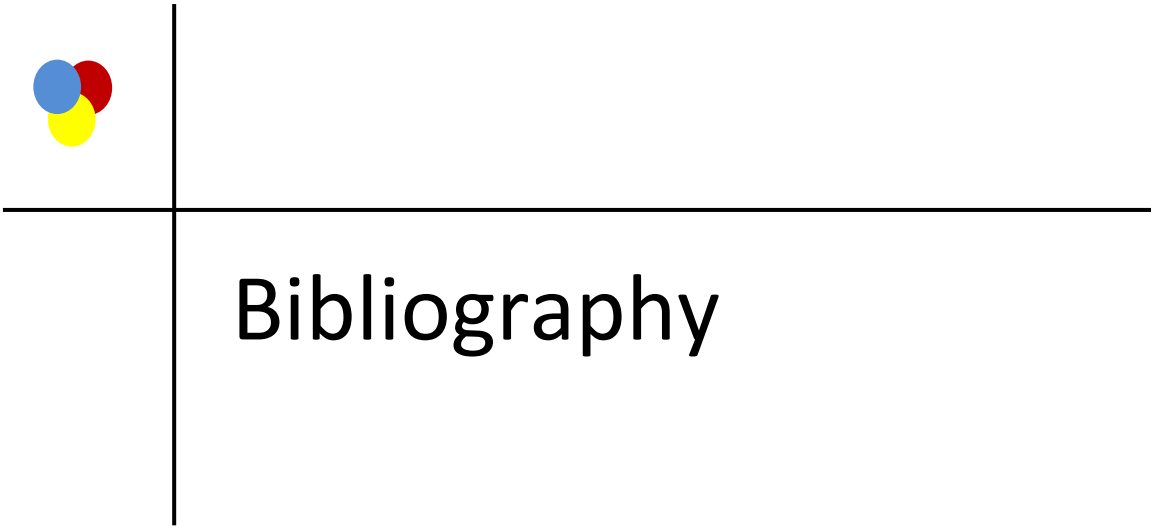

Bibliography

Bibliography

[1] Ai, D., Yang, J., Fan, J., Cong, W., and Wang, Y. Adaptive tensor-based principal component analysis for low-dose CT image denoising. *PloS one 10*, 5 (2015), e0126914.

[2] Al-Ameen, Z., Al-Ameen, S., and Sulong, G. Latest methods of image enhancement and restoration for computed tomography: A concise review. *Applied Medical Informatics 36*, 1 (2015), 1.

[3] Al-Ameen, Z., and Sulong, G. Attenuating noise from computed tomography medical images using a coefficients-driven total variation denoising algorithm. *International Journal of Imaging Systems and Technology 24*, 4 (2014), 350–358.

[4] Al-Ameen, Z., Sulong, G., Rehman, A., Al-Rodhaan, M., Saba, T., and Al-Dhelaan, A. Phase-preserving approach in denoising computed tomography medical images. *Computer Methods in Biomechanics and Biomedical Engineering: Imaging & Visualization* (2014), 1–11.

[5] Antoniadis, A., and Fan, J. Regularization of wavelet approximations. *Journal of the American Statistical Association* (2011).

[6] Bayram, I., and Kamasak, M. E. Directional total variation. *IEEE Signal Processing Letters 19*, 12 (2012), 781–784.

[7] Beck, A., and Teboulle, M. Fast gradient-based algorithms for constrained total variation image denoising and deblurring problems. *IEEE Transactions on Image Processing 18*, 11 (2009), 2419–2434.

[8] Beekman, F. J., and Kamphuis, C. Ordered subset reconstruction for X-ray CT. *Physics in medicine and biology 46*, 7 (2001), 1835.

[9] Bhadauria, H., and Dewal, M. Efficient denoising technique for CT images to enhance brain hemorrhage segmentation. *Journal of digital imaging 25*, 6 (2012), 782–791.

[10] Bhadauria, H., and Dewal, M. Medical image denoising using adaptive fusion of curvelet transform and total variation. *Computers & Electrical Engineering 39*, 5 (2013), 1451–1460.

[11] Blu, T., and Luisier, F. The SURE-LET approach to image denoising. *IEEE Transactions on Image Processing 16*, 11 (2007), 2778–2786.

[12] Borsdorf, A. *Adaptive filtering for noise reduction in X-ray computed tomography*. Logos, 2009.

[13] Borsdorf, A., Kappler, S., Raupach, R., and Hornegger, J. Analytic noise propagation for anisotropic denoising of CT images. In *2008 IEEE Nuclear Science Symposium Conference Record* (2008), IEEE, pp. 5335–5338.

[14] Borsdorf, A., Raupach, R., Flohr, T., and Hornegger, J. Wavelet based noise reduction in CT-images using correlation analysis. *IEEE transactions on medical imaging 27*, 12 (2008), 1685–1703.

[15] Borsdorf, A., Raupach, R., and Hornegger, J. Wavelet based noise reduction by identification of correlations. In *Joint Pattern Recognition Symposium* (2006), Springer, pp. 21–30.

[16] Brooks, R. A., and Di Chiro, G. Principles of computer assisted tomography (CAT) in radiographic and radioisotopic imaging. *Physics in medicine and biology 21*, 5 (1976), 689.

[17] Buades, A., Coll, B., and Morel, J.-M. A review of image denoising algorithms, with a new one. *Multiscale Modeling & Simulation 4*, 2 (2005), 490–530.

[18] Cai, J.-F., Osher, S., and Shen, Z. Convergence of the linearized bregman iteration for 1-norm minimization. *Mathematics of Computation 78*, 268 (2009), 2127–2136.

[19] Cai, J.-F., Osher, S., and Shen, Z. Linearized bregman iterations for compressed sensing. *Mathematics of Computation 78*, 267 (2009), 1515–1536.

[20] Cai, J.-F., Osher, S., and Shen, Z. Split bregman methods and frame based image restoration. *Multiscale modeling & simulation 8*, 2 (2009), 337–369.

[21] Candès, E. J., and Donoho, D. L. New tight frames of curvelets and optimal representations of objects with piecewise C2 singularities. *Communications on pure and applied mathematics 57*, 2 (2004), 219–266.

[22] Candes, E. J., Wakin, M. B., and Boyd, S. P. Enhancing sparsity by reweighted 1 minimization. *Journal of Fourier analysis and applications 14*, 5-6 (2008), 877–905.

[23] Catté, F., Lions, P.-L., Morel, J.-M., and Coll, T. Image selective smoothing and edge detection by nonlinear diffusion. *SIAM Journal on Numerical analysis 29*, 1 (1992), 182–193.

[24] Chambolle, A. An algorithm for total variation minimization and applications. *Journal of Mathematical imaging and vision 20*, 1-2 (2004), 89–97.

[25] Chambolle, A., and Pock, T. A first-order primal-dual algorithm for convex problems with applications to imaging. *Journal of Mathematical Imaging and Vision 40*, 1 (2011), 120–145.

[26] Chang, S. G., Yu, B., and Vetterli, M. Adaptive wavelet thresholding for image denoising and compression. *IEEE transactions on image processing 9*, 9 (2000), 1532–1546.

[27] Chen, H., Wang, C., Song, Y., and Li, Z. Split bregmanized anisotropic total variation model for image deblurring. *Journal of Visual Communication and Image Representation 31* (2015), 282–293.

[28] Chew, E., Weiss, G., Brooks, R., and Di Chiro, G. Effect of CT noise on detectability of test objects. *American Journal of Roentgenology 131*, 4 (1978), 681–685.

[29] Cormack, A. M. Early two-dimensional reconstruction and recent topics stemming from it. *Science 209*, 4464 (1980), 1482–1486.

[30] Cousins, C., Miller, D., Bernardi, G., et al. International commission on radiological protection. *ICRP publication 120* (2011), 1–125.

[31] Da Cunha, A. L., Zhou, J., and Do, M. N. The nonsubsampled contourlet transform: theory, design, and applications. *IEEE transactions on image processing 15*, 10 (2006), 3089–3101.

[32] Da-tong, H. Acceptance testing of CT scanner. *CHINESE JOURNAL OF RADIOLOGY* (1994), 09.

[33] Dabov, K., Foi, A., Katkovnik, V., and Egiazarian, K. Image denoising by sparse 3-D transform-domain collaborative filtering. *IEEE Transactions on image processing 16*, 8 (2007), 2080–2095.

[34] Darbon, J., and Sigelle, M. Image restoration with discrete constrained total variation part I: Fast and exact optimization. *Journal of Mathematical Imaging and Vision 26*, 3 (2006), 261–276.

[35] Deng, J., Li, H., and Wu, H. A CT image denoise method using curvelet transform. In *Communication Systems and Information Technology*. Springer, 2011, pp. 681–687.

[36] Denis, L., Tupin, F., Darbon, J., and Sigelle, M. Sar image regularization with fast approximate discrete minimization. *IEEE Transactions on Image Processing 18*, 7 (2009), 1588–1600.

[37] Do, M. N., and Vetterli, M. The contourlet transform: an efficient directional multiresolution image representation. *IEEE Transactions on image processing 14*, 12 (2005), 2091–2106.

[38] Dobson, D. C., and Santosa, F. Recovery of blocky images from noisy and blurred data. *SIAM Journal on Applied Mathematics 56*, 4 (1996), 1181–1198.

[39] Donoho, D. L., and Johnstone, J. M. Ideal spatial adaptation by wavelet shrinkage. *Biometrika 81*, 3 (1994), 425–455.

[40] Duan, J., Lu, W., Tench, C., Gottlob, I., Proudlock, F., Samani, N. N., and Bai, L. Denoising optical coherence tomography using second order total generalized variation decomposition. *Biomedical Signal Processing and Control 24* (2016), 120–127.

[41] Elbakri, I. A., and Fessler, J. A. Efficient and accurate likelihood for iterative image reconstruction in X-ray computed tomography. In *Medical Imaging 2003* (2003), International Society for Optics and Photonics, pp. 1839–1850.

[42] Eom, I. K., and Kim, Y. S. Wavelet-based denoising with nearly arbitrarily shaped windows. *IEEE Signal Processing Letters 11*, 12 (2004), 937–940.

[43] Esedolu, S., and Osher, S. J. Decomposition of images by the anisotropic rudin-osher-fatemi model. *Communications on pure and applied mathematics 57*, 12 (2004), 1609–1626.

[44] Fathi, A., and Naghsh-Nilchi, A. R. Efficient image denoising method based on a new adaptive wavelet packet thresholding function. *IEEE transactions on image processing 21*, 9 (2012), 3981–3990.

[45] feng Li, X., Xu, J., Luo, J., Cao, L., and Zhang, S. Intensity image denoising for laser active imaging system using nonsubsampled contourlet transform and sure approach. *Optik-International Journal for Light and Electron Optics 123*, 9 (2012), 808–813.

[46] Fessler, J. A., Ficaro, E. P., Clinthorne, N. H., and Lange, K. Grouped-coordinate ascent algorithms for penalized-likelihood transmission image reconstruction. *IEEE Transactions on Medical Imaging 16*, 2 (1997), 166–175.

[47] Firoiu, I., Isar, A., and Isar, D. A bayesian approach of wavelet based image denoising in a hyperanalytic multi-wavelet context. *WSEAS Trans Signal Process 6* (2010), 155–164.

[48] GAN, Y.-g., RONG, Y.-x., LI, Y.-t., et al. Clinical study on the influence of helical CT at low-dose chest scanning in airway post processing images of children. *J]. Chinese Journal of Radiation Mediation and Protection 26*, 4 (2006), 405–407.

[49] Gao, H.-Y. Wavelet shrinkage denoising using the non-negative garrote. *Journal of Computational and Graphical Statistics 7*, 4 (1998), 469–488.

[50] Gao, H.-Y., and Bruce, A. G. Waveshrink with firm shrinkage. *Statistica Sinica* (1997), 855–874.

[51] Ghadrdan, S., Alirezaie, J., Dillenseger, J.-L., and Babyn, P. Low-dose computed tomography image denoising based on joint wavelet and sparse representation. In *2014 36th Annual International Conference of the IEEE Engineering in Medicine and Biology Society* (2014), IEEE, pp. 3325–3328.

[52] Giraldo, J. C. R., Kelm, Z. S., Guimaraes, L. S., Yu, L., Fletcher, J. G., Erickson, B. J., and McCollough, C. H. Comparative study of two image space noise reduction methods for computed tomography: bilateral filter and nonlocal means. In *2009 Annual International Conference of the IEEE Engineering in Medicine and Biology Society* (2009), IEEE, pp. 3529–3532.

[53] Goldstein, T., and Osher, S. The split bregman method for L1-regularized problems. *SIAM journal on imaging sciences 2*, 2 (2009), 323–343.

[54] Gonzalez, R. C., Woods, R. E., et al. Digital image processing, 2002.

[55] Guo, K., and Labate, D. Optimally sparse multidimensional representation using shearlets. *SIAM journal on mathematical analysis 39*, 1 (2007), 298–318.

[56] Gupta, D., Anand, R., and Tyagi, B. Despeckling of ultrasound medical images using nonlinear adaptive anisotropic diffusion in nonsubsampled shearlet domain. *Biomedical Signal Processing and Control 14* (2014), 55–65.

[57] Hanzouli, H., Lapuyade-Lahorgue, J., Monfrini, E., Delso, G., Pieczynski, W., Visvikis, D., and Hatt, M. PET/CT image denoising and segmentation based on a multi observation and a multi scale markov tree model. In *2013 IEEE Nuclear Science Symposium and Medical Imaging Conference (2013 NSS/MIC)* (2013), IEEE, pp. 1–4.

[58] Hashemi, S., Beheshti, S., Cobbold, R. S., and Paul, N. S. Non-local total variation based low-dose computed tomography denoising. In *2014 36th Annual International Conference of the IEEE Engineering in Medicine and Biology Society* (2014), IEEE, pp. 1083–1086.

[59] Hounsfield, G. N. Computerized transverse axial scanning (tomography): Part 1. description of system. *The British journal of radiology 46*, 552 (1973), 1016–1022.

[60] Hsieh, J. Computed tomography: principles, design, artifacts, and recent advances. SPIE Bellingham, WA.

[61] Hu, Y., and Jacob, M. Higher degree total variation (HDTV) regularization for image recovery. *IEEE Transactions on Image Processing 21*, 5 (2012), 2559–2571.

[62] Jain, A. K. *Fundamentals of digital image processing*. Prentice-Hall, Inc., 1989.

[63] Jain, P., and Tyagi, V. Lapb: Locally adaptive patch-based wavelet domain edge-preserving image denoising. *Information Sciences 294* (2015), 164–181.

[64] Jain, P., and Tyagi, V. A survey of edge-preserving image denoising methods. *Information Systems Frontiers 18*, 1 (2016), 159–170.

[65] Jansen, M., and Bultheel, A. Empirical bayes approach to improve wavelet thresholding for image noise reduction. *Journal of the American Statistical Association* (2011).

[66] Jiang, W., Cui, H., Zhang, F., Rong, Y., and Chen, Z. Oriented total variation l1/2 regularization. *Journal of Visual Communication and Image Representation 29* (2015), 125–137.

[67] Jones, D., Shrimpton, P. C., and Britain, G. *Survey of* CT *practice in the UK. Part 3: Normalised organ doses calculated using Monte Carlo techniques*. National Radiological Protection Board Chilton, UK, 1991.

[68] Junzheng, Z. Strengthening control of medical exposure by new basic standards for radiological protection in china [j]. *Radialization Protection 2* (2004), 001.

[69] Kalra, M. K., Maher, M. M., Toth, T. L., Hamberg, L. M., Blake, M. A., Shepard, J.-A., and Saini, S. Strategies for CT radiation dose optimization 1. *Radiology 230*, 3 (2004), 619–628.

[70] Katsaggelos, A. K. *Digital image restoration*. Springer Publishing Company, Incorporated, 2012.

[71] Kazubek, M. Wavelet domain image denoising by thresholding and wiener filtering. *IEEE Signal Processing Letters 10*, 11 (2003), 324–326.

[72] Ke, L., and Zhang, R. Multiscale wiener filtering method for low-dose CT images. In *2010 3rd International Conference on Biomedical Engineering and Informatics* (2010), vol. 1, IEEE, pp. 428–431.

[73] Kingsbury, N. The dual-tree complex wavelet transform: a new efficient tool for image restoration and enhancement. In *Signal Processing Conference (EUSIPCO 1998), 9th European* (1998), IEEE, pp. 1–4.

[74] Knas, M., and Cierniak, R. Computed tomography images denoising with markov random field model parametrized by prewitt mask. In *Image Processing & Communications Challenges 6*. Springer, 2015, pp. 53–58.

[75] Knaup, M., Kachelrieb, M., and Kalender, W. A. 3D and 4D imaging from multi-threaded cone-beam CT scans. In *IEEE Nuclear Science Symposium Conference Record, 2005* (2005), vol. 4, IEEE, pp. 5–pp.

[76] Krommweh, J., and Ma, J. Tetrolet shrinkage with anisotropic total variation minimization for image approximation. *Signal processing 90*, 8 (2010), 2529–2539.

[77] Kumar, B. S. Image denoising based on non-local means filter and its method noise thresholding. *Signal, image and video processing 7*, 6 (2013), 1211–1227.

[78] La Rivière, P. J., Bian, J., and Vargas, P. A. Penalized-likelihood sinogram restoration for computed tomography. *IEEE transactions on medical imaging 25*, 8 (2006), 1022–1036.

[79] Landi, G., and Piccolomini, E. L. An efficient method for nonnegatively constrained total variation-based denoising of medical images corrupted by poisson noise. *Computerized Medical Imaging and Graphics 36*, 1 (2012), 38–46.

[80] Lange, K., and Fessler, J. A. Globally convergent algorithms for maximum a posteriori transmission tomography. *IEEE Transactions on Image Processing 4*, 10 (1995), 1430–1438.

[81] Lanzolla, A., Andria, G., Attivissimo, F., Cavone, G., Spadavecchia, M., and Magli, T. Denoising filter to improve the quality of CT images. In *Instrumentation and Measurement Technology Conference, 2009. I2MTC'09. IEEE* (2009), IEEE, pp. 947–950.

[82] Le Pogam, A., Hanzouli, H., Hatt, M., Le Rest, C. C., and Visvikis, D. Denoising of PET images by combining wavelets and curvelets for improved preservation of resolution and quantitation. *Medical image analysis 17*, 8 (2013), 877–891.

[83] Li, T., Li, X., Wang, J., Wen, J., Lu, H., Hsieh, J., and Liang, Z. Nonlinear sinogram smoothing for low-dose X-ray CT. *IEEE Transactions on Nuclear Science 51*, 5 (2004), 2505–2513.

[84] Li, W., Li, Q., Gong, W., and Tang, S. Total variation blind deconvolution employing split bregman iteration. *Journal of Visual Communication and Image Representation 23*, 3 (2012), 409–417.

[85] Li, Z., Yu, L., Trzasko, J. D., Lake, D. S., Blezek, D. J., Fletcher, J. G., McCollough, C. H., and Manduca, A. Adaptive nonlocal means filtering based on local noise level for CT denoising. *Medical physics 41*, 1 (2014), 011908.

[86] Lou, Y., Zeng, T., Osher, S., and Xin, J. A weighted difference of anisotropic and isotropic total variation model for image processing. *SIAM*

Journal on Imaging Sciences 8, 3 (2015), 1798–1823.

[87] Lu, L., Jin, W., and Wang, X. Non-local means image denoising with a soft threshold. *IEEE Signal Processing Letters 22*, 7 (2015), 833–837.

[88] Luisier, F., Blu, T., and Unser, M. A new SURE approach to image denoising: Interscale orthonormal wavelet thresholding. *IEEE Transactions on image processing 16*, 3 (2007), 593–606.

[89] Malfait, M., and Roose, D. Wavelet-based image denoising using a markov random field a priori model. *IEEE transactions on image processing 6*, 4 (1997), 549–565.

[90] Mallat, S. G. A theory for multiresolution signal decomposition: the wavelet representation. *IEEE transactions on pattern analysis and machine intelligence 11*, 7 (1989), 674–693.

[91] Manduca, A., Yu, L., Trzasko, J. D., Khaylova, N., Kofler, J. M., McCollough, C. M., and Fletcher, J. G. Projection space denoising with bilateral filtering and CT noise modeling for dose reduction in CT. *Medical physics 36*, 11 (2009), 4911–4919.

[92] Mayo, J., Hartman, T. E., Lee, K. S., Primack, S., Vedal, S., and Müller, N. CT of the chest: minimal tube current required for good image quality with the least radiation dose. *AJR. American journal of roentgenology 164*, 3 (1995), 603–607.

[93] McCollough, C. H., Primak, A. N., Braun, N., Kofler, J., Yu, L., and Christner, J. Strategies for reducing radiation dose in CT. *Radiologic Clinics of North America 47*, 1 (2009), 27–40.

[94] Mechlem, K., Allner, S., Mei, K., Pfeiffer, F., and Noël, P. B. Dictionary-based image denoising for dual energy computed tomography. In *SPIE Medical Imaging* (2016), International Society for Optics and Photonics, pp. 97830E–97830E.

[95] Mettler Jr, F. A., Wiest, P. W., Locken, J. A., and Kelsey, C. A. CT scanning: patterns of use and dose. *Journal of radiological Protection 20*, 4 (2000), 353.

[96] Mignotte, M. A post-processing deconvolution step for wavelet-based image denoising methods. *IEEE Signal Processing Letters 14*, 9 (2007), 621.

[97] Mihcak, M. K., Kozintsev, I., and Ramchandran, K. Spatially adaptive statistical modeling of wavelet image coefficients and its application to denoising. In *Acoustics, Speech, and Signal Processing, 1999. Proceedings., 1999 IEEE International Conference on* (1999), vol. 6, IEEE, pp. 3253–3256.

[98] Mihcak, M. K., Kozintsev, I., Ramchandran, K., and Moulin, P. Low-complexity image denoising based on statistical modeling of wavelet coefficients. *IEEE Signal Processing Letters 6*, 12 (1999), 300–303.

[99] Minasyan, S., Astola, J., Egiazarian, K., and Guevorkian, D. Parametric haar-like transforms in image denoising. In *2006 International Conference on Image Processing* (2006), IEEE, pp. 2629–2632.

[100] Mohan, J., Krishnaveni, V., and Guo, Y. A survey on the magnetic resonance image denoising methods. *Biomedical Signal Processing and Control 9* (2014), 56–69.

[101] Mohideen, K., Perumal, A., Krishnan, N., and Sathik, M. Image denoising and enhancement using multiwavelet with hard threshold in digital mammographic images. *Int. Arab J. e-Technol. 2*, 1 (2011), 49–55.

[102] Motwani, M. C., Gadiya, M. C., Motwani, R. C., and Harris, F. C. Survey of image denoising techniques. In *Proceedings of GSPX* (2004), pp. 27–30.

[103] Moulin, P., and Liu, J. Analysis of multiresolution image denoising schemes using generalized gaussian and complexity priors. *IEEE Transactions on Information Theory 45*, 3 (1999), 909–919.

[104] Naidich, D. P., Marshall, C. H., Gribbin, C., Arams, R. S., and McCauley, D. I. Low-dose CT of the lungs: preliminary observations. *Radiology 175*, 3 (1990), 729–731.

[105] Naimi, H., Adamou-Mitiche, A. B. H., and Mitiche, L. Medical image denoising using dual tree complex thresholding wavelet transform and wiener

filter. *Journal of King Saud University-Computer and Information Sciences 27*, 1 (2015), 40–45.

[106] Nasri, M., and Nezamabadi-pour, H. Image denoising in the wavelet domain using a new adaptive thresholding function. *Neurocomputing 72*, 4 (2009), 1012–1025.

[107] Nikolova, M. Local strong homogeneity of a regularized estimator. *SIAM Journal on Applied Mathematics 61*, 2 (2000), 633–658.

[108] Nitta, N., Takahashi, M., Murata, K., and Morita, R. Ultra low-dose helical CT of the chest. *AJR. American journal of roentgenology 171*, 2 (1998), 383–385.

[109] Nuyts, J., De Man, B., Dupont, P., Defrise, M., Suetens, P., and Mortelmans, L. Iterative reconstruction for helical CT: a simulation study. *Physics in medicine and biology 43*, 4 (1998), 729.

[110] Okada, M. Noise evaluation and filter design in CT images. *IEEE transactions on biomedical engineering*, 9 (1985), 713–719.

[111] Osher, S., Burger, M., Goldfarb, D., Xu, J., and Yin, W. An iterative regularization method for total variation-based image restoration. *Multiscale Modeling & Simulation 4*, 2 (2005), 460–489.

[112] OUYANG, H.-B., QUAN, H.-M., TANG, Y., AND ZENG, Y.-Z. Image de-noising algorithm using adaptive bayes threshold by subband based on nsct. *Electronic Design Engineering 23* (2011), 069.

[113] PAN, T. Computed tomography: from photon statistics to modern cone-beam CT. *Journal of Nuclear Medicine 50*, 7 (2009), 1194–1194.

[114] PERONA, P., AND MALIK, J. Scale-space and edge detection using anisotropic diffusion. *IEEE Transactions on pattern analysis and machine intelligence 12*, 7 (1990), 629–639.

[115] PRAKASH, O., AND KHARE, A. Medical image denoising based on soft thresholding using biorthogonal multiscale wavelet transform. *International Journal of Image and Graphics 14*, 01n02 (2014), 1450002.

[116] QIU, T., WANG, A., YU, N., AND SONG, A. LLSURE: local linear sure-based edge-preserving image filtering. *IEEE Transactions on Image Processing 22*, 1 (2013), 80–90.

[117] RABBANI, H. Image denoising in steerable pyramid domain based on a local laplace prior. *Pattern Recognition 42*, 9 (2009), 2181–2193.

[118] RABBANI, H., NEZAFAT, R., AND GAZOR, S. Wavelet-domain medical image denoising using bivariate laplacian mixture model. *IEEE transactions on biomedical engineering 12*, 56 (2009), 2826–2837.

[119] Romberg, J. K., Choi, H., and Baraniuk, R. G. Bayesian wavelet-domain image modeling using hidden markov trees. In *Image Processing, 1999. ICIP 99. Proceedings. 1999 International Conference on* (1999), vol. 1, IEEE, pp. 158–162.

[120] Rudin, L. I., and Osher, S. Total variation based image restoration with free local constraints. In *Image Processing, 1994. Proceedings. ICIP-94., IEEE International Conference* (1994), vol. 1, IEEE, pp. 31–35.

[121] Rudin, L. I., Osher, S., and Fatemi, E. Nonlinear total variation based noise removal algorithms. *Physica D: Nonlinear Phenomena 60*, 1 (1992), 259–268.

[122] Rutherford, R., Pullan, B., and Isherwood, I. Measurement of effective atomic number and electron density using an EMI scanner. *Neuroradiology 11*, 1 (1976), 15–21.

[123] Sanches, J. M., Nascimento, J. C., and Marques, J. S. Medical image noise reduction using the sylvester–lyapunov equation. *IEEE transactions on image processing 17*, 9 (2008), 1522–1539.

[124] Sandborg, M. Computed tomography: Physical principles and biohazards.

[125] Sankur, B., and Sezgin, M. Image thresholding techniques: A survey over categories. *Pattern Recognition 34*, 2 (2001), 1573–1583.

[126] Schauer, D. A., and Linton, O. W. National council on radiation protection and measurements report shows substantial medical exposure increase 1. *Radiology 253*, 2 (2009), 293–296.

[127] Sendur, L., and Selesnick, I. W. Bivariate shrinkage functions for wavelet-based denoising exploiting interscale dependency. *IEEE Transactions on signal processing 50*, 11 (2002), 2744–2756.

[128] Shao, W.-j., Ni, J., and Zhu, C. A hybrid method of image restoration and denoise of CT images. In *2012 Sixth International Conference on Internet Computing for Science and Engineering* (2012), IEEE, pp. 117–121.

[129] Shih, C.-T., Chang, S.-J., Liu, Y.-l., and Wu, J. Noise reduction of low-dose computed tomography using the multi-resolution total variation minimization algorithm. In *SPIE Medical Imaging* (2013), International Society for Optics and Photonics, pp. 86682H–86682H.

[130] Shui, P.-L. Image denoising algorithm via doubly local wiener filtering with directional windows in wavelet domain. *IEEE Signal Processing Letters 12*, 10 (2005), 681–684.

[131] Shui, P.-L., Zhou, Z.-F., and Li, J.-X. Image denoising algorithm via best wavelet packet base using wiener cost function. *IET Image Processing 1*, 3 (2007), 311–318.

[132] Silva, J. S., Silva, A., and Santos, B. S. Image denoising methods for tumor discrimination in high-resolution computed tomography. *Journal of digital imaging 24*, 3 (2011), 464–469.

[133] Skiadopoulos, S., Karatrantou, A., Korfiatis, P., Costaridou, L., Vassilakos, P., Apostolopoulos, D., and Panayiotakis, G. Evaluating image denoising methods in myocardial perfusion single photon emission computed tomography (SPECT) imaging. *Measurement Science and Technology 20*, 10 (2009), 104023.

[134] Sun, C., Tang, C., Zhu, X., and Ren, H. Exponential total variation model for noise removal, its numerical algorithms and applications. *AEU-International Journal of Electronics and Communications 69*, 3 (2015), 644–654.

[135] Tikhonov, A., and Arsenin, V. Y. *Methods for solving ill-posed problems*. John Wiley and Sons, Inc, 1977.

[136] Tomasi, C., and Manduchi, R. Bilateral filtering for gray and color images. In *Computer Vision, 1998. Sixth International Conference on* (1998), IEEE, pp. 839–846.

[137] Trinh, D. H., Luong, M., Rocchisani, J.-M., Pham, C. D., Pham, H. D., and Dibos, F. An optimal weight method for CT image denoising. *Journal of Electronic Science and Technology 10*, 2 (2012), 124–129.

[138] Vandeghinste, B., Goossens, B., Van Holen, R., Vanhove, C., Pižurica, A., Vandenberghe, S., and Staelens, S. Iterative CT reconstruction using shearlet-based regularization. *IEEE Transactions on Nuclear Science 60*, 5 (2013), 3305–3317.

[139] Velisavljevic, V., Beferull-Lozano, B., Vetterli, M., and Dragotti, P. L. Directionlets: anisotropic multidirectional representation with separable filtering. *IEEE Transactions on Image Processing 15*, 7 (2006), 1916–1933.

[140] Venturas, S., and Flaounas, I. Study of radon transformation and application of its inverse to nmr. *Algorithms in Molecular Biology 4* (2005).

[141] Vidakovic, B. Nonlinear wavelet shrinkage with bayes rules and bayes factors. *Journal of the American Statistical Association 93*, 441 (1998), 173–179.

[142] Vogel, C. R. A multigrid method for total variation-based image denoising. In *Computation and control IV*. Springer, 1995, pp. 323–331.

[143] Vogel, C. R., and Oman, M. E. Iterative methods for total variation denoising. *SIAM Journal on Scientific Computing 17*, 1 (1996), 227–238.

[144] Wang, L., Zou, Y.-K., and Zhang, H.-J. A medical image denoising arithmetic based on wiener filter parallel model of wavelet transform. In *Image and Signal Processing, 2009. CISP'09. 2nd International Congress on* (2009), IEEE, pp. 1–4.

[145] Wang, X., Shi, G., Niu, Y., and Zhang, L. Robust adaptive directional lifting wavelet transform for image denoising. *IET image processing 5*, 3 (2011), 249–260.

[146] Wang, Z., Bovik, A. C., Sheikh, H. R., and Simoncelli, E. P. Image quality assessment: from error visibility to structural similarity. *IEEE transactions on image processing 13*, 4 (2004), 600–612.

[147] Weickert, J. *Anisotropic diffusion in image processing*, vol. 1. Teubner Stuttgart, 1998.

[148] Wotao, Y., Stanley, O., Donald, G., and Jerome, D. Bregman iterative algorithms for l1-minimization with applications to compressed sensing. *SIAM Journal on Imaging Sciences 1*, 1 (2008), 143–168.

[149] Wu, H., Zhang, W., Gao, D., Yin, X., Chen, Y., and Wang, W. Fast CT image processing using parallelized non-local means. *Journal of medical and biological engineering 31*, 6 (2011), 437–441.

[150] Xiaohua, Z., Jiang, S., Jingyun, S., Zhengqian, Y., Shijun, L., and Yongming, X. The relationship between image quality and CT dose index of multi-slice low-dose chest CT. *Chinese Journal of Radiology 37*, 10 (2003), 945–950.

[151] Xu, F., and Mueller, K. Accelerating popular tomographic reconstruction algorithms on commodity PC graphics hardware. *IEEE Transactions on nuclear science 52*, 3 (2005), 654–663.

[152] Xu, F., and Mueller, K. Real-time 3D computed tomographic reconstruction using commodity graphics hardware. *Physics in medicine and biology 52*, 12 (2007), 3405.

[153] Yan, J., and Lu, W.-S. New algorithms for sparse representation of discrete signals based on p-2 optimization. In *Communications, Computers and Signal Processing (PacRim), 2011 IEEE Pacific Rim Conference on* (2011), IEEE, pp. 73–78.

[154] Yan, J., and Lu, W.-S. Power-iterative strategy for p-2 optimization for compressive sensing: Towards global solution. In *2011 Conference Record of the Forty Fifth Asilomar Conference on Signals, Systems and Computers (ASILOMAR)* (2011), IEEE, pp. 1153–1157.

[155] Yan, J., and Lu, W.-S. Smoothed p-2 solvers for signal denoising. In *2012 IEEE International Conference on Acoustics, Speech and Signal Processing (ICASSP)* (2012), IEEE, pp. 3801–3804.

[156] Yan, J., and Lu, W.-S. Image denoising by generalized total variation regularization and least squares fidelity. *Multidimensional Systems and Signal Processing 26*, 1 (2015), 243–266.

[157] Yasuda, N., and Kodera, Y. Design of a noise-dependent shrinkage function in wavelet shrinkage of X-ray CT image. *International journal of computer assisted radiology and surgery 4*, 4 (2009), 353–366.

[158] YASUDA NARUOMI, I. Y., and YOSHIE, K. Improvement of image quality in chest MDCT using nonlinear wavelet shrinkage with trimmed-thresholding. *International Journal of Radiology 61*, 12 (2005), 1599–1608.

[159] Zhang, H., Zhang, L., Sun, Y., and Zhang, J. Projection domain denoising method based on dictionary learning for low-dose CT image reconstruction. *Journal of X-ray science and technology 23*, 5 (2015), 567–578.

[160] Zheng, X., Liao, Z., Hu, S., Li, M., and Zhou, J. Improving spatial adaptivity of nonlocal means in low-dosed CT imaging using pointwise fractal dimension. *Computational and mathematical methods in medicine 2013* (2013).

[161] Zibulevsky, M., and Elad, M. L1-L2 optimization in signal and image processing. *IEEE Signal Processing Magazine 27*, 3 (2010), 76–88.

List of Publications

List of Publications

1. Kumar M, Diwakar M. Reconstruction of 3D Shape from CT Images using Propagation Based Shape from Shading Approach. In Proceedings of Elsevier on Digital Signal and Image Processing, 2014 (pp. 145-150).

2. Diwakar M, Kumar M. CT image noise reduction based on adaptive wiener filtering with Wavelet packet thresholding. In Proceedings of IEEE on Parallel, Distributed and Grid Computing (PDGC), 2014 International Conference on 2014 Dec 11 (pp. 94-98).

3. Diwakar M, Kumar M. CT image denoising based on complex wavelet transform using local adaptive thresholding and Bilateral filtering. In Proceedings of ACM conference on the Third International Symposium on Women in Computing and Informatics 2015 Aug 10 (pp. 297-302).

4. Kumar M, Diwakar M. A New Locally Adaptive Patch Variation Based CT Image Denoising. International Journal of Image, Graphics and Signal Processing. 2016 Jan 1;8(1):43.

5. Kumar M, Diwakar M. CT image denoising using locally adaptive shrinkage rule in tetrolet domain. Journal of King Saud University-Computer and Information Sciences. 2016 Mar 31.
   (Published online in Science direct, http://dx.doi.org/10.1016/j.jksuci.2016.03.003).

6. Kumar M, Diwakar M. Edge Preservation Based CT Image Denoising Using Wavelet and Curvelet Transforms. In Proceedings of Springer on Fifth International Conference on Soft Computing for Problem Solving 2016 (pp. 771-782).

7. Kumar M, Diwakar M. A new exponentially directional weighted function based

CT image denoising using total variation. Journal of King Saud University-Computer and Information Sciences. 2016 Dec 22. (Published online in Science direct, http://dx.doi.org/10.1016/j.jksuci.2016.12.002).

8. Diwakar M, Kumar M. A Hybrid Method Based CT Image Denoising Using Nonsubsampled Contourlet and Curvelet Transforms. In Proceedings of Springer on Computer Vision and Image Processing 2017 (pp. 571-580).

9. Diwakar M, Kumar M. Edge Preservation Based CT Image Denoising Using Wiener Filtering and Thresholding in Wavelet Domain. In Proceedings of IEEE on Parallel, Distributed and Grid Computing (PDGC), 2016. (In Press)

10. Kumar M, Diwakar M. CT image denoising using NLM and wavelet packet thresholding. Communicated in INFOCOMP Journal of Computer science, 2016.

Journal of King Saud University – Computer and Information Sciences (2016) xxx, xxx–xxx

King Saud University

Journal of King Saud University – Computer and Information Sciences

www.ksu.edu.sa
www.sciencedirect.com

CT image denoising using locally adaptive shrinkage rule in tetrolet domain

Manoj Kumar, Manoj Diwakar *

Babasaheb Bhimrao Ambedkar University, Lucknow, India

Received 11 December 2015; revised 24 February 2016; accepted 17 March 2016

KEYWORDS

Image denoising;
Wavelet transform;
Tetrolet transform;
Shrinkage rule

Abstract In Computed Tomography (CT), image degradation such as noise and detail blurring is one of the universal problems due to hardware restrictions. The problem of noise in CT images can be solved by image denoising. The main aim of image denoising is to reduce the noise as well as preserve the important features such as edges, corners, textures and sharp structures. Due to the large capability of noise suppression in noisy signals according to neighborhood pixels or coefficients, this paper presents a new technique to denoise CT images with edge preservation in tetrolet domain (Haar-type wavelet transform) where a locally adaptive shrinkage rule is performed on high frequency tetrolet coefficients in such a way that noise can be reduced more effectively. The experimental results of the proposed scheme are excellent in terms of noise suppression and structure preservation. The proposed scheme is compared with some standard existing methods where it is observed that performance of the proposed scheme is superior to the existing methods in terms of visual quality, MSE, PSNR and Image Quality Index (IQI).

1. Introduction

CT examination is widely used in medical science for detection of diseases such as lung cancer. Higher radiation dose used for clinical CT scanning may increase the risk of cancer in the patients (Zhoubo et al., 2014). However, it is mentioned in the guidelines of CT scanning that the use of radiation should be as low as reasonably required. But many times, we have to compromise with these guidelines to achieve good quality CT images. On the other-side, low-dose CT imaging may produce a noisy image which degrade the diagnostic performance. Thus, there is a need to develop the techniques which can control the noise in low dose CT scan images.

Various techniques have been investigated for controlling noise in CT scan imaging. Broadly, these techniques can be categorized in three major parts : projection based denoising, iterative reconstruction (IR) based denoising and post processing based image denoising.

Projection based techniques such as projection space denoising with bilateral filtering and CT noise modeling for dose reduction in CT imaging (Manduca et al., 2009) work on raw data or sinogram, where noise filtering is applied on

* Corresponding author.
E-mail address: manoj.diwakar@gmail.com (M. Diwakar).
Peer review under responsibility of King Saud University.

ELSEVIER Production and hosting by Elsevier

http://dx.doi.org/10.1016/j.jksuci.2016.03.003

Please cite this article in press as: Kumar, M., Diwakar, M. CT image denoising using locally adaptive shrinkage rule in tetrolet domain. Journal of King Saud University – Computer and Information Sciences (2016), http://dx.doi.org/10.1016/j.jksuci.2016.03.003

raw data or sinogram and reconstructed image comes in the form of denoised image. Many iterative reconstruction approaches for noise suppression in CT have also been investigated, for example, ordered subset reconstruction for X-ray CT scan (Beekman and Kamphuis, 2001) that optimizes statistical objective functions. Iterative reconstruction techniques have an advantage of using noise statistics directly in the projections during the reconstruction process, the disadvantage, however, is the high computational cost. Post processing based methods can denoise directly to the reconstructed CT images by applying linear or nonlinear filters (Motwani et al., 2004). Several linear or nonlinear filtering methods for noise reduction in the projection data have been proposed. Linear filters such as Wiener filter (Li and Zhang, 2010; Naimi et al., 2015) in the wavelet domain gives optimal results when the signal distortion is estimated by Gaussian approximation and the accuracy is measured by calculating Mean Square Error (MSE). Most of the techniques like bilateral filtering (Durand and Dorsey, 2002; Manduca et al., 2009), total variation denoising (Chambolle, 2004; Goldstein and Osher, 2009), nonlocal means (NLM) denoising (Buades et al., 2005), local linear SURE based edge-preserving image filtering (LLSURE) (Qiu et al., 2013) and K-singular value decomposition (K-SVD) algorithm (Aharon et al., 2006) take an advantage of statistical properties of objects in image space and preserve clinical structures such as sharp edges, similarities between neighboring pixels, etc. In transform-domain denoising techniques, the input data are decomposed into its scale-space representation (Mallat, 1989). Various thresholding techniques for noise reduction have been introduced with wavelet such as efficient image denoising method based on a new adaptive wavelet packet thresholding function (Fathi and Naghsh-Nilchi, 1989), ideal spatial adaptation via wavelet shrinkage (Chang et al., 2000), SURE-LET approach for image denoising (Thierry and Florian, 2007), etc. For CT image denoising, selection of a threshold value is a cumbersome task for edge preservation and noise suppression. By selecting a small threshold value, the resultant image may left noisy while large threshold value may produce blurring on the edges of resultant image. To deal with this situation, an appropriate algorithm is to be selected to estimate a threshold value. Three major algorithms to estimate threshold value are VISUShrink, SUREShrink and BayesShrink. VISUShrink (Donoho and Johnstone, 1994) is non-adaptive universal threshold, which depends only on the number of samples and known for finding smoothed images. Its threshold choice can be large due to its dependence on the number of pixels in the images. From literature, it can be observed that threshold estimation of VISUShrink tends to over-smooth the signal while SUREShrink (Donoho, 2010) uses a hybrid of the universal and the SURE [Stein's Unbiased Risk Estimator] thresholds, and performs better than VISUShrink. BayesShrink (Abramovitch et al., 1998) minimizes the Bayes' risk estimator function assuming generalized Gaussian approximation and thus finds adaptive threshold value. In most of the cases, BayesShrink provides better outcomes in comparison to both VISUShrink and SUREShrink. Thresholding is one of the strategies to clean the pixels or images. In wavelet based thresholding, small wavelet coefficients in high frequency bands are removed and large wavelet coefficients are preserved. Hard and soft thresholding are very popular methods for thresholding. In hard thresholding (Donoho, 2010), each coefficient value is compared with estimated threshold value and values less than threshold are replaced by zero. In soft thresholding (Prakash and Khare, 2014), the replacement process is same as in hard thresholding, additionally rest of coefficients are modified by subtracting threshold value from those coefficients. Comparing the two, Soft thresholding gives better performance for visual appearance of images. Due to hard thresholding, image artifacts may be generated near the edges on denoised CT images. Soft thresholding has a limitation with large coefficient values which may not be good for more sophisticated CT images. Other thresholding schemes have also been proposed, which take the advantages of both soft and hard thresholding. Some well-known shrinkage rules are hyperbola function (Vidakovic, 1998), firm thresholding (Gao and Bruce, 1997), garrote thresholding (Gao, 1998) and SCAD thresholding (Antoniadis and Fan, 2001).

Recently, some researchers extended the idea of shrinkage with geometric wavelets methods (Krommweh, 2010) such as ridgelet, curvelets, contourlets, directionlet and tetrolet. CT image denoising is a challenging task because of finding correct noise variation, relationship between coefficients and achieving an optimal tradeoff between denoising and blurring or artifacts. To overcome these challenges, we propose a method for CT image denoising based on the variation of neighborhood pixels or coefficients.

This paper is organized as follows. In Section 2, a brief introduction of tetrolet transform is described. In Section 3, we describe the proposed methodology for CT image denoising where a locally adaptive shrinkage rule is performed in tetrolet transform. In Section 4, we describe the experimental results and compare with some existing denoising methods. Finally, conclusions are drawn in Section 5.

2. Tetrolet transform

The idea of tetrolet transform comes from a famous computer game 'Tetris', where five geometric patterns (as shown in Fig. 1 (a)) are used with rotation and reflection properties (Krommweh, 2010). These geometric patterns are known as tetrominoes. Tetrolet transform is a powerful tool for signal and image processing tasks because of local enhancement through tetrominoes, multi-resolution analysis, sub-banding and localization in both frequency and time domain. All the tetrominoes are connected with a four equal sized squares. In tetrolet transform, an image $X[i,j]_{i,j=1}^{N}$ with $N = 2^P,\ P \in N$ is divided into 4×4 blocks. Each block is covered with any four free tetrominoes, which is responsible for enhancing the local structure using properties of rotations and reflections. These four tetrominoes (I_o, I_1, I_2, I_3) are mapped in a unique order (0, 1, 2, 3) by applying bijective mapping (L) with their corresponding order. For each tetromino subset (I_v), the discrete basis functions (Krommweh, 2010) are defined as follows:

$$\phi_{I_v}[i,j] := \begin{cases} 1/2; & (i,j) \in I_v \\ 0; & \text{otherwise} \end{cases}$$

$$\psi^l_{I_v}[i,j] := \begin{cases} \in [l, L(i,j)]; & (i,j) \in I_v \\ 0; & \text{otherwise} \end{cases}$$

for $l = 1, 2, 3$, $\psi^l_{I_v}$ represents tetrolets and ϕ_{I_v} is scaling function. Haar wavelet transform matrix W has four fixed 2×2

squares with 117 solution for disjoint covering of a 4×4 board.

$$W = (\in [m,n])_{m,n=0}^{3} = \frac{1}{2}\begin{pmatrix} 1 & 1 & 1 & 1 \\ 1 & 1 & -1 & -1 \\ 1 & -1 & 1 & -1 \\ 1 & -1 & -1 & 1 \end{pmatrix}$$

There are 117 kinds of tilings for covering of a 4×4 block with any four tetrominoes (Jain and Tyagi, 2015). Fig. 1(b) represents one of the covering from 117 kinds of tilings and Fig. 1(c) represents its local structure.

3. Proposed methodology

Generally, the distribution of noise in CT images follows the Poisson distribution due to statistical fluctuations on X-ray projected data (Rabbani et al., 2009). However, different reconstruction algorithms can change the distribution of noise model. Thus by Central Limit Theorem (CLT), the noise can be best modeled by Gaussian distribution (Rabbani, 2009; Ali and Sukanesh, 2011; Zhu et al., 2012). The CLT in CT images can be obtained by adding values from many different projections into each voxel of CT images (Hashemi et al., 2015; Borsdorf et al., 2008; Naimi et al., 2015). With the assumption that the CT images are corrupted by Gaussian noise with zero mean and different variances, the scheme is proposed using locally adaptive shrinkage rule in tetrolet domain.

Let, the noisy image $X(i,j)$ be expressed as:

$$X(i,j) = Y(i,j) + \eta(i,j) \quad (1)$$

where, η is an additive noise, Y is noiseless image. The block diagram of the proposed scheme is shown in Fig. 2. For denoising of noisy CT scanned images, tetrolet transform plays a major role to enhance the local information of an image because of multi-scale geometric property.

In our proposed scheme, tetrolet transform is used to decompose input noisy CT image into low (LL) and high (LH, HL, HH) frequency subbands. Generally, physicians prefer original noisy images more willingly in comparison to smooth images for more sophisticated CT images. Therefore, low frequency tetrolet subbands are not processed. The perfect optimization for estimating a threshold value is an almost impossible task for image denoising. Thus as an alternative, an iterative method (Gupta et al., 2014) is used to get an

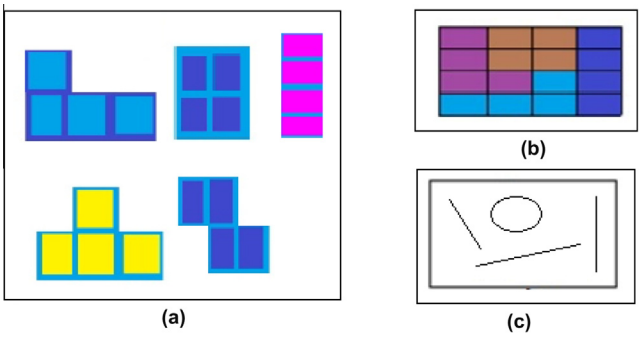

Figure 1 Tetromeno patterns with example. (a) Five tetromeno patterns. (b) One of the disjoint covering from 117 kind of tilings. (c) Corresponding local structure of (b).

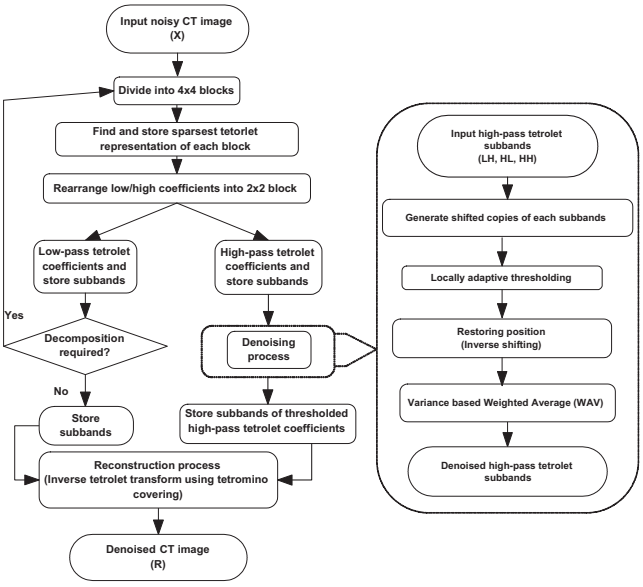

Figure 2 Proposed scheme.

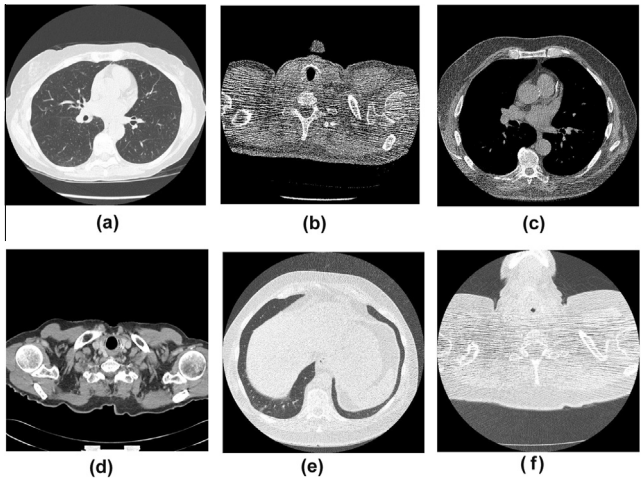

Figure 3 Original CT image data set.

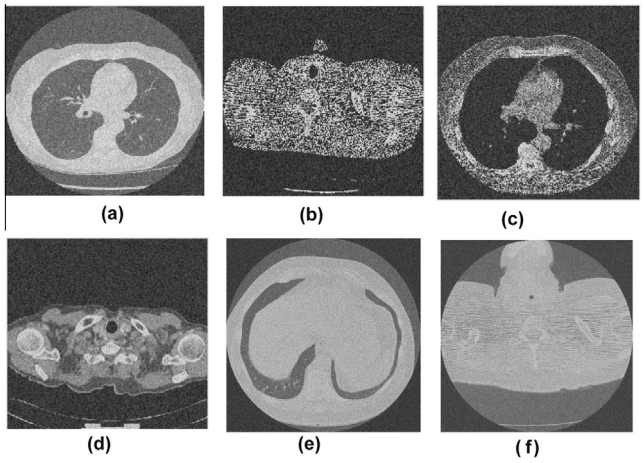

Figure 4 Noisy CT image data set $\sigma = 20$.

Table 1 Average correlation values between multiple thresholded high frequency subbands.

L	X^{LH}						X^{HL}						X^{HH}					
	CT1	CT2	CT3	CT4	CT5	CT6	CT1	CT2	CT3	CT4	CT5	CT6	CT1	CT2	CT3	CT4	CT5	CT6
L = 1	0.9996	0.9934	0.9826	0.9656	0.9967	0.9989	0.9843	0.9992	0.9965	0.9892	0.9971	0.9992	0.9787	0.9692	0.9856	0.9801	0.9985	0.9994
L = 2	0.9732	0.9810	0.9721	0.9591	0.9741	0.9641	0.9571	0.9843	0.9669	0.9801	0.9793	0.9635	0.9619	0.9491	0.9624	0.9612	0.9703	0.9667
L = 3	0.9510	0.9583	0.9634	0.9310	0.9545	0.9431	0.9391	0.9623	0.9503	0.9511	0.9572	0.9410	0.9592	0.9312	0.9478	0.9598	0.9458	0.9498
L = 4	0.9497	0.9304	0.9331	0.9006	0.9365	0.9211	0.9131	0.9378	0.9395	0.9402	0.9476	0.9351	0.9271	0.9020	0.9378	0.9327	0.9309	0.9274
L = 5	0.9158	0.9043	0.9163	0.8912	0.9019	0.9143	0.9023	0.9191	0.9112	0.9229	0.9086	0.9071	0.9067	0.8932	0.9106	0.9208	0.9069	0.9104

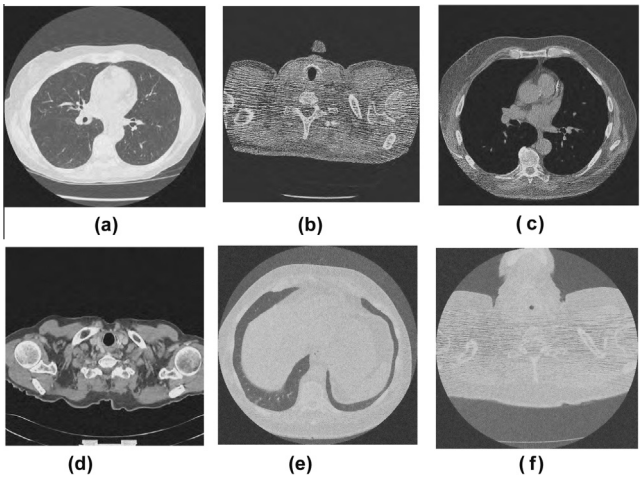

Figure 5 Results of LLSURE.

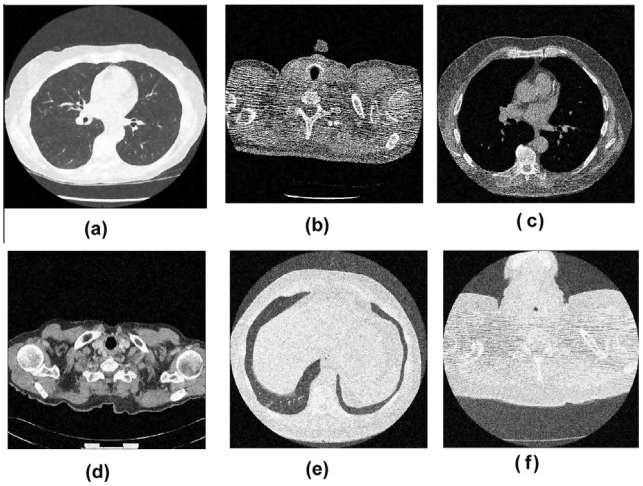

Figure 6 Results of Bilateral filtering.

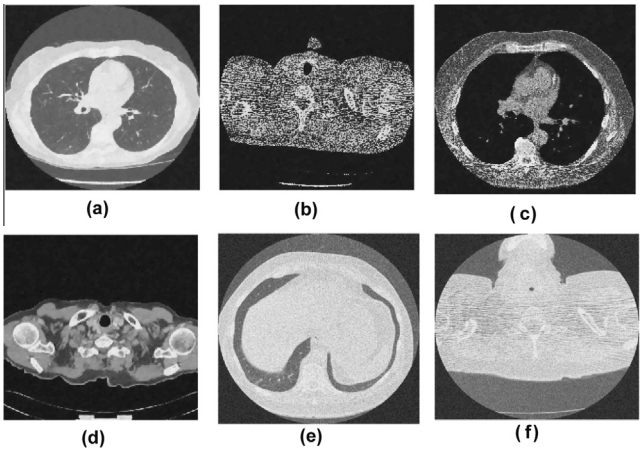

Figure 7 Results of total variation denoising.

optimum thresholded value for each coefficient. To accomplish this, we made several high-frequency tetrolet subbands by shifting the coefficient position in the direction of x- and/or y-axis circularly which are known as shifted copies of respective high-frequency tetrolet subbands. These shifted high frequency subbands are thresholded separately by applying locally adaptive shrinkage rule using estimated threshold value and averaged to get final denoised coefficients.

In our proposed scheme, BayesShrink method is used to estimate the threshold value. BayesShrink is a mathematical framework where it is assumed that each high frequency subbands of tetrolet coefficients are generalized by Gaussian distribution to estimate the threshold value that minimizes the Bayesian risk. To denoise high frequency subbands, a threshold value is estimated and thresholding is performed. The threshold value can be estimated as,

$$\lambda = \frac{\sigma_\eta^2}{\sigma_Y} \tag{2}$$

where the noise variance (σ_η^2) can be estimated using robust median estimator method (Borsdorf et al., 2008) and defined as:

$$\sigma_\eta^2 = \left[\frac{median(|X(i,j)|)}{0.6745}\right]^2 \tag{3}$$

and variance σ_W^2 of noiseless image can be extracted as,

$$\sigma_Y^2 = max\left(\sigma_X^2 - \sigma_\eta^2, 0\right) \tag{4}$$

where $\sigma_X^2 = \frac{1}{w}\sum_{i=1}^{w} X_i^2$ and w represents the number of pixels in a selected block.

In our proposed scheme, a thresholding shrinkage rule (Gao and Bruce, 1997) is used to denoise high frequency tetrolet subbands which helps to avoid the limitations of both hard and soft thresholding. This function also helps to minimize the overall mean-squared error. The thresholding function can be expressed as:

$$\hat{X}' := \begin{cases} X, & \text{if } |X| > \lambda_2 \\ sign(X)\frac{\lambda_2(|X|-\lambda_1)}{\lambda_2-\lambda_1}, & \text{if } \lambda_1 < |X| \leqslant \lambda_2 \\ 0, & \text{Otherwise} \end{cases} \tag{5}$$

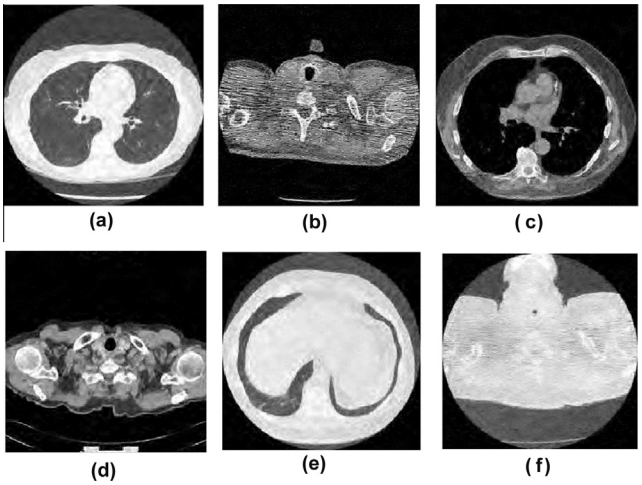

Figure 8 Results of SURELET.

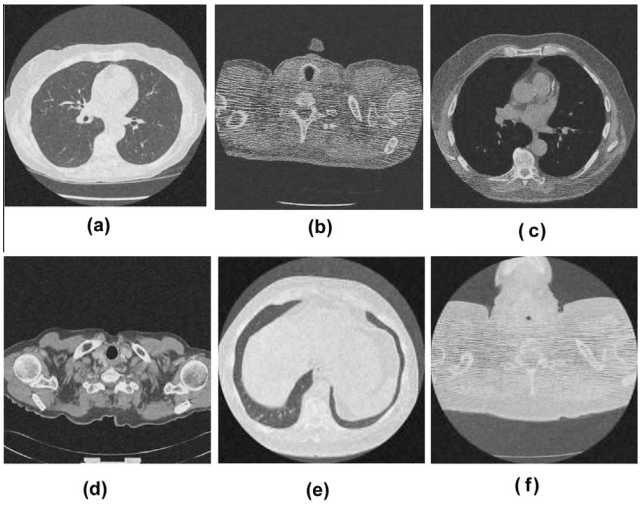

Figure 9 Results of Bayes thresholding.

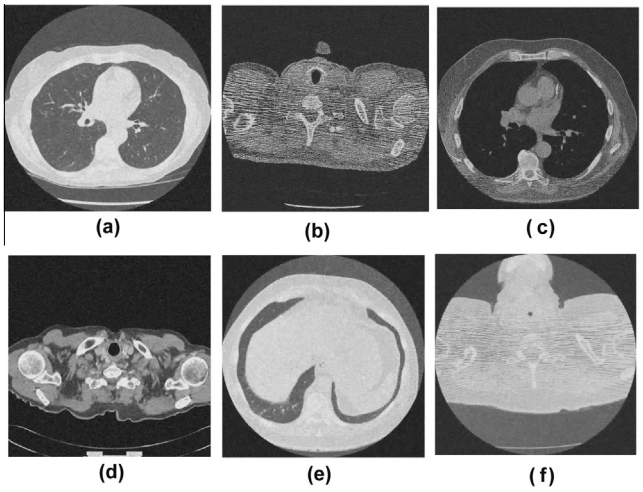

Figure 10 Results of biorthogonal wavelet thresholding.

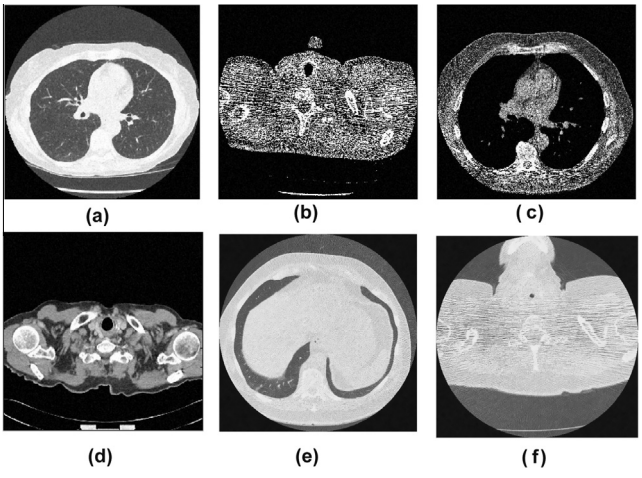

Figure 11 Results of proposed scheme.

After thresholding process, all shifted copies of high frequency tetrolet subbands are restored by shifting coefficients into their original position and patch wise variance based weighted average is performed to get final thresholded high frequency tetrolet subbands. Finally, inverse tetrolet decomposition is performed to obtain final denoised CT image.

Our proposed method consist the following steps:

Step 1: Apply tetrolet decomposition on noisy input CT image to obtain low and high frequency subbands as below:

(a) Divide the image into 4×4 blocks.

(b) Set the decomposition level and tetromino covering values (by, 117).

(c) Find and store sparsest tetrolet representation of each block.

(d) Rearrange low/high coefficients into 2×2 blocks and obtain low and high frequency subbands.

(e) Extraction of further decomposition on low frequency subband:

- For each level, low frequency subbands are decomposed. Decomposed subbands are known as child node for respective parent node.
- Calculate the entropy as a cost function (Fathi and Naghsh-Nilchi, 1989) of each child nodes as well as parent nodes.
- In top down approach manner, check the cost value. If the cost of parent node is greater than total cost of child nodes; Continue further decomposition. Otherwise; Stop decomposition and eliminate children nodes.

Step 2: Prepare k number of shifted copies of high frequency tetrolet subbands by shifting the coefficient positions in the direction of the x- and/or y-axis circularly.

$$X'(i,j)_{s^{\gamma}} = circular\_shift\{X(i,j)_s, [i_{shift}, j_{shift}]\} \quad (6)$$

where $\gamma = 1 \ldots k$, the value of k depends on the length of respective high frequency tetrolet subband.

Step 3: For each decomposition level (L):

(a) Calculate local noise variance using Eq. (3)

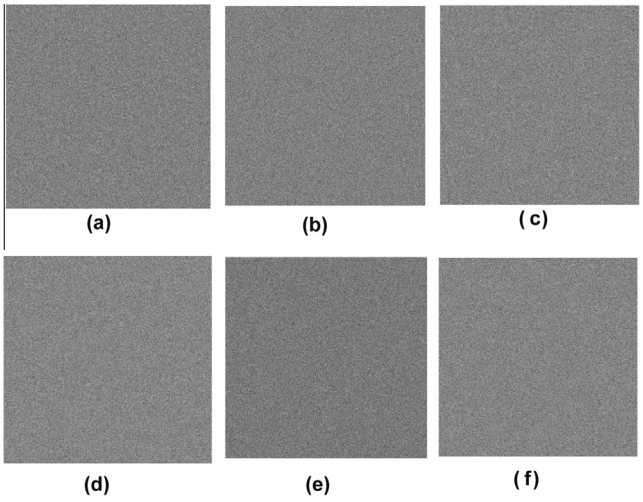

Figure 12 Difference between original and noisy image.

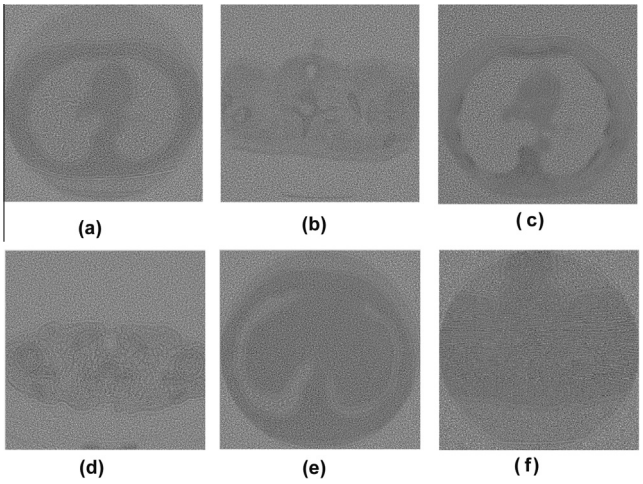

Figure 14 Difference between original and bilateral filtered image.

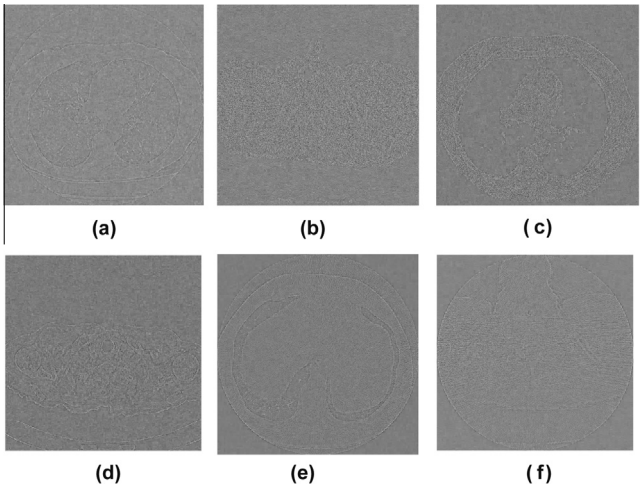

Figure 13 Difference between original and LLSURE filtered image.

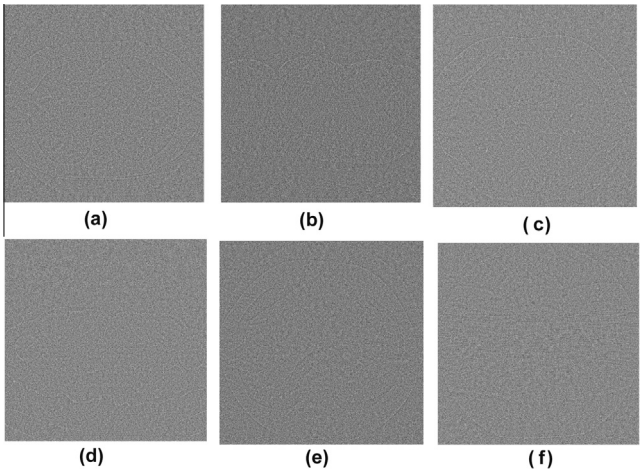

Figure 15 Difference between original and total variation denoised image.

Please cite this article in press as: Kumar, M., Diwakar, M. CT image denoising using locally adaptive shrinkage rule in tetrolet domain. Journal of King Saud University – Computer and Information Sciences (2016), http://dx.doi.org/10.1016/j.jksuci.2016.03.003

(b) For each tetrolet coefficients in each subband (s):
(i) Compute threshold value λ_1 using Eq. (2)
(ii) Compute threshold value λ_2, by setting $\lambda_2 = 0.9 \cdot \lambda_1$
(iii) Apply shrinkage rule using Eq. (5)

Step 4: After thresholding on each subband, perform the inverse shift. The resulting thresholded high frequency tetrolet coefficients $(\widehat{X}'(i,j)_{s^{\gamma}})$ are shifted back to the original position and the multiple high frequency tetrolet modified subbands are stored.

$$X''(i,j)_{s^{\gamma}} = circular\_shift\{\widehat{X}'(i,j)_{s^{\gamma}}, [-i_{shift}, -j_{shift}]\} \tag{7}$$

Step 5: To get final denoised high frequency tetrolet subbands, perform patch wise variance based weighted average on multiple high frequency tetrolet modified subbands, as given below (Jain and Tyagi, 2015):

$$\widehat{X}(i,j)_s = \sum_{\gamma=1}^{k} \alpha_{s^{\gamma}} \cdot X''(i,j)_{s^{\gamma}} \tag{8}$$

where $\alpha_{s^{\gamma}} = \frac{var^{-1}(X''_{w,s^{\gamma}})}{\sum_{\gamma=1}^{k} var^{-1}(X''_{w,s^{\gamma}})}$, $var^{-1}(\cdot)$ represents inverse of the variance, $\hat{X}(i,j)_s$ is the final thresholded value for the coefficient at position (i,j) in the subband s and w is local neighborhood which is used to calculate the local variance.

Step 6: Perform the tetrolet reconstruction, to get the final denoised CT image.

4. Experimental results and discussion

The experimental evaluation is performed on noisy CT images with size 512x512. The CT scanned test images shown in Fig. 3 (a–f) are obtained from public access database (https://eddie.via.cornell.edu/cgibin/datac/logon.cgi). The proposed image denoising scheme is applied to all test images corrupted by additive Gaussian white noise at four different noise levels (σ): 10, 20, 30, and 40. Fig. 3(a–f) is considered as CT image 1, 2, 3, 4, 5 and 6 respectively. Fig. 4(a–f) shows noisy test image data set with $(\sigma) = 20$.

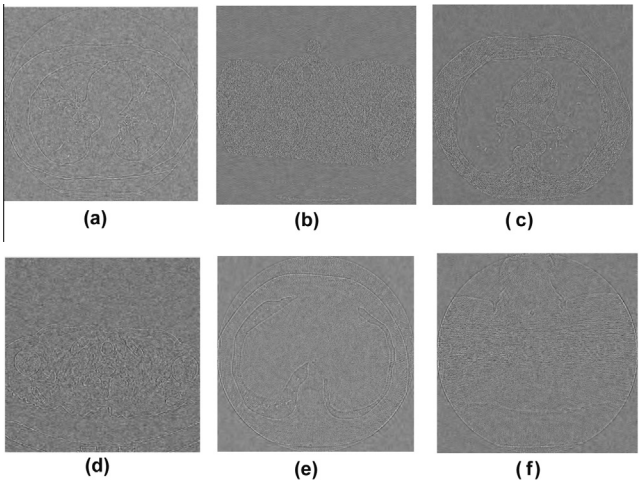

Figure 16 Difference between original and SURELET filtered image.

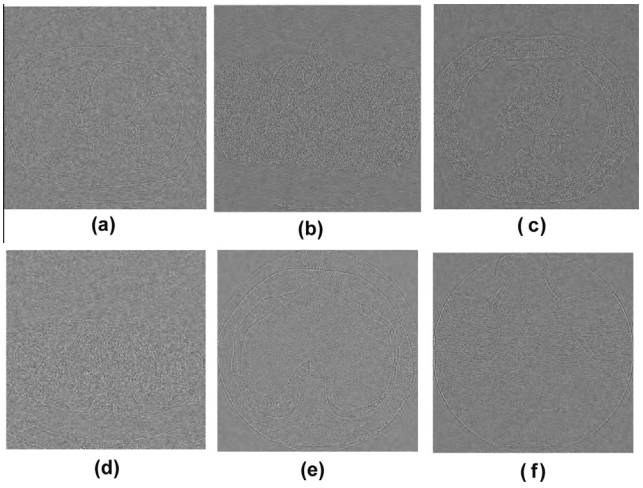

Figure 17 Difference between original and Bayes denoised image.

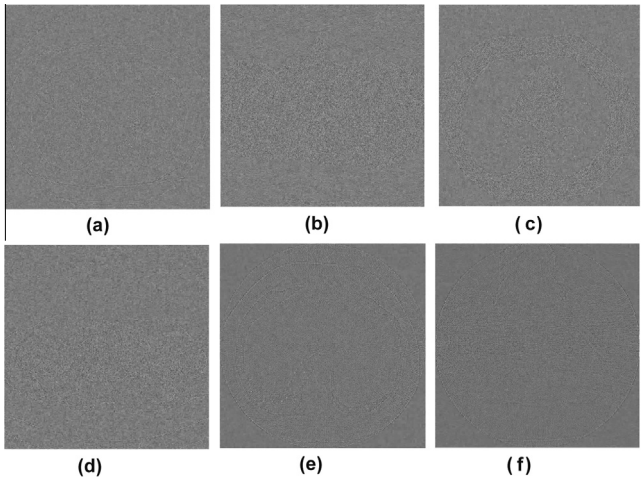

Figure 18 Difference between original and biorthogonal wavelet based denoised image.

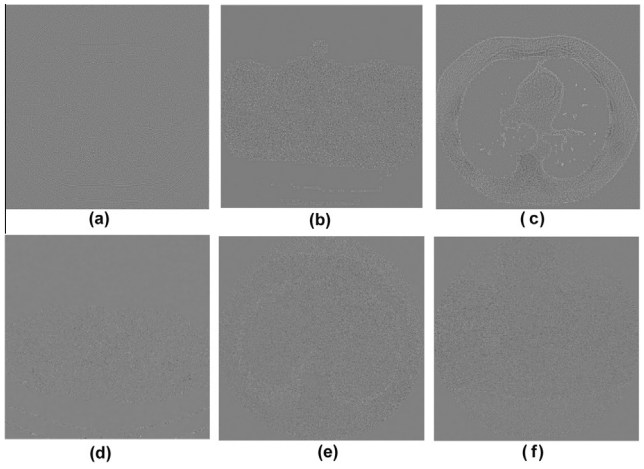

Figure 19 Difference between original and proposed scheme based denoised image.

Table 2 MSE, PSNR and IQI of CT denoised images.

Image	σ	MSE				PSNR				IQI			
		10	20	30	40	10	20	30	40	10	20	30	40
CT1	LLSURE (Qiu et al., 2013)	40.20	116.17	205.15	281.24	32.09	27.45	25.01	23.64	0.9968	0.9019	0.8864	0.8670
	Bilateral (Durand and Dorsey, 2002)	50.35	102.58	154.19	231.24	31.11	28.02	26.25	24.49	0.9952	0.9174	0.8972	0.8711
	TV (Goldstein and Osher, 2009)	40.55	96.17	145.90	258.27	32.05	28.30	26.49	24.01	0.9976	0.9175	0.8831	0.8540
	SURELET (Thierry and Florian, 2007)	46.99	102.82	158.88	227.02	31.41	28.01	26.12	24.57	0.9951	0.9168	**0.8961**	0.8702
	Bayes (Chang et al., 2000)	39.27	96.62	145.23	258.27	32.19	28.28	26.51	24.01	0.9971	0.9147	0.8832	0.8521
	Bior (Prakash and Khare, 2014)	38.91	93.77	147.59	239.92	32.23	28.41	26.54	24.33	0.9973	0.9139	0.8812	0.8510
	Proposed	**34.76**	**88.32**	**119.42**	**207.05**	**32.72**	**28.67**	**27.36**	**24.97**	**0.9993**	**0.9298**	0.8949	**0.8841**
CT2	LLSURE (Qiu et al., 2013)	39.90	95.73	155.98	258.27	32.12	28.32	26.20	24.01	0.9971	0.9028	0.8953	0.8669
	Bilateral (Durand and Dorsey, 2002)	44.06	**78.17**	153.13	289.78	31.69	**29.20**	26.28	23.51	0.9975	**0.9198**	0.8721	0.8611
	TV (Goldstein and Osher, 2009)	40.65	92.27	145.57	235.00	32.04	28.48	26.50	24.42	0.9973	0.9061	0.8801	0.8506
	SURELET (Thierry and Florian, 2007)	50.82	100.24	155.62	219.72	31.07	28.12	26.21	24.71	0.9952	0.9168	0.8962	0.8712
	Bayes (Chang et al., 2000)	40.18	96.40	146.58	253.55	32.09	28.29	26.47	24.09	0.9976	0.9154	0.8851	0.8552
	Bior (Prakash and Khare, 2014)	39.09	100.01	152.08	241.03	32.21	28.13	26.39	24.31	0.9961	0.9148	0.8863	0.8521
	Proposed	**33.57**	80.18	**123.90**	**207.52**	**32.87**	29.09	**27.20**	**24.96**	**0.9993**	0.9081	**0.8999**	**0.8875**
CT3	LLSURE (Qiu et al., 2013)	51.53	100.01	151.73	252.39	31.01	28.13	26.32	24.11	0.9941	0.8801	0.8781	0.8649
	Bilateral (Durand and Dorsey, 2002)	49.09	80.55	152.78	266.73	31.22	29.07	26.29	23.87	0.9979	0.9080	0.8832	0.8642
	TV (Goldstein and Osher, 2009)	**40.18**	102.82	152.78	258.27	**32.09**	28.01	26.29	24.01	**0.9984**	0.8960	0.8728	0.8572
	SURELET (Thierry and Florian, 2007)	46.99	81.29	125.62	210.90	31.41	29.03	27.14	24.89	0.9950	0.8920	0.8705	0.8613
	Bayes (Chang et al., 2000)	42.08	98.19	144.90	235.54	31.89	28.21	26.52	24.41	0.9947	0.9073	0.8837	0.8609
	Bior (Prakash and Khare, 2014)	43.15	94.20	133.68	225.98	31.78	28.39	26.87	24.59	0.9933	0.9061	0.8828	0.8660
	Proposed	40.27	**73.29**	**125.04**	**207.05**	32.08	**29.48**	**27.16**	**24.97**	0.9961	**0.9089**	**0.8879**	**0.8663**
CT4	LLSURE (Qiu et al., 2013)	59.44	102.82	159.61	230.18	30.39	28.01	26.10	24.51	0.9942	0.8998	0.8709	0.8553
	Bilateral (Durand and Dorsey, 2002)	**43.15**	86.11	155.62	258.27	**31.78**	28.78	26.21	24.01	**0.9981**	0.9031	0.8789	0.8601
	TV (Goldstein and Osher, 2009)	56.37	100.94	141.93	232.85	30.62	28.09	26.61	24.46	0.9962	0.8914	0.8682	0.8565
	SURELET (Thierry and Florian, 2007)	51.53	102.11	154.55	246.64	31.01	28.04	26.24	24.21	0.9953	0.9012	0.8869	0.8659
	Bayes (Chang et al., 2000)	55.09	92.48	147.25	244.38	30.72	28.47	26.45	24.25	0.9976	0.9023	0.8843	0.8636
	Bior (Prakash and Khare, 2014)	52.49	89.55	144.57	225.98	30.93	28.61	26.53	24.59	0.9978	0.9043	0.8813	0.8661
	Proposed	46.78	**83.96**	**139.66**	**216.31**	31.43	**28.89**	**26.68**	**24.78**	0.9979	**0.9059**	**0.8892**	**0.8693**
CT5	LLSURE (Qiu et al., 2013)	44.88	92.27	140.95	268.58	31.61	28.48	26.64	23.84	0.9971	0.8812	0.8633	0.8567
	Bilateral (Durand and Dorsey, 2002)	50.24	103.53	196.82	268.28	31.12	27.98	25.19	23.91	0.9934	0.8966	0.8712	0.8533
	TV (Goldstein and Osher, 2009)	55.09	100.48	151.73	260.66	30.72	28.11	26.32	23.97	0.9932	0.8734	0.8609	0.8598
	SURELET (Thierry and Florian, 2007)	49.21	95.95	138.06	249.50	31.21	28.31	26.73	24.16	0.9953	0.9012	0.8769	0.8619
	Bayes (Chang et al., 2000)	44.47	86.71	132.15	246.64	31.65	28.75	26.92	24.21	0.9960	0.8912	0.8883	0.8610
	Bior (Prakash and Khare, 2014)	44.06	89.75	**131.54**	241.03	31.69	28.60	**26.94**	24.31	0.9967	0.8971	**0.8895**	0.8601
	Proposed	**41.69**	**85.91**	133.37	**237.72**	**31.93**	**28.79**	26.88	**24.37**	**0.9979**	**0.9097**	0.8812	**0.8625**
CT6	LLSURE (Qiu et al., 2013)	50.35	85.52	147.59	286.47	31.11	28.81	26.44	23.56	0.9965	0.8909	0.8616	0.8407
	Bilateral (Durand and Dorsey, 2002)	47.98	82.42	137.42	276.74	31.32	28.97	26.75	23.71	0.9943	0.9078	0.8702	0.8653
	TV (Goldstein and Osher, 2009)	39.72	**81.67**	155.62	239.92	32.14	**29.01**	26.21	24.33	0.9961	**0.9117**	0.8714	0.8575
	SURELET (Thierry and Florian, 2007)	48.09	92.91	140.30	221.86	31.31	28.45	26.66	24.67	0.9948	0.9013	0.8709	0.8617
	Bayes (Chang et al., 2000)	49.09	87.51	144.90	239.37	31.22	28.71	26.52	24.34	0.9977	0.9064	0.8811	0.8672
	Bior (Prakash and Khare, 2014)	49.66	88.12	138.06	231.24	31.17	28.68	26.73	24.49	0.9971	0.9001	0.8898	0.8688
	Proposed	**38.91**	88.32	**135.54**	**219.82**	**32.23**	28.67	**26.81**	**24.71**	**0.9971**	0.9108	**0.8903**	**0.8691**

4.1. Experimental evaluation

With the motivation that in most of the cases, denoising is dependent on the neighborhood pixels or coefficients, our scheme is designed where high frequency tetrolet coefficients are thresholded by changing neighborhood coefficients using circular shifting and multiple thresholded high frequency subbands are obtained as discussed in proposed methodology

Please cite this article in press as: Kumar, M., Diwakar, M. CT image denoising using locally adaptive shrinkage rule in tetrolet domain. Journal of King Saud University – Computer and Information Sciences (2016), http://dx.doi.org/10.1016/j.jksuci.2016.03.003

section. In our proposed scheme, two threshold values (λ_1 and λ_2) are used in thresholding function. The threshold value (λ_1) can be obtained from Eq. (2). Another threshold value (λ_2) is used to provide less sensitivity for small variations in the data and also for smaller overall mean-squared error (Minasyan et al., 2006). The value of (λ_2) should be between zero to λ_1. Here all experimental results are obtained by setting the threshold value (λ_2) as $\lambda_2 = 0.9\lambda_1$. The results may slightly vary by setting different values of λ_2. The variation between multiple thresholded high frequency subbands can be observed by correlation values. Table 1 shows the obtained average correlation values between multiple thresholded high frequency subbands ($\sigma = 20$).

To achieve maximum edge preserving and effective noise reduction, patch wise variance based weighted average is performed on multiple thresholded high frequency subbands where the patch size is used as 3×3. Using inverse tetrolet decomposition, final denoised image is obtained.

4.2. Performance evaluation

The performance of CT image denoising schemes can be measured using MSE, PSNR and Image Quality Index (IQI).

For input image (X) and denoised image (R), the IQI can be defined as:

$$\mathrm{IQI} = \frac{4\sigma_{XR}\overline{X}\,\overline{R}}{(\sigma_X^2 + \sigma_R^2)\left[(\overline{X})^2 + (\overline{R})^2\right)\Big]} \tag{9}$$

where,
$\overline{X} = \frac{1}{N}\sum_{i=1}^{N} X_i$, $\overline{R} = \frac{1}{N}\sum_{i=1}^{N} R_i$, $\sigma_X^2 = \frac{1}{N-1}\sum_{i=1}^{N}(X_i - \overline{X})^2$, $\sigma_R^2 = \frac{1}{N-1}\sum_{i=1}^{N}(R_i - \overline{R})^2$ and $\sigma_{XR} = \frac{1}{N-1}\sum_{i=1}^{N}(X_i - \overline{X})(R_i - \overline{R})$.

The quality of image index range lies between 1 and -1. The best value 1 represents an identical value of input image pixel and denoised image pixel. The lowest value -1 shows that the pixel values are uncorrelated.

Peak Signal-to-Noise Ratio (PSNR) is an important factor to evaluate denoising performance. The higher PSNR values represent more similarity between the denoised and original images. For input image (X) and denoised image (R), the PSNR is expressed as:

$$PSNR = 10 \times \log_{10}\left(\frac{255\times255}{MSE}\right) \tag{10}$$

where, Mean Square Error (MSE) is defined as

$$MSE = \frac{1}{mn}\sum_{i=0}^{m-1}\sum_{j=0}^{n-1}[X(i,j) - R(i,j)]^2$$

4.3. Comparisons

To validate the superiority of the proposed scheme, its performance is compared in terms of visual quality, MSE, PSNR and Image Quality Index (IQI) of the denoised images using some standard existing methods. For strong comparison, both wavelet and non-wavelet based existing standard methods are used. The existing methods used for comparison are LLSURE (Qiu et al., 2013), Bilateral filtering (Durand and Dorsey, 2002), Total variation (Goldstein and Osher, 2009), SURELET (Thierry and Florian, 2007), wavelet based Bayes thresholding using Daubechies 8 (DB8) (Chang et al., 2000) and medical image denoising based on soft thresholding using bi-orthogonal 1.3 (bior 1.3) multiscale wavelet transform (Prakash and Khare, 2014).

Figs. 5–11 are showing the results of LLSURE (Qiu et al., 2013), Bilateral filtering (Durand and Dorsey, 2002), Total variation (Goldstein and Osher, 2009), SURELET (Thierry and Florian, 2007), wavelet based Bayes thresholding (Chang et al., 2000), medical image denoising based on soft thresholding using biorthogonal multiscale wavelet transform (Prakash and Khare, 2014) and proposed scheme respectively. The image quality is measured by visual inspection as there is no generally accepted objective way to judge the image quality of a denoised image. There are two criteria widely used in the literature are: (1) visibility of the artifacts and (2) preservation of edge details. The performance of LLSURE method as shown in Fig. 5, is not satisfactory, specially in homogenous regions and near the edges. The method of Bilateral filtering as shown in Fig. 6, provides smoother edge preserved results in homogenous regions. For higher noise level, edge preservation of small detail parts are not satisfactory for clinical purpose. The results of Total Variation (TV) denoising as shown in Fig. 6, give edge preserved smooth denoised images but texture is not as good as for clinical purpose. The results of SURELET, wavelet based denoising using Bayes thresholding and Biorthogonal wavelet thresholding as shown in Figs. 8–10 respectively are providing smoother edge preserved results in homogenous regions. As the noise level increases, Bayes and Biorthogonal wavelet thresholding methods failed to provide the smooth data over the homogenous regions. SURELET also failed to provide satisfactory results on the edges over the higher noise level. The proposed scheme performs several intermediate results using variation and averaging on high frequency coefficients to get final denoised image. The proposed denoising method employs a locally adaptive thresholding where all tetrolet coefficients of each high-frequency subbands are thresholded using the coefficients in their local neighborhoods. It is observed that the results of proposed scheme provide better outcomes for effectively noise reduction and edge preservation of the CT images. Fig. 12 shows the difference between the original and noisy images. Figs. 13–19 show the results as the difference between the original images and the filtered ones for each method where visually it can be observed that proposed scheme gives better outcomes in most of the cases. Table 2 shows MSE, PSNR (in dB) and IQI values of the denoised images relative to their original images for proposed and existing methods. The best values among all the methods are represented in bold. The results shown in Table 2 demonstrate that in most of the cases, the proposed method is superior to all other methods.

5. Conclusions

An alternate post processing approach of iterative method has been proposed to denoise the CT images using locally adaptive thresholding rule in tetrolet domain. Patch wise variance based weighted average gives the strength to get finer details and effective denoising. The proposed method can be implemented very simply and more efficiently than many existing denoising methods. In most of the cases, the MSE, PSNR and IQI values of proposed scheme are better in comparison to existing methods. Apart from MSE, PSNR and IQI, the visual quality of

Please cite this article in press as: Kumar, M., Diwakar, M. CT image denoising using locally adaptive shrinkage rule in tetrolet domain. Journal of King Saud University – Computer and Information Sciences (2016), http://dx.doi.org/10.1016/j.jksuci.2016.03.003

proposed scheme over the CT images is better in terms of clinically relevant details. Experimental results demonstrate that our proposed method: (i) effectively eliminate the noise in CT images, (ii) preserve the edge and geometrical structures, and (iii) retain clinically relevant details.

References

Abramovitch, F., Sapatinas, T., Silverman, B.W., 1998. Wavelet thresholding via a Bayesian approach. J. Roy Stat. Soc. 60 (4), 725–749.

Aharon, M., Elad, M., Bruckstein, A., 2006. K-SVD: an algorithm for designing overcomplete dictionaries for sparse representation'. IEEE Trans. Signal Process 54, 4311–4322.

Ali, S.H., Sukanesh, R., 2011. An efficient algorithm for denoising MR and CT images using digital curvelet transform. Adv. Exp. Med. Biol. 696, 471–480.

Antoniadis, A., Fan, J., 2001. Regularization of wavelet approximations. J. Am. Stat. Assoc. 96 (455), 939–967.

Beekman, F.J., Kamphuis, C., 2001. Ordered subset reconstruction for X-ray CT. Int. J. Med. Phys. Res. Practice 46, 1835–1844.

Borsdorf, A., Raupach, R., Flohr, T., HorneggerTanaka, J., 2008. Wavelet based noise reduction in CT-images using correlation analysis. IEEE Trans. Med. Imaging 27 (12), 1685–1703.

Buades, A., Coll, B., Morel Song, J.M., 2005. A review of image denoising algorithms, with a new one. SIAM J. Multiscale Model. Simul. 4 (2), 490–530.

Chambolle, A., 2004. An algorithm for total variation minimization and applications. J. Matter Image Visual., J. Roy Stat. Soc. 20 (1), 89–97.

Chang, S.G., Yu, B., Vetterli, M., 2000. Adaptive wavelet thresholding for image denoising and compression. IEEE Trans. Image Process. 9 (9), 1532–1546.

Donoho, D.L., 2010. De-noising by soft-thresholding. IEEE Trans. Inf. Theory 41 (3), 613–627, Signal Process 90(8) pp. 2529–2539, 2010.

Donoho, D.L., Johnstone, I.M., 1994. Ideal spatial adaptation via wavelet shrinkage. Biometrika 81, 425–455.

Durand, F., Dorsey, J., 2002. Fast bilateral filtering for the display of high dynamic range images. ACM Trans. Graphics 21 (3), 257–266.

Fathi, A., Naghsh-Nilchi, A.R., 1989. Efficient image denoising method based on a new adaptive wavelet packet thresholding function. IEEE Trans. Image Process. 21 (9), 3981–3990.

Gao, H.Y., 1998. Wavelet shrinkage denoising using the nonnegative garrote. J. Comput. Graph. Stat. 7 (4), 469–488.

Gao, H.Y., Bruce, A.G., 1997. WaveShrink with firm shrinkage. Stat. Sin. 7, 855–874.

Goldstein, T., Osher, S., 2009. The split Bregman method for L1 regularized problems. SIAM J. Imaging Sci. 2 (2), 323–343.

Gupta, D., Anand, R.S., Tyagi, B., 2014. Despeckling of ultrasound medical images using nonlinear adaptive anisotropic diffusion in nonsubsampled shearlet domain. Biomed. Signal Process. Control 14, 55–65.

Hashemi, S.M., Paul, N.S., Beheshti, S., Cobbold, R.S.C., 2015. Adaptively tuned iterative low dose CT image denoising. Comput. Math. Methods Med.

Jain, P., Tyagi, V., 2015. An adaptive edge-preserving image denoising technique using tetrolet transforms. J. Visual Comput. 31 (5), 657–674.

Jain, P., Tyagi, V., 2015. LAPB: locally adaptive patch-based wavelet domain edge-preserving image denoising. J. Inf. Sci. 294, 164–181.

Krommweh, J., 2010. Tetrolet shrinkage with anisotropic total variation minimization for image approximation. Signal Process. 90 (8), 2529–2539.

Li, K., Zhang, R., 2010. Multiscale wiener filtering method for low-dose CT images. IEEE Biomed. Eng. Inf.s, 428–431.

Mallat, S., 1989. A theory for multiresolution signal decomposition: the wavelet representation. IEEE Trans. Pattern Anal. Mach. Intell. 11 (7), 674–693.

Manduca, A., Yu, L., Trzasko, J.D., Khaylova, N., Kofler, J.M., McCollough, C.M., Fletcher, J.G., 2009. Projection space denoising with bilateral filtering and CT noise modeling for dose reduction in CT. Int. J. Med. Phys. Res. Practice 36 (11), 4911–4919.

Minasyan, S., Astola, J., Egiazarian, K., Guevorkian, D., 2006. Parametric Haar-like transforms in image denoising. IEEE Int. Conf. Image Process., 2629–2632

Motwani, M.C., Gadiya, M.C., Motwani, R.C., Harris, F.C., 2004. Survey of image denoising techniques. In: Proceedings of Global Signal Processing Expo and Conference (GSPx '04), pp. 27–30.

Naimi, H., Adamou-Mitiche, A.B.H., Mitiche, L., 2015. Medical image denoising using dual tree complex thresholding wavelet transform and Wiener filter. J. King Saud Univ.-Comput. Inf. Sci. 27 (1), 40–45.

Prakash, O., Khare, A., 2014. Medical image denoising based on soft thresholding using biorthogonal multiscale wavelet transform. Int. J. Image Graphics 14 (01n02), 1450002.

Qiu, T., Wang, A., Yu, N., Song, A., 2013. LLSURE: local linear surebased edge-preserving image filtering. IEEE Trans. Image Process. 22 (1), 80–90.

Rabbani, H., 2009. Image denoising in steerable pyramid domain based on a local Laplace prior. Pattern Recognit. 42 (9), 2181–2193.

Rabbani, H., Nezafat, R., Gazor, S., 2009. Wavelet-domain medical image denoising using bivariate laplacian mixture model. IEEE Trans. Biomed. Eng. 56 (12), 2826–2837.

Thierry, B., Florian, L., 2007. The SURE-LET approach to image denoising. IEEE Trans. Image Process. 16 (11), 2778–2786.

Vidakovic, B., 1998. Nonlinear wavelet shrinkage with Bayes rules and Bayes factors. J. Am. Stat. Assoc. 93 (441), 173–179.

Zhoubo, Li, Lifeng, Yu., Joshua, D. Trzasko, David, S. Lake, Daniel, J. Blezek, Joel, G. Fletcher, Cynthia, H. McCollough, Manduca, A., 2014. Adaptive nonlocal means filtering based on local noise level for CT denoising. Int. J. Med. Phys. Res. Practice 41 (1), 011908.

Zhu, F., Carpenter, T., Gonzalez, D.R., Atkinson, M., Wardlaw, J., 2012. Computed tomography perfusion imaging denoising using Gaussian process regression. Phys. Med. Biol. 57 (12), N183–N198.

Please cite this article in press as: Kumar, M., Diwakar, M. CT image denoising using locally adaptive shrinkage rule in tetrolet domain. Journal of King Saud University – Computer and Information Sciences (2016), http://dx.doi.org/10.1016/j.jksuci.2016.03.003

I.J. Image, Graphics and Signal Processing, **2016, 1, 43-50**
Published Online January 2016 in MECS (http://www.mecs-press.org/)
DOI: 10.5815/ijigsp.2016.01.05

A New Locally Adaptive Patch Variation Based CT Image Denoising

Manoj Kumar
Department of Computer Science Babasaheb Bhimrao Ambedkar University Lucknow, India
E-mail: mkjnuiitr@gmail.com

Manoj Diwakar
Department of Computer Science Babasaheb Bhimrao Ambedkar University Lucknow, India
E-mail: manoj.diwakar@gmail.com

Abstract—The main aim of image denoising is to improve the visual quality in terms of edges and textures of images. In Computed Tomography (CT), images are generated with a combination of hardware, software and radiation dose. Generally, CT images are noisy due to hardware/software fault or mathematical computation error or low radiation dose. The analysis and extraction of medical relevant information from noisy CT images are challenging tasks for diagnosing problems. This paper presents a novel edge preserving image denoising technique based on wavelet transform.

The proposed scheme is divided into two phases. In first phase, input CT image is separately denoised using different patch size where denoising is performed based on thresholding and its method noise thresholding. The outcome of first phase provides more than one denoised images. In second phase, block wise variation based aggregation is performed in wavelet domain.

The final outcomes of proposed scheme are excellent in terms of noise suppression and structure preservation. The proposed scheme is compared with existing methods and it is observed that performance of proposed method is superior to existing methods in terms of visual quality, PSNR and Image Quality Index (IQI).

Index Terms—Image denoising, Thresholding, Method noise, Correlation analysis, Aggregation.

I. Introduction

Computed Tomography (CT) is an important tool to detect the internal problems in human body such as depiction of lesions in human organs, skull fracture, brain hemorrhage and many more. CT scan images provide extraordinary sensitive medical relevant information which may helpful to diagnose the problems. However, high radiation dose, low contrast, noise and artifacts are some major drawbacks in computed tomography. Still, it is widely used because of low cost, easy availability, short execution time and excellent sharp images. The impact of radiation dose is directly related to CT image quality. High radiation dose may improve the image quality but it may harm to patients. Low radiation dose may degrade the image quality in terms of noise. Due to noisy CT images, the experts may not comfortable to diagnose the problems.

Various techniques have been investigated to control the noise in CT scan imaging. Projection based techniques such as projection space denoising with bilateral filtering and CT noise modeling for dose reduction in CT imaging [1] work on raw data or sinogram, where noise filtering is performed on raw data or sinogram and the denoised image is reconstructed. Many iterative reconstruction approaches for noise suppression in CT have also been proposed such as ordered subset based reconstruction for X-ray CT scan [2] optimizes the statistical functions and improve low dose CT images. Most of other techniques e.g., bilateral filtering [1, 3], total variation denoising [4, 5], nonlocal means (NLM) denoising [6, 7] and k-SVD [8] take the advantages of statistical properties of objects in image space and preserve clinical structures such as sharp edges, similarities between neighboring pixels, etc. In transform-domain denoising techniques, the input data is decomposed into its scale-space representation [9]. Linear filters such as Wiener filter [10] in the wavelet domain give optimal results when the signal distortion is estimated as Gaussian approximation and the accuracy is measured by calculating Mean Square Error (MSE). Various thresholding techniques for noise reduction have also been introduced with wavelet transform such as efficient image denoising method based on a new adaptive wavelet packet thresholding function [11, 12], ideal spatial adaptation via wavelet shrinkage [13, 14] etc. Thresholding is one of the important tools for denoising. VISUShrink [13, 15] is a non-adaptive universal threshold, which depends only on number of samples and known to find smoothed images because its threshold choice can be large due to its dependence on the number of pixels in the images. SUREShrink [13, 16] uses a hybrid of the universal and the SURE [Steins Unbiased Risk Estimator] thresholds, and performs better than VISUShrink. BayesShrink [17-19] minimizes the Bayes risk estimator function assuming generalized Gaussian approximation and thus finds adaptive threshold value. Chang et al. [20] proposed the use of adaptive wavelet thresholding for image denoising, by modeling the

wavelet coefficients as a generalized Gaussian random variable, whose parameters are estimated locally (i.e., within a given neighborhood). In image space, CT images can be denoised directly without access to raw data. CT image denoising is a challenging task because of finding correct noise variation, relationship between coefficients and achieving an optimal trade-off between denoising and blurring or artifacts [21-23]. To surmount these challenges, we propose a maximum edge preserving and noise reduction method. Experimentally, it is observed that each wavelet coefficients are affected with different patch size. With different patch size, the estimated threshold value may not be the same and may affect images in terms of local features and noise. With this consideration, we propose a scheme for CT image denoising based on the variation in multiple thresholded values which are obtained by different patch sizes.

The paper is organized as follows. Section 2 gives a brief overview of wavelet based shrinkage. In section 3, the proposed method is presented in details. Experimental results, including discussions and comparison with other denoising methods, are given in section 4. Finally, conclusions are summarized in section 5.

II. Image Denoising by Wavelet Shrinkage

Wavelet transform is a powerful tool for signal and image processing tasks because of multi-resolution analysis, sub-banding and localized in both, frequency and time domain. Two dimensional DWT transforms the signals into low frequency (LL) and high frequency components (LH; HL; HH), as shown in Fig. 1.

With the assumption, the CT images are corrupted by Gaussian noise with zero mean and different variances, the noisy CT image can be expressed as:

$$X(m,n) = Y(m,n) + \eta(m,n) \tag{1}$$

Where, $\eta(m,n)$ is a noise coefficient, $Y(m,n)$ and $X(m,n)$ are noiseless and noisy images respectively.

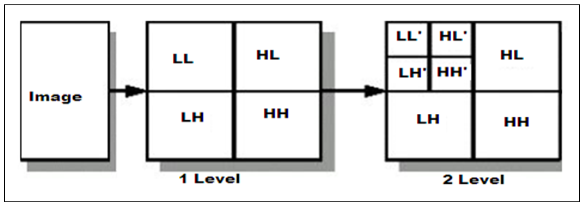

(a)

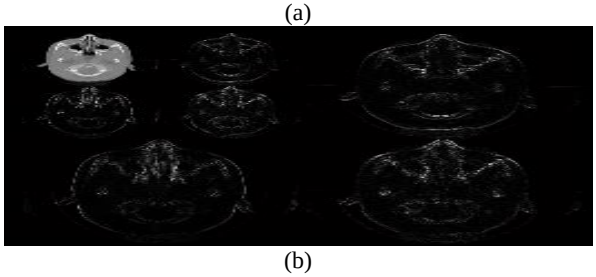

(b)

Fig.1. (a) First and Second Level 2-D Wavelet Decomposition (b) 2D-DWT Decomposition on CT image up-to two levels.

Before applying wavelet thresholding, two important tasks must be performed which are responsible for the results and computational complexity. First, a wavelet basis is chosen for determining its decomposing layers such as haar, db2, etc. Second, decomposition level is chosen for thresholding on all subbands for all levels. Wavelet based noise shrinkage can be expressed with the following major steps:

Step 1: Perform discrete wavelet transform (DWT) on input noisy CT image to obtain approximation and detail parts.

Step 2: Perform the denoising using following steps:

i. Estimate noise variance
ii. Apply thresholding on detail parts

Step 3: Apply inverse discrete wavelet transform (Inverse DWT) to obtain final denoised image.

A. Threshold Selection

For CT images, selection of a threshold value is not an easy task. By selecting small threshold value, the resultant image may be noisy. For large threshold value, the resultant image may blur on the edges. The selection of optimal threshold value is necessary and important task for preserving clinical details and suppression of noise.

The threshold λ can be selected as:

$$\lambda = \left(\frac{\sigma_\eta^2}{\sigma_Y} \right) \tag{2}$$

Where the noise variance can be estimated using robust median estimation method (Abramovitch et al. 1998) as follows:

$$\sigma_\eta^2 = \left[\frac{median(|X(m,n)|)}{0.6745} \right]^2, \tag{3}$$

Where, $X(m,n)$ ϵ HH_L, L represents respective level in wavelet decomposition. The standard deviation of noise less image (σ_Y) can be estimated as:

$$\sigma_Y^2 = \max(\sigma_X^2 - \sigma_\eta^2, 0) \tag{4}$$

Where, $\sigma_X^2 = \frac{1}{b}\sum_{i=1}^{b} X_i^2$, and b represent patch size of an input image.

B. Thresholding process

After selecting a threshold value, the process of

thresholding is applied by selecting an appropriate algorithm. Hard thresholding and soft thresholding methods are very popular for thresholding. In hard thresholding, each coefficient value is compared with threshold value and values less than threshold are replaced by zero. In Soft thresholding, replacement process is same as in hard thresholding, additionally rest of coefficients are modified by subtracting threshold values. In comparison of both, Soft thresholding gives better performance for visual appearance of images. The soft thresholding can be expressed as:

$$\hat{Y} := \begin{cases} 0 & if\ |X| \le \lambda \\ sign(X)(|X| - \lambda) & if\ |X| > \lambda \end{cases} \quad (5)$$

III. Proposed Methodology

The perfect optimization for estimating a threshold value is an almost impossible task for image denoising. Estimated threshold value may be varying according to different patch sizes. With the consideration that the small variation of neighborhood size will not much affect the threshold estimated value, a new locally adaptive different patch size based thresholding scheme is proposed, where some limited patch sizes are selected. The patch sizes can be extracted as: If $X(m,n)$ is the size of image, then for high frequency subband's first patch size will be $(m/2, n/2)$. Similarly, $k-1$ numbers of subband are generated by dividing previous patch size by 2.

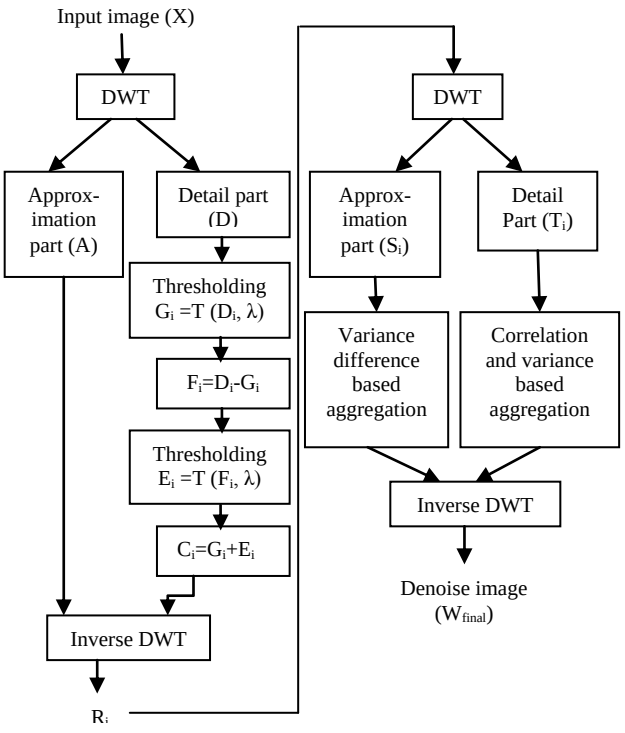

Fig.2. Flow Chart of Proposed Scheme

With the assumption, that the CT image is corrupted by Gaussian noise, the proposed method as shown in fig. 2 can be summarized as:

1) Select the maximum size of input noisy CT image $X(m,n)$ where $m = 2^k$ and $n = 2^k$.
2) Apply DWT on input image to obtain low frequency (A) and high frequency (D) subbands.
3) High frequency subbands (D_i) are patching wise threshold (for $i = 1\ to\ k-1$) using equation (5) according to respective patch size.

$$G_i = T(D_i, \lambda) \quad (6)$$

Where, λ is an estimated noise level calculated using equation (3).

4) Apply method noise using input high frequency (D) subband and thresholded high frequency subband (G_i) as:

i) Subtract G_i from D and get F_i as,

$$F_i = D - G_i \quad (7)$$

ii) Apply patch wise thresholding on F_i .

$$E_i = T(F_i, \lambda) \quad (8)$$

iii) Add G_i and E_i and get C_i ,

$$C_i = G_i + E_i \quad (9)$$

5) Apply inverse DWT, using low frequency (A) and thresholded high frequency (C_i) subbands. The output (R_i) comes in the form of $k-1$ denoised images.
6) To obtain final denoised image, perform the following steps:

i) Separately apply DWT on R_i images to obtain their approximation (S_i) and detail parts (T_i).
ii) Estimate the variance at each pixel of approximation part at level 2 of all denoise images (R_i) in block of size 3 × 3.
iii) Variance (*Var*) difference on approximation part of denoised images (R_i), as below:

$$\tau = \frac{1}{k-2} \sum_{j=1}^{k-2} \alpha_j \quad (10)$$

where,

$$\alpha_j = Var(S_j) - Var(S_{j+1}),\ j = 1\ to\ k-2$$

The value of τ is normalized in the range [0 1] and used as a weight factor for the next process.

iv) Variance difference based aggregation process is based on weight factors τ and perform on approximation part as per the following relationship:

$$B_{final} = H + Q \tag{11}$$

where,

$$H = \frac{1}{k-1}\sum_{f=1}^{\frac{k-1}{2}} \frac{\tau}{f}(S_f);\ Q = \frac{1}{k-1}\sum_{g=\frac{k-1}{2}+1}^{k-1}\left(1-\left(\frac{\tau}{(k-g)}\right)\right)(S_g)$$

v) Variance based aggregation (Jain et al. 2015) using correlation (Corr) is performed on detail parts using following relationship:

$$C_{final} = \begin{cases} T_1^b, & If\ \mathrm{Corr}(T_i, T_{i+1}) > \mathrm{Th} \\ \sum_{i=1}^{k-1} \beta^b T_i^b, & Otherwise \end{cases} \tag{12}$$

where,

$$\beta^b = \frac{Var^{-1}(T_1^b)}{\sum_{i=1}^{k-1} Var^{-1}(T_i^b)}$$

T_i represents detail part of all denoised images (R_i) with block size b. T_h represents a defined threshold value to differentiate between correlated and uncorrelated coefficients. The function $Var^{-1}(.)$ can be estimated as inverse variance.

7) Apply inverse DWT using B_{final} and C_{final} to obtain final denoised image (W_{final}).

In proposed scheme, noisy CT image is denoised in wavelet domain where noise on high frequency coefficients of each subband in *L* level has been suppressed using Bayes shrink and method noise thresholding with different patch sizes. In method noise, the thresholded patch is subtracted with original patch. The outcome of subtraction is again thresholded and added into the thresholded original patch. This method noise thresholding process is used to observe, how much local features of clinical details are missing at the time of thresholding and can be recovered as shown in Step 4. With different patch size, separate multiple denoised images are obtained. To get final denoised image, separately DWT is performed on all denoised images. In approximation part of all denoised images, a weight value τ is estimated using variance difference between different denoised images. This weight value is incorporated into denoised images and aggregation relationship has been performed as shown in Step 6(iv). In detail part, patch wise correlation coefficient values are obtained between all denoised images. Correlation value lies in the interval [-1; 1], where 1 means perfect correlation, 0 no correlation, and -1 perfect anti-correlation. To find correlated and uncorrelated values, correlation values are normalized in the range of [0; 1]. The correlation values closer to 1 indicate that the similarity structure is present between the images. The lower values (near to 0) indicate that the corresponding value includes only noise and, therefore, can be suppressed. If correlation value is greater with a defined threshold (T_h) value then keep the largest patch size denoised coefficient value of subband, otherwise, perform variance based weighted average between all denoised coefficients of subband as given in Step 6(v). Thus, final denoised CT image can be obtained using inverse wavelet transform.

IV. Experimental Results

The experimental evaluation is performed on low quality CT images with size 512x512. The CT scanned test images shown in fig.3(a-c) is obtained from public access database(https://eddie.via.cornell.edu/cgibin/datac/logon.cgi), and CT scanned test image shown in fig. 3(d) is obtained from a Diagnosis Center. The proposed image denoising method is applied on all test images corrupted by additive Gaussian white noise at six different noise level (σ): 10, 15, 20, 25, 30, and 35. Fig. 3(a), 3(b), 3(c) and 3(d) are considered as CT images 1, 2, 3 and 4, respectively. Fig. 4(a-d) are showing noisy test image data set with σ = 25.

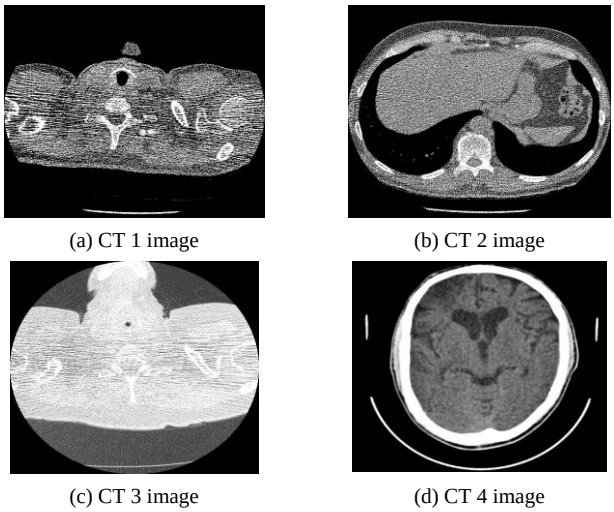

(a) CT 1 image (b) CT 2 image

(c) CT 3 image (d) CT 4 image

Fig.3. Input Test CT Image Dataset

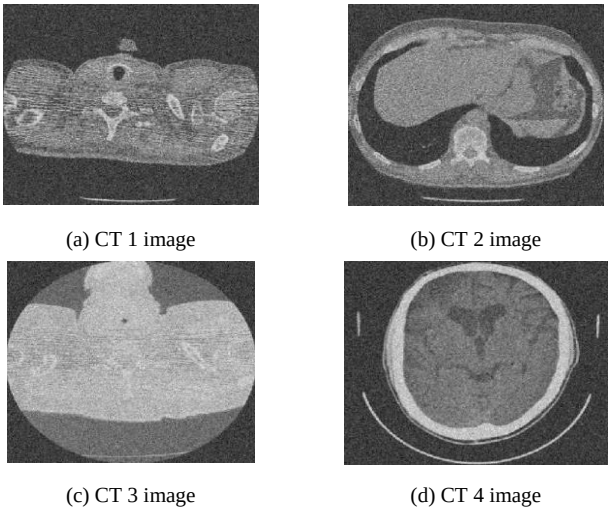

(a) CT 1 image (b) CT 2 image

(c) CT 3 image (d) CT 4 image

Fig.4. Noisy CT Image Dataset (σ=25)

A. Evaluation of different patch size

$k-1$ numbers of patch sizes are used to denoise the images using proposed methodology. The outcome of thresholding may be differ with differ local patch sizes. As $k-1$ numbers of patch size are used separately for thresholding, $k-1$ numbers of thresholded subband are obtained respectively. To verify the effect of different patch sizes for thresholding, an average correlation value is obtained between $k-1$ thresholded subband for all test images. Table 1 shows the average values of the correlations using a 7x7 window for all CT image dataset.

Table 1. Average Values of the Correlations between K-1 Denoised Images using Different Patch Size

Level (L)	*L=1*	*L=2*	*L=3*	*L=4*
CT 1 image	0.9501	0.9385	0.8976	0.8793
CT 2 image	0.9729	0.9462	0.8991	0.8592
CT 3 image	0.9201	0.8976	0.8715	0.8358
CT 4 image	0.8973	0.8695	0.8413	0.8187

B. Performance evaluation

Peak Signal-to-noise Ratio (PSNR) is an important factor to evaluate denoising performance. The high PSNR value represents more similarity between the denoising and original image than lower PSNR value. The objective quality of the denoised image is measured by PSNR as:

$$PSNR = 10\log_{10}\frac{255^2}{mse} \quad \text{dB} \qquad (13)$$

Where *mse* is the mean square error between the original and the denoised image:

$$mse = \frac{1}{mn}\sum_{i=1}^{m}\sum_{j=1}^{n}[X(i,j)-W(i,j)]^2 \qquad (14)$$

Image quality index (IQI) is another important factor to analyse the performance of image denoising in terms of correlation, luminance distortion and contrast distortion. For input image (X) and denoised image (W), the IQI can be defined as:

$$IQI = \frac{4\sigma_{XW}\,\bar{X}\,\bar{W}}{(\sigma_X^2+\sigma_W^2)[(\bar{X})^2+(\bar{W})^2]}$$

where,

$$\bar{X}=\frac{1}{N}\sum_{i=1}^{N}X_i,\ \bar{W}=\frac{1}{N}\sum_{i=1}^{N}W_i,\ \sigma_X^2=\frac{1}{N-1}\sum_{i=1}^{N}(X_i-\bar{X})^2,$$

$$\sigma_W^2=\frac{1}{N-1}\sum_{i=1}^{N}(W_i-\bar{W})^2$$

and

$$\sigma_{XW}=\frac{1}{N-1}\sum_{i=1}^{N}(X_i-\bar{X})(W_i-\bar{W})$$

The quality of image index range lies between 1 and -1. The highest value 1 represents an identical value of input image pixel and denoised image pixel. The lowest value -1 shows that the pixels values are uncorrelated.

C. Experimental evaluation

To evaluate the results of proposed scheme, the parameters are kept fixed throughout the comparisons as in other methods. The result evaluation is performed on the CT images with the size of 512x512, can be expressed as 2^9x2^9. As per proposed scheme, we can evaluate the total number of patch sizes are k-1 i.e 8 and patch size can be expressed as: 256x256, 128x128, 64x64, 32x32, 16x16, 8x8, 4x4 and 2x2. Using these patch sizes, 8 denoised images are obtained. The method noise helps to recover details, textures and edges from denoised images which represent the performance and limitations of denoising algorithm. It is observed from the experimental results that too small blocks may affect the denoised image as block artifacts and too large block size may affect the details as a poor quality edges. Therefore, we apply aggregation process to get final denoised image using multiple denoised images. To aggregate the denoisied images, correlation values are measured on high frequency subbands using block size 3x3 for all test images where a threshold value (T_h) is set as 0.96. Above the threshold value is considered as similarity, so large patch size of denoised coefficients are opted. For below threshold value, variation based weighted average is used with block size 3x3. Similarly, variance difference based aggregation is performed on low frequency subband. Final output comes in the form of single denoised image.

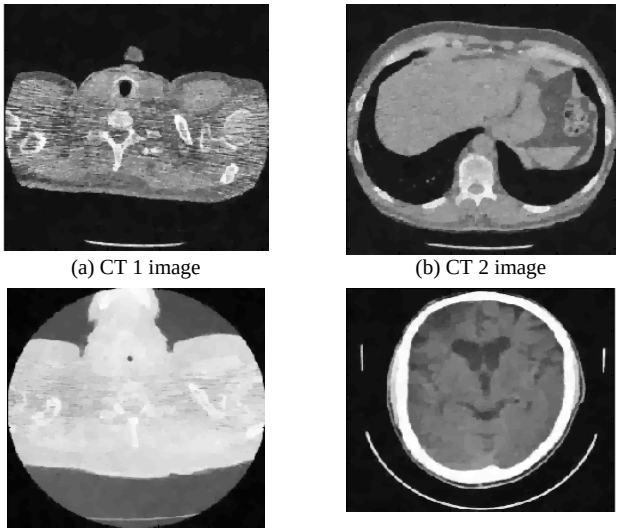

(a) CT 1 image (b) CT 2 image

(c) CT 3 image (d) CT 4 image

Fig.5. Results of Total Variation Denoising

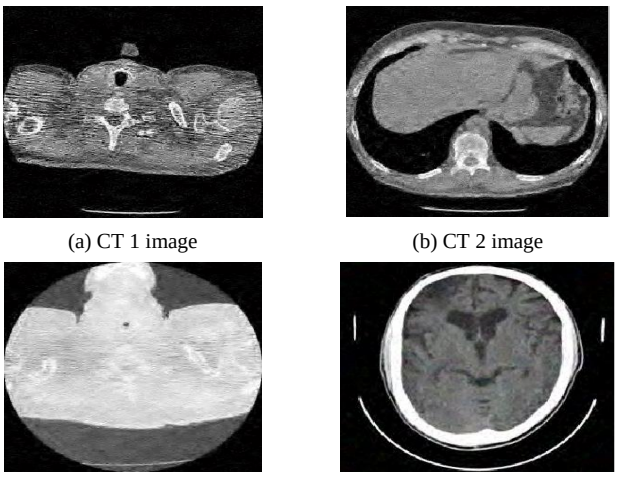

(a) CT 1 image (b) CT 2 image

(c) CT 3 image (d) CT 4 image

Fig.6. Results of SURELET

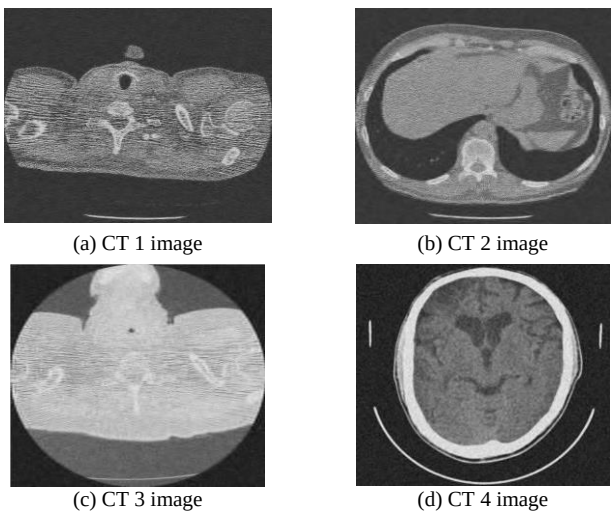

(a) CT 1 image (b) CT 2 image

(c) CT 3 image (d) CT 4 image

Fig.7. Results of Bayes Thresholding

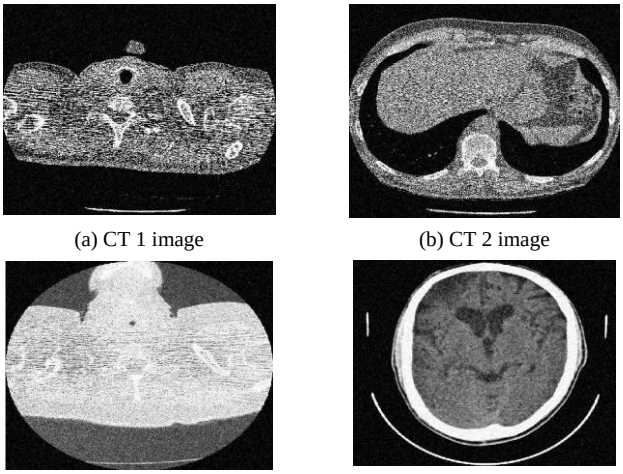

(a) CT 1 image (b) CT 2 image

(c) CT 3 image (d) CT 4 image

Fig.8. Results of Proposed Scheme

Table 2. PSNR of Denoised Images

	σ	TV method	SURELET method	Bayes method	Proposed method
CT 1 image	10	32.14	33.25	31.50	**33.39**
	15	30.95	**31.45**	29.96	31.44
	20	29.45	**30.10**	28.21	30.05
	25	27.98	29.68	28.01	**29.85**
	30	26.31	28.47	27.25	**28.54**
	35	25.26	26.19	25.31	**26.88**
CT 2 image	10	31.54	32.12	30.98	**32.47**
	15	30.87	30.64	29.42	31.05
	20	28.95	29.08	28.47	**29.53**
	25	28.48	28.64	27.26	**28.96**
	30	27.69	28.03	26.17	**28.11**
	35	25.83	26.96	25.34	**26.97**
CT 3 image	10	32.33	33.19	31.98	**33.89**
	15	31.29	31.25	30.67	**31.87**
	20	29.84	**30.98**	28.68	30.91
	25	27.15	29.27	28.34	**29.31**
	30	26.29	28.54	27.52	**28.67**
	35	24.36	26.65	24.64	**26.73**
CT 4 image	10	32.65	33.65	31.63	**33.79**
	15	**31.35**	31.24	29.26	**31.35**
	20	29.64	30.19	28.31	**30.61**
	25	27.45	29.34	28.72	**29.36**
	30	26.64	28.21	27.37	**28.42**
	35	25.39	**26.94**	25.61	26.61

D. Comparisons

To validate the superiority of the proposed scheme, its performance is compared in terms of visual quality, PSNR, and Image Quality Index (IQI) of the denoised images using the various methods available in literature such as Total Variation (TV) (Goldstein et al. 2009), SURELET (Donoho et al. 1995) and Bayes methods (Abramovitch et al. 1998). In all the cases, db8 is used for wavelet decomposition and soft-thresholding is used to

threshold wavelet coefficients. In WT-based thresholding and proposed scheme, three levels of decomposition are used. Tables 2 & 3, respectively show the PSNR (in dB) and IQI values of the denoised images relative to their original images using proposed and existing methods.

The best values amongst all the methods are represented in bold. The results shown in tables demonstrate that in most of the cases, the proposed method is superior to all other methods. The results of TV denoising method as shown in fig. 5 gives edge preserved smooth denoised image but texture is not as good as for clinical purpose.

The results of wavelet based denoising using Bayes and SURELET are shown in fig. 6 & 7 respectively. Both methods are providing smoother results in homogenous regions. As the noise level increases, Bayes method fail to provide smoothed data over the homogenous regions and SURELET also fail to provide satisfactory results on the edges. To overcome these limitations of other methods, the proposed scheme is prepared, where multi estimated threshold values are obtained through different patch sizes, method noise is applied, k-1 denoised images are obtained and finally a aggregation process is applied to provide a single edge preserved noise suppressed image. The obtained results of proposed scheme as shown in fig. 8, gives better results in terms of visual aspects and performance metrics. The result of proposed scheme show improved texture, noise suppression and sharp preserved edges.

Table 3. IQI of Denoised Images

	σ	TV method	SURELET method	Bayes method	Proposed method
CT 1 image	10	0.9931	0.9912	0.9924	**0.9976**
	15	0.9534	0.9856	0.9762	**0.9865**
	20	0.9312	0.9541	0.9365	**0.9597**
	25	0.8972	0.9165	0.9174	**0.9248**
	30	0.8903	0.8954	0.8832	**0.8962**
	35	**0.8894**	0.8762	0.8614	0.8747
CT 2 image	10	0.9817	0.9828	0.9751	**0.9889**
	15	0.9789	0.9794	0.9745	**0.9831**
	20	0.9421	**0.9654**	0.9241	0.9521
	25	0.8452	0.8684	0.8922	**0.9047**
	30	0.8364	0.8361	0.8632	**0.8740**
	35	0.8189	0.8314	0.8614	**0.8694**
CT 3 image	10	0.9874	0.9812	0.9914	**0.9965**
	15	0.9514	0.9614	0.9762	**0.9893**
	20	0.9423	0.9591	0.9432	**0.9614**
	25	0.9102	0.9241	**0.9397**	0.9235
	30	0.8964	0.8931	0.8942	**0.9131**
	35	0.8831	0.8894	0.8913	**0.8941**
CT 4 image	10	0.9871	0.9974	0.9954	**0.9979**
	15	0.9642	0.9831	0.9645	**0.9846**
	20	0.9409	0.9641	0.9469	**0.9698**
	25	0.9123	0.9352	0.9231	**0.9411**
	30	0.8991	0.8978	0.8945	**0.9006**
	35	0.8647	0.8649	**0.8791**	0.8771

V. Conclusions

In this paper, a scheme is proposed based on locally patch thresholding, its method noise thresholding and aggregation. Due to selective patch sizes, the cost computation is reduced in compare of iterative methods. The proposed scheme is taking the advantage of thresholding to denoised same pixel with different patch size. A gap in patch size is maintained by apply a rule to divide by 2 of previous patch size. A method noise with selective patch size may also help for more denoised and edge preserved patch. An aggregation scheme helps to provide a single final edge preserved and noise suppressed CT image. Final outcomes of proposed scheme are good in terms of noise suppression and edge preservation. All the results of proposed scheme are compared by existing methods. In most of the cases, the performance of proposed scheme is giving better values in terms of PSNR and IQI. Apart from performance metrics, the visual quality of proposed scheme over the CT images is also better in terms of clinically relevant details. Experimental results demonstrate that our proposed scheme: (i) effectively eliminate the noise in CT images, (ii) preserve the edge and structural information, and (iii) retain clinically relevant details.

References

[1] A. Manduca, L. Yu, J. D. Trzasko, N. Khaylova, J. M. Kofler, C. M. McCollough and J. G. Fletcher, "Projection space denoising with bilateral filtering and CT noise modeling for dose reduction in CT," International Journal of Medical Physics Research and Practice, Vol. 36, No. 11, pp.4911-4919, 2009.

[2] D. Kim, S. Ramani and J. A. Fessler," Accelerating X-ray CT ordered subsets image reconstruction with Nesterov's first-order methods" In Proc. Intl. Mtg. on Fully 3D Image Recon. in Rad. and Nuc. Med pp. 22-5, 2013.

[3] F. Durand and J. Dorsey, "Fast bilateral filtering for the display of high dynamic range images," ACM Transactions on Graphics, Vol. 21, No. 3, pp.257–266, 2002.

[4] T. Goldstein and S. Osher, "The Split Bregman Method for L1 Regularized Problems," SIAM Journal on Imaging Sciences, Vol. 2, No. 2, pp.323-34, 2009.

[5] A. Chambolle, "An algorithm for total variation minimization and applications," Journal of Matter Image and Visualization', Journal Roy Statistic Society, Vol. 20, No. 1, pp.89–97, 2004.

[6] A. Buades, B. Coll and J. M. Morel Song, "A review of image denoising algorithms, with a new one," SIAM Journal on Multiscale Modeling and Simulation, Vol. 4, No. 2, pp.490–530, 2005.

[7] Z. Li, L.Yu, J. D. Trzasko, D. S. Lake, D. J. Blezek, J. G. Fletcher, C. H. McCollough and A. Manduca, "Adaptive nonlocal means filtering based on local noise level for CT denoising," International Journal of Medical Physics Research and Practice, Vol. 41, No. 1, 2014.

[8] M. Aharon, M. Elad and A. Bruckstein, "K-SVD: An algorithm for designing overcomplete dictionaries for sparse representation', IEEE Trans. Signal Process, Vol. 54, pp.4311–4322, 2006.

[9] S. Mallat, "A theory for multiresolution signal decomposition: the wavelet representation," IEEE Trans. on Pattern Anal. Mach. Intell. , Vol. 11, No. 7, pp.674–693, 1989.

[10] K. Li and R. Zhang, "Multiscale wiener filtering method for low-dose CT images," IEEE Biomedical Engineering and Informatics, pp.428–431, 2010.

[11] A. Fathi and A. R. Naghsh-Nilchi, "Efficient image denoising method based on a new adaptive wavelet packet

thresholding function," IEEE Trans Image Process, Vol. 21, No. 9, pp.3981–3990, 1989.
[12] M. Malfait and D. Roose, "Wavelet based image denoising using a Markov Random Field a priori model," IEEE Transactions on Image Processing, Vol. 6, No. 4, pp.549–565, 1997.
[13] D. L. Donoho and I. M. Johnstone, "Ideal spatial adaptation via wavelet shrinkage," Biometrika, Vol. 81, pp.425–455, 1994.
[14] A. Borsdorf, R. Raupach, T. Flohr and J. Hornegger Tanaka, "Wavelet Based Noise Reduction in CT-Images Using Correlation Analysis," IEEE Transactions on Medical Imaging, Vol. 27, No. 12, pp.1685–1703, 2008.
[15] M. C. Motwani, M. C. Gadiya, R. C. Motwani and F. C. Harris, "Survey of Image Denoising Techniques," Proceedings of Global Signal Processing Expo and Conference (GSPx '04), pp.27–30, 2004.
[16] D. L. Donoho, "De-noising by soft-thresholding," IEEE Transactions on Information Theory, Vol. 41, No. 3, pp.613–627., Signal Process. Vol. 90 no. 8 pp 2529-2539, 2010, 1995.
[17] P. Moulin and J. Liu "Analysis of multiresolution image denoising schemes using generalized Gaussian and complexity priors," IEEE Infor. Theory, Vol. 45, No. 3, pp.909–919, 1999.
[18] F. Abramovitch, T. Sapatinas, and B. W. Silverman "Wavelet thresholding via a Bayesian approach," Journal Roy Statistic Society, Vol. 60, No. 4, pp.725– 749, 1998.
[19] J. Romberg, H. Choi and R. G. Baraniuk, "Bayesian wavelet domain image modeling using hidden Markov models," IEEE Transactions on Image Processing, Vol. 10, pp.1056–1068, 2001.
[20] S. G. Chang, B. Yu and M. Vetterli, "Adaptive wavelet thresholding for image denoising and compression," IEEE Trans. on Image Proc, Vol. 9, No. 9, pp.1532–1546, 2000.
[21] L. Xinhao, M. Tanaka and M. Okutomi, "Single- Image Noise Level Estimation for Blind Denoising," IEEE Transactions on Image Processing , Vol. 22, No. 12, pp.5226–5237, 2013.
[22] H. S. Bhadauria and M. L. Dewal, "Efficient Denoising Technique for CT images to Enhance Brain Hemorrhage Segmentation," International Journal of Digit Imaging, Vol.25, No. 6, pp. 782–791, 2012.
[23] P. Jain and V. Tyagi, "LAPB: Locally adaptive patch-based wavelet domain edge-preserving image denoising," Journal of Information Sciences, Vol. 294, pp. 164–181, 2015.

Authors' Profiles

Manoj Kumar: He has achieved his master degree (M. C. A.) from JNU, New Delhi and Ph.D from IIT Roorkee, India. Currently, he is working as Assistant Professor in the Department of Computer Science, Babasaheb Bhimrao Ambedkar University, Lucknow, India. His research interest includes Computer Graphics, Vision, & Image processing, Medical imaging and Pattern recognition. He has published various research papers in national and international journals & conferences.

Manoj Diwakar: He has achieved his B.Tech degree from Dr. R. M. L. Awadh University, Faizabad and M.Tech from MITS, Gwalior, India. He is currently pursuing his Ph. D. in the Department of Computer Science, Babasaheb Bhimrao Ambedkar University, Lucknow, India. His research interests include Image processing, Information Security and Medical imaging. He has published various research papers in national and international journals & conferences.

